In vitro induction and *in vivo* engraftment of lung bud tip progenitor cells derived from human pluripotent stem cells

Alyssa J. Miller[1,2], David R. Hill[2], Melinda S. Nagy[2], Yoshiro Aoki[4], Briana R. Dye[5], Alana M. Chin[2], Sha Huang[2], Felix Zhu[2], Eric S. White[2], Vibha Lama[4], Jason R. Spence[1,2,3*]

1. Program in Cellular and Molecular Biology
2. Department of Internal Medicine
3. Department of Cell and Developmental Biology
4. Division of Pulmonary and Critical Care Medicine
University of Michigan Medical School, Ann Arbor, Michigan 48109

5. Department of Biomedical Engineering
University of Michigan College of Engineering, Ann Arbor, Michigan 48109

* Author for correspondence:
Email: spencejr@umich.edu
ORCID: http://orcid.org/0000-0001-7869-3992

Author Contributions: AJM and JRS conceived the study. AJM, MSN, BRD, SH, YA, AMC, and ESW conducted experiments. AJM, DRH, BRD, SH, MSN, YA, AMC, FZ, VL and JRS analyzed and interpreted results. ESW also provided critical materials and reagents. AJM and JRS wrote the manuscript. All authors read, edited and approved the final content of the manuscript.

Conflicts of Interest: The authors have no conflicts to declare.

Abbreviations:
Bone Morphogenic Protein, BMP
Fibroblast Growth Factor, FGF
All-Trans Retinoic Acid, RA
Human Lung Organoid, HLO

Summary:
The bud tip epithelium of the branching mouse and human lung contains multipotent progenitors that are able to self-renew and give rise to all mature lung epithelial cell types. The current study aimed to understand the developmental signaling cues that regulate bud tip progenitor cells in the human fetal lung, which are present during branching morphogenesis, and to use this information to induce a bud tip progenitor-like population from human pluripotent stem cells (hPSCs) *in vitro.* We identified that FGF7, CHIR-99021 and RA maintained isolated human fetal lung bud tip progenitor cells in an undifferentiated state *in vitro*, and led to the induction of a 3-dimensional lung-like epithelium from hPSCs. 3-dimensional hPSC-derived lung tissue was initially patterned, with airway-like interior domains and bud tip-like progenitor domains at the periphery. Bud tip-like domains could be isolated, expanded and maintained as a nearly homogeneous population by serial passaging. Comparisons between human fetal lung bud tip cells and hPSC-derived bud tip-like cells were carried out using immunostaining, *in situ* hybridization and transcriptome-wide analysis, and revealed that *in vitro* derived tissue was highly similar to native lung. hPSC-derived bud tip-like structures survived *in vitro* for over 16 weeks, could be easily frozen and thawed and maintained multi-lineage potential. Furthermore, hPSC-derived bud tip progenitors had successful short-term engrafment into the proximal airways of injured immunocompromised NSG mouse lungs, where they began to express markers of proximal airway cells.

Introduction:
During development, the lung undergoes branching morphogenesis, where a series of stereotyped epithelial bifurcations give rise to the branched, tree-like architecture of the adult lung (Metzger et al., 2008). A population of rapidly proliferating progenitor cells resides at the tips of the epithelium throughout the branching process ('bud tip progenitors') (Branchfield et al., 2015; Rawlins et al., 2009). This population, which expresses *Id2* and *Sox9* in mice, has the capability to differentiate into both mature airway and alveolar cell types. At early stages of branching morphogenesis, this population of progenitors gives rise to proximal airway cells, while at later time points these progenitors give rise to mature alveolar cells (Rawlins, 2009).

Studies utilizing genetic mouse models have shown that lung branching morphogenesis and proximal-distal patterning are regulated by a series of complex mesenchymal-epithelial interactions that involve multiple signaling events, transcription factors, and dynamic regulation of the physical environment (Domyan and Sun, 2010; Hines and Sun, 2014; Kim and Nelson, 2012; Morrisey et al., 2013; Morrisey and Hogan, 2010; Rawlins, 2010; Rock and Hogan, 2011; Varner and Nelson, 2014). These studies have identified major roles for several signaling pathways in these processes, including Wnt, Fibroblast Growth Factor (Fgf), Bone Morphogenic Protein (Bmp), Sonic Hedgehog (Shh), Retinoic Acid (RA) and Hippo signaling among others (Abler et al., 2009; Bellusci et al., 1997a;

1997b; 1996; Cornett et al., 2013; Desai et al., 2006; 2004; Domyan et al., 2011; Goss et al., 2009; Harris-Johnson et al., 2009; Herriges et al., 2015; Lange et al., 2015; Lu et al., 2009; Mahoney et al., 2014; Motoyama et al., 1998; Sekine et al., 1999; Shu et al., 2005; Weaver et al., 2000; White et al., 2006; Yin et al., 2011; 2008; Y. Zhang et al., 2016; Zhao et al., 2014). However, due to the complex and intertwined nature of these signaling networks, perturbations in one pathway often affect signaling activity of others (Hines and Sun, 2014; Morrisey et al., 2013; Ornitz and Yin, 2012). To date, how multiple signaling networks interact to generate, maintain, and prompt cell fate decisions in bud tip progenitors remains poorly understood. Furthermore, emerging evidence suggests that there are significant differences in gene expression between the developing human and mouse lungs (Y.-W. Chen et al., 2017; Nikolić et al., 2017),.

The aforementioned understanding of murine lung development has been used as a guide to successfully direct differentiation of human pluripotent stem cells into differentiated lung lineages and 3-dimensional lung organoids (Y.-W. Chen et al., 2017; Dye et al., 2016b; 2015; Firth et al., 2014; Ghaedi et al., 2013; Gilpin et al., 2014; Gotoh et al., 2014; Huang et al., 2013; Konishi et al., 2015; Longmire et al., 2012; McCauley et al., 2017). However, specifically inducing and maintaining the bud tip progenitor cell population from hPSCs has remained elusive. For example, our own studies have shown that hPSCs can be differentiated into human lung organoids (HLOs) that possess airway-like epithelial structures and alveolar cell types; however, it was not clear if HLOs passed through a bud tip progenitor-like stage, mimicking all stages of normal development *in vivo* (Dye et al. 2015). More recent evidence from others has demonstrated that putative bud tip progenitor cells can be induced from hPSCs; however, these cells were rare, had low cloning efficiency, and their multilineage differentiation potential was not assessed (Y.-W. Chen et al., 2017). Thus, generation of a robust population of bud tip progenitor cells from hPSCs would shed additional mechanistic light on how these cells are regulated, would provide a platform for further investigation into mechanisms of lung lineage cell fate specification, and would add a layer of control to existing directed differentiation protocols allowing them to pass through this developmentally important progenitor transition.

In order to gain insight into the signaling cues required for *in vitro* growth and maintenance of progenitor identity, we conducted a low-throughput screen using isolated mouse bud tip cultures that were subsequently used to inform experiments in human fetal lung tissue and in hPSC-derived tissue. We determined that FGF7 promoted an initial expansion of human bud tip progenitors, and that the addition of CHIR-99021 (a GSK3β inhibitor that acts to stabilize β-catenin) and All-trans Retinoic Acid (RA) (3-Factor conditions, herein referred to as '3F') were required growth/expansion of human fetal bud tip organoids that maintained their progenitor identity. Our results also confirmed recent studies suggesting that bud tip progenitor cells in the developing human lung express SOX2, which is exclusively expressed in the proximal airway in the

embryonic mouse lung, identifying an important species-specific difference (Y.-W. Chen et al., 2017; Hashimoto et al., 2012; Nikolić et al., 2017; Que et al., 2007).

When applied to hPSC-derived foregut spheroid cultures, we observed that 3F conditions promoted growth into larger organoid structures with a patterned epithelium that had airway-like and bud tip-like domains. Bud tip-like domains possessed cells with a molecular profile similar to human fetal bud tip organoids. Bud tip domains could be further enriched and expanded by serial passaging and underwent multilineage differentiation *in vitro*. Transplantation studies revealed that hPSC-derived bud tip progenitors could engraft into the epithelium of immunocompromised mice and respond to systemic factors. Taken together, these studies provide an improved mechanistic understanding of human lung bud tip progenitor cell regulation and highlight the importance of using developing tissues to provide a framework for improving differentiation of hPSCs into specific lineages.

Results:

Characterizing human fetal lung bud tip progenitors

During branching morphogenesis, the distal epithelial bud tips are comprised of progenitor cells that remain in the progenitor state until the branching program is complete (Chang et al., 2013) and will give rise to all the mature cell types of the lung epithelium (Rawlins et al., 2009). In mice, this population of progenitor cells is known to express several transcription factors, including *Sox9*, *Nmyc* and *Id2* (Chang et al., 2013; Moens et al., 1992; Okubo et al., 2005; Perl et al., 2005; Rawlins et al., 2009; Rockich et al., 2013). However, progenitor cells in the human lung are less well studied. Moreover, in order to generate hPSC-derived bud tip-like progenitor cells *de novo,* we wanted to use human fetal lung tissue as a benchmark, given the possibility that unknown species-specific differences may exist. Thus, we carried out an immunohistochemical analysis using well-established protein markers that are present during mouse lung development (Figure 1A-C, Figure 1 – Supplement 1) on human lungs during the psuedoglandular stage of branching morphogenesis between 10-20 weeks gestation. We also conducted RNAsequncing on freshly isolated lung bud tip domains and compared this to adult lung to identify genes that were differentially expressed in human bud tip progenitors (Figure 1D-E). Consistent with the developing mouse lung (Perl et al., 2005; Rockich et al., 2013), we observed that SOX9 is expressed in bud tip domains of the branching epithelium (Figure 1A, Figure 1 – Supplement 1A). In contrast to the developing murine lung, we observed SOX2 expression in these bud tip progenitor domains until 16 weeks of gestation, at which time SOX2 expression was lost from this population (Figure 1A, Figure 1 – Supplement 1A). We also observed expression of *ID2* by *in situ*

hybridization (Figure 1B), with bud tip localization becoming increasingly intense in the bud tips as branching progressed, up through 20 weeks gestation (Figure 1 – Figure Supplement 1F). Bud tips began to express Pro-SFTPC by 12 weeks, and expression increased in the bud tips until 20 weeks, the latest time point examined (Figure 1C; Figure 1 – Figure Supplement 1D). SOX9+ bud tip cells did not express several other lung epithelial markers including SFTPB, PDPN, RAGE or HOPX (Figure 1C). Again, this expression contrasted with mice, where early bud tip progenitors were shown to co-express *Pdpn* and *Sftpc* (Treutlein et al., 2014). SOX9+ cells also did not express the SFTPB, a marker of mature AECII cells, at any time points examined (Figure 1C, Figure 1 – Figure Supplement 1D). We also examined expression of several proximal airway markers, including P63, acetylated-Tubulin (AC-TUB), FOXJ1, SCGB1A1 and MUC5AC and noted that expression was absent from the bud tip progenitors (negative staining data not shown). Interestingly, we observed that makers associated with AECI cells in the mature lung, PDPN and HOPX, were expressed in the transition zone/small airways directly adjacent to the SOX9+ bud tip domain and in the proximal airways at all time points examined (10-20 weeks of gestation) but that this region did not begin to express the AECI maker RAGE until 16 weeks of gestation (Figure 1C; Figure 1 – Figure Supplement 1 B, C, E). RNAsequencing of isolated, uncultured human fetal lung bud tips (n=2; 59 days and 89 days gestation; isolation procedure Figure 2A-B) supported protein staining analysis of human fetal buds. Differential expression analysis to identify genes enriched in the human fetal bud tips (isolated human fetal bud tips vs. whole adult lung) identified 7,166 genes that were differentially expressed (adjusted P-value < 0.01; Figure 1D). We then generated a curated heatmap to show genes corresponding to the proteins/mRNA examined in Figure 1A-C and highlighted in the literature as being known markers lung epithelial cells (Figure 1E). We also generated a curated heatmap to compare differentially enriched genes identified in our analysis with a recently published list of 37 transcription factors found to be enriched in human fetal lung bud tips (Nikolić et al., 2017) (Figure 1F). In total, 20 of the 37 transcription factors previously reported in human fetal buds were also enriched in the bud tip enriched genes identified in our analysis (Figure 1F). Gene set enrichment analysis (GSEA) confirmed that this was a highly significant enrichment of fetal lung bud tip associated transcription factors (NES = -1.8, adjusted P-value=9.1e-5). Combined, this data provides a profile of the protein and gene expression in human fetal lung buds prior to 15 weeks gestation (summarized in Figure 2G).

Murine bud tip growth *in vitro*

In order to establish an experimental framework that would allow us to efficiently work with rare/precious human tissue samples, we first conducted a low-throughput screen using mouse epithelial bud tips to identify factors that promoted tissue expansion and maintenance of SOX9 expression. Bud tips were isolated from lungs of embryonic day (E) 13.5 *Sox9*-eGFP mice and cultured in a Matrigel droplet (Figure 1- Figure Supplement 2A). Isolated *Sox9*-eGFP lung bud

tips were shown to express GFP and to have the same level of *Sox9* mRNA as their wild type (WT) counterparts by QRT-PCR analysis (Figure 1- Figure Supplement 2B,C).

Signaling pathways examined included FGF, WNT, BMP and RA signaling (Bellusci et al., 1997b; Cardoso et al., 1997; Min et al., 1998; Nyeng et al., 2008; Sekine et al., 1999; Volckaert et al., 2013) and the screen included FGF7, FGF10, BMP4, All Trans Retinoic Acid (hereafter referred to as 'RA') and CHIR-99021 (a GSK3β inhibitor that acts to stabilize β-catenin) (Figure 1- Figure Supplement 2D). Treating isolated E13.5 mouse bud tips with no growth factors (basal media, control) or individual growth factors showed that FGF7 robustly promoted growth, expansion and survival of isolated buds for up to two weeks (Figure 1- Figure Supplement 1D). Interestingly, the same concentration of FGF7 and FGF10 did not have the same effect on lung bud outgrowth. To test the possibility that ligand activity may explain experimental differences, we treated buds with a 50-fold excess of FGF10 (500ng/mL, compared to 10ng/mL). A high concentration of FGF10 led to modest growth of buds and was sufficient to keep buds alive in culture, but cultures did not exhibit robust growth seen with low levels of FGF7 (Figure 1- Figure Supplement 2E).

FGF7 alone does not maintain *Sox9* in culture

In order to determine if FGF7 was promoting expansion of *Sox9*+ distal progenitors cells, we performed a lineage trace utilizing *Sox9*-Cre^{ER};*Rosa26*^{Tomato} mice. Tamoxifen was given to timed pregnant dams at E12.5, and epithelial lung buds were isolated 24 hours later, at E13.5 (Figure 1 - Figure Supplement 2F). Isolated distal buds were placed *in vitro* in basal media (control) or with FGF7. The *Sox9*-Cre^{ER};*Rosa26*^{Tomato} lineage labeled population expanded over time (Figure 1 - Figure Supplement 2F). However, we also noted that *Sox9* mRNA expression was significantly reduced over time (Figure 1 – Figure Supplement 2G), and SOX9 protein was absent after 14 days in culture (Figure 1 – Figure Supplement 4C), suggesting that FGF7 promoted an initial growth of *Sox9*+ bud tip progenitor cells, but did not maintain SOX9 expression.

FGF7, CHIR-99021 and RA are sufficient to maintain the expression of SOX9 *in vitro*

Given that FGF7 promoted robust expansion of bud tips *in vitro* but did not maintain SOX9 expression, we sought to identify additional growth factors that may interact with FGF signaling to maintain expression *in vitro.* To do this, we grew bud tips in 5F media, and removed one growth factor at a time and examined the effect on growth and expression of *Sox9* and *Sox2* (Figure 1 – Figure Supplement 3). Bud tips were grown in 5F-1 media for two weeks in culture. Removing FGF10, CHIR-99021, RA or BMP4 from 5F culture media did not affect the ability of isolated buds to expand, although various growth factor combinations generated starkly different morphological structures (Figure 1-

Figure Supplement 3A). QRT-PCR analysis of buds after 5 days in culture showed that removing BMP4 led to a statistically significant increase in *Sox9* mRNA expression levels when compared to other culture conditions (Figure 1 - Figure Supplement 3B), and led to gene expression levels that were closest in expression levels of freshly isolated WT E13.5 lung buds (Figure 1 - Figure Supplement 3B). Removing any other single factor did not lead to statically significant changes in *Sox9* expression (Figure 1 – Figure Supplement 3E) relative to buds grown with 5F-BMP4. *Sox2* gene expression was generally low in isolated E13.5 lung buds, and in all culture conditions after 5 days *in vitro* (Figure 1- Figure Supplement 3C).

Based the data demonstrating that FGF7 is critical for *in vitro* expansion of isolated murine bud tips and data showing that BMP4 led to a decrease in *Sox9* expression, we screened combinations of the remaining factors (FGF7 +/- FGF10, CHIR-99021, RA) to determine a minimal set of factors that could maintain the SOX9+ identity of bud tip progenitor cells (Figure 1 – Figure Supplement 4). We found that all conditions supported robust growth (Figure 1- Figure Supplement 4A) and expression of *Sox9* while maintaining low levels of *Sox2* (Figure 1- Figure Supplement 4C-E). Cultured buds treated with 4-factor '4F' or 3-Factor conditions ('3F'; FGF7, CHIR-99021, RA) maintained *Sox9* mRNA expression at the highest levels, mirroring expression levels in freshly isolated epithelial buds at E13.5 (Figure 1 – Figure Supplement 4E). Immunofluorescence and whole mount immunostaining of buds after 2 weeks in culture supported QRT-PCR data and showed that 3F and 4F conditions supported robust SOX9 protein expression (Figure 1- Figure Supplement 4C, D). Finally, to demonstrate that *Sox9*+ progenitors are expanded over time *in vitro*, lineage tracing experiments utilizing *Sox9*-Cre^{ER};*Rosa26*^{Tomato} mice, in which Tamoxifen was administered to timed pregnant dams at E12.5 and epithelial lung buds were isolated at E13.5, showed an expansion of labeled progenitors over the 2 week period in culture (Figure 1- Figure Supplement 4B).

Collectively, the experiments conducted in isolated mouse bud tips suggest that a minimum set of 3 factors (FGF7, CHIR-99021, RA) are sufficient to allow growth of mouse bud tip progenitor cells and to maintain SOX9 expression *in vitro.*

In vitro growth and maintenance of human fetal distal epithelial lung progenitors

Until recently, almost nothing was known about the functional regulation of human fetal epithelial bud tip progenitor cells (Nikolić et al., 2017). We asked if conditions supporting mouse bud tip progenitors also supported growth and expansion of human bud tip progenitors *in vitro*. Distal epithelial lung buds were enzymatically and mechanically isolated from the lungs of 3 different biological specimens at 12 weeks of gestation (84-87 days; n=3) and cultured in a Matrigel droplet (Figure 2A-B), where they formed cystic organoid structures that will

hereafter be referred to as 'fetal progenitor organoids' (Figure 2E; Figure 2 – Figure Supplement 1A). Consistent with paraffin embedded whole lung tissue (Figure 1), whole mount immunostaining revealed that human bud tip epithelial progenitors express both SOX9 and SOX2 at 12 weeks (Figure 2C).

When human bud tips were cultured *in vitro*, we observed that FGF7 promoted an initial expansion of tissue *in vitro* after 2 and 4 weeks, but structures began to collapse by 6 weeks in culture (Figure 2 - Figure Supplement 1A). All other groups tested permitted expansion and survival of buds in culture for 6 weeks or longer (Figure 21 - Figure Supplement 1A). Immunofluorescence demonstrated that human fetal progenitor organoids exposed to 3F or 4F supported robust protein expression of both SOX2 and SOX9 and QRT-PCR showed that these organoids expressed highest levels of the distal progenitor markers *SOX9, SOX2, ID2 and NMYC* (Figure 2 - Figure Supplement 1B-C). In contrast, culture in only 2 factors (FGF7+CHIR-99021, or FGF7+RA) did not support robust bud tip progenitor marker expression (Figure 2 - Figure Supplement 1B-C). QRT-PCR also showed that fetal progenitor organoids cultured in 3F or 4F media expressed very low levels of the proximal airway markers *P63, FOXJ1* and *SCGB1A1* and expressed HOPX at levels similar to the fetal lung (Figure 2 - Figure Supplement 2D-E). Consistent with low mRNA expression, protein staining for several markers was not detected in fetal progenitor organoids treated for 4 weeks in 3F media for, including P63, FOXJ1, SCGB1A1, MUC5AC, HOPX, RAGE, and SFTPB (n=8; negative data not shown). On the other hand, SOX9, SOX2 and pro-SFTPC was robustly expressed in human bud tip progenitor organoids grown in 3F medium, as demonstrated by immunofluorescence in sections or by whole mount staining. *ID2* expression was also detected using *in situ* hybridization. (Figure 2H). These gene/protein expression patterns are consistent with expression in human fetal bud tips earlier than 16 weeks of gestation.

To confirm our immunofluorescence and QRT-PCR data, we performed bulk RNA-sequencing on tissue from the distal portion of fetal lungs (epithelium plus mesenchyme) (n=3), on freshly isolated bud tips (n=3) and on 3F grown human fetal bud tip progenitor organoids after 4 weeks in culture (n=2 biological samples, run with statistical triplicates). Analysis revealed a high degree of similarity between these samples with respect to epithelial progenitor gene expression (Figure 2I). Additionally, we identified genes highly enriched in isolated fetal bud tips by conducting differential expression analysis on RNAseq data, comparing whole human adult lung versus uncultured isolated lung buds (12 weeks gestation) and versus cultured fetal progenitor organoids (12 weeks gestation, cultured for 2 weeks) (Figure 2J). The top 1000 upregulated genes relative to adult for each group were identified (log2FoldChange < 0; adjusted p-value < 0.05), and common upregulated genes were identified. 431 (27.5%) of the genes were commonly upregulated in fetal bud tips and cultured fetal organoids, which was highly statistically significant (p-value=1.4e-278 for overlapping genes, as determined by a hypergeometric test)(Figure 2J).

Lastly, we tested if fetal progenitor organoid cells could engraft into the airways of injured NSG mice (Figure 2 - Figure Supplement 2A). Adult male mice were injured with naphthaline, which severely damaged the lung epithelium within 24 hours (Figure 2- Figure Supplement 2B). Fetal progenitor organoids were digested into single cells and delivered by intratracheal gavage of mice 24 hours after injury (n=6 mice injected). Seven days after the cells were injected, patches of human cells that had engrafted into the proximal mouse airway in 3 out of the 4 surviving mice as determined by expression of a human specific mitochondrial marker (HuMito, Figure 2 - Figure Supplement 2D)(Dye et al., 2016a). Compared to human fetal lung bud organoids, which robustly expressed SOX9 and SOX2 on the day of injection (Figure 2 - Figure Supplement 2C), engrafted NKX2.1+ human cells did not express SOX9 or Pro-SFTPC but maintained expression of SOX2 (Figure 2 - Figure Supplement 2D; negative Pro-SFTPC staining not shown). Protein staining for differentiated cell markers indicated that engrafted human cells did not express detectable levels of proximal airway markers SCGB1A1, MUC5AC, FOXJ1, CHGA and P63, nor differentiated alveolar cell markers SFTPB, ABCA3, HOPX, RAGE and PDPN, suggesting that these cells had not taken on a fully differentiated cell fate by 7 days post injection (negative data not shown).

FGF7, CHIR-99021, RA induces a bud tip progenitor-like population of cells from hPSC-derived foregut spheroids

Given the robustness by which 3F medium (FGF7, CHIR-99021, RA) supported mouse and human lung bud progenitor growth and maintenance *in vitro*, we sought to determine whether these culture conditions could promote a lung bud tip progenitor-like population from hPSCs. NKX2.1+ ventral foregut spheroids were generated as previously described (Dye et al., 2016b; 2015), and were cultured in a droplet of Matrigel and overlaid with serum-free medium containing FGF7, CHIR-99021,RA. Spheroids were considered to be “day 0” on the day they were placed in Matrigel (Figure 3A-B). Foregut spheroids cultured in 3F medium generated patterned organoids (hereafter referred to as 'hPSC-derived patterned lung organoids'; PLOs) that grew robustly, survived for over 16 weeks in culture, and could be frozen, thawed and re-cultured (Figure 2- Figure Supplement 1A-E). PLOs passed through predictable and consistent phases of epithelial morphogenesis (Figure 3B, Figure 2 - Figure Supplement 1C-D). Epithelial folding began around 3 weeks in culture; after which regions in the periphery began to form budded structures that underwent repeated rounds of outgrowth and apparent bifurcation (Figure 3B, Figure 3 – Figure supplement 1C-D), asterisks mark bifurcating buds in D). Budded regions formed balloon-like structures after roughly 10 weeks in culture (Figure 3B). In order to passage patterned lung organoids, the organoids were manually removed from their Matrigel droplets without disrupting the structure, and replated in fresh matrigel every two weeks.

At 2 and 6 weeks, PLOs co-expressed NKX2.1 and SOX2 in >99% of all cells (99.41 +/- 0.82% and 99.06 +/- 0.83%, respectively), while 16 week old PLOs possessed 93.7 +/- 4.6% NKX2.1+/SOX2+ cells (Figure 3C-D). However, PLOs at this later time point appeared as though they were deteriorating (Figure 3B). Interestingly, no mesenchymal cell types were detected in patterned lung organoid cultures at 2, 6 or 16 weeks by immunofluorescence (VIMENTIN, α-SMOOTH MUSCLE ACTIN, PDGFRα; negative immunostaining data not shown).

PLOs also exhibited regionalized proximal-like and distal-like domains. In 100% of analyzed PLOs (n=8) Peripheral budded regions contained cells that co-stained for SOX9 and SOX2, whereas interior regions of the PLOs contained cells that were positive only for SOX2, suggesting these organoids had proximal-like and distal-like regions corresponding to airway and bud tip progenitor regions in the developing human lung (Figure 3E-F). Budded regions of PLOs contained SOX9+ cells that also expressed pro-SFTPC, similar to what is seen in human fetal bud tip cells (Figure 3G; Figure 1C). SOX9+/SOX2+ bud tip regions persisted within PLOs for over 100 days in culture (~16 weeks, the longest time examined) (Figure 3 – Figure Supplement 1F). QRT-PCR analysis showed that *SOX2*, *NMYC*, and *ID2* expression levels are similar between whole fetal human lung and 54 day PLOs, while SOX9 mRNA was expressed at lower levels in whole PLOs (Figure 3 - Figure Supplement 2A). Comparison of freshly isolated 12 week human fetal bud tips and microdissected bud regions from PLOs demonstrated that PLO buds have similar expression of *SOX9, SOX2, ID2* and *NMYC* (Figure 3 - Figure Supplement 2B), while expression of differentiation markers are significantly lower in PLOs compared to whole 14 week human fetal lungs (Figure 3- Figure Supplement 2C-D).

Interior regions of PLOs contained a small proportion of cells that showed positive immunostaining for the club cell marker SCGB1A1 (~9%) and the goblet cell marker MUC5AC (~1%), with similar morphology to adult human proximal airway secretory cells (Figure 3I-L). Some apical staining of acetylated tubulin was present in the cells within the interior regions of PLOs, but no *bona fide* cilia were noted and FOXJ1 was not detected by protein stain in any PLOs (Figure 2I). Additionally, the basal cell marker P63 was absent from PLOs (Figure 2I), as was staining for markers of lung epithelial cell types including HOPX, RAGE, PDPN, ABCA3, SFTPB, and CHGA (negative data not shown).

Expansion of bud tip progenitor-like cells from patterned lung organoids

Patterned lung organoids could be passaged by mechanically shearing the epithelial structures using a 27-gauge needle, followed by embedding in fresh Matrigel and growth in 3F medium (Figure 4A-B). Patterned lung organoids could undergo initial needle passage as early as 2 weeks and as late as 10 weeks with similar results, meaning this population can be generated from hPSCs in as little as 24 days (9 days to achieve foregut spheroids, 14 days to expand patterned

lung organoids, 1 day to grow needle passaged organoids) but could be grown and expanded for up to 18 weeks (Figure 4A). Following needle shearing, many small cysts were re-established within 24 hours and could be serially passaged every 7-10 days (Figure 4C). Interestingly, we noted that patterned structures were not re-established following passaging. The cysts that formed after needle passaging were NKX2.1+/SOX2+ (Figure 4 – Figure Supplement 1A) and the majority of cells expressed SOX9 (Figure 4D,E), therefore these cysts were called 'bud tip organoids'. When compared to PLOs, bud tip organoids possessed a much higher proportion of SOX9+ cells (42.5% +/- 6.5%, n=5; vs. 88.3% +/- 2.3%, n=9; Figure 4E).

Examination of proliferation by KI67 immunofluorescent staining revealed that bud tip organoids contained significantly higher number of proliferating cells when compared to PLOs (38.24% +/- 4.7%, n=9 for bud tip organoids vs. 4.9% +/- 0.6%, n=5 for PLOs; Figure 4F-I). In PLOs, we noted that proliferation was largely restricted to SOX9+ budded regions, but only a small proportion of SOX9+ cells were proliferating (8.1% +/- 0.9%, n=5), whereas bud tip organoids had a much higher proportion of proliferative SOX9+ cells (40.2% +/- 4.3%, n=9) (Figure 3I). Together, this data suggests that needle passaging enriches the highly proliferative bud tip regions of PLOs.

Bud tip organoids were further characterized and compared to the bud tips in human fetal lungs using *in situ* hybridization and immunofluorescence (Figure 4 – Figure Supplement 1; Figure 1). Bud tip organoids exhibited protein staining patterns consistent with 14-16 week fetal lungs, including co-staining of SOX9 and pro-SFTPC (Figure 4 - Figure Supplement 1D). We also noted that bud tip organoids were positive for *ID2* based on *in situ hybridization* and whole transcriptome comparisons using RNAseq (Figure 4K; Figure 4 - Figure supplement 1C). Additionally, bud tip organoids were negative for SFTPB, ABCA3, HOPX, RAGE and PDPN, similar to what was observed in the developing human fetal bud tip cells (Figure 1 and Figure 1 – Figure Supplement 1 vs. Figure 4 - Figure Supplement 1B, E). Furthermore, no positive protein staining was detected for the proximal airway markers P63, FOXJ1, AC-TUB, MUC5AC, SCGB1A1 or CHGA (negative data not shown).

In addition to targeted analysis comparing bud tip organoids and the human fetal lung, we also conducted and unbiased comparison using RNA-sequencing by comparing: hPSC-derived bud tip organoids; whole peripheral (distal) human fetal lung tissue; freshly isolated fetal bud tips; human fetal lung progenitor organoids; undifferentiated hPSCs; and hPSC-derived lung spheroids. Principal component analysis (PCA) revealed the highest degree of similarity between hPSC-derived bud tip organoids, patterned lung organoids and human fetal organoids (Figure 4J). Interestingly, freshly isolated bud tips and whole distal human fetal lungs had a high degree of similarity, clustered separately from both fetal and hPSC-derived organoids. On the other hand, cultured human fetal organoids, PLOs and bud tip organoids clustered together. These transcriptional

differences are likely due to molecular changes that are induced in the tissue culture environment compared to the environment of the native lung, but also highlight the high degree of molecular similarity of human fetal and hPSC-derived organoids grown *in vitro* (Figure 1J).

Differentially expression of RNAseq data was used to conduct several comparisons: 1) uncultured isolated lung buds (59 days and 89 days (8-12 weeks) gestation) versus whole adult lung tissue; 2) cultured fetal progenitor organoids (12 weeks gestation, cultured for 2 weeks) versus whole adult lung tissue; 3) hPSC-derived bud tip organoids versus whole adult lung tissue (Figure 4L). The top 1000 upregulated genes in each group relative to adult were identified (log2FoldChange < 0; adjusted p-value < 0.05), and overlapping genes were identified. A hypergeometric means test found that the shared genes between isolated human bud tips and hPSC-derived bud tip organoids were highly significant, with 377 (23.2%) overlapping genes (p-value=9.3e-901; Figure 4L), as were the shared genes between cultured fetal progenitor organoids and hPSC-derived bud tip organoids, with 477 (31.3%) overlapping genes (p-value=1.2e-1021) (Figure 4M). Both of these comparisons were highly statistically significant. Of note, when all three groups were compared, a core group of 285 common upregulated genes were identified representing 14.3% of genes included in the comparison, including several genes previously associated with human or mouse fetal bud tips (Nikolić et al., 2017; Rockich et al., 2013) (Figure 4N; *COL2A1, ETV4, E2F8, FGF20, HMGA2, MYBL2, RFX6, SALL4, SOX9, SOX11*), as well as many genes associated with cell cycle and proliferation (*CCNA2, CCNB1, CCNB2, CDC6, CDC20, CDC25A, CDC25C, CDCA3, CDCA5, MKI67*)

hPSC-derived bud tip organoids maintain multilineage potential *in vitro*

Since we had demonstrated that CHIR-99021 and RA were required along with FGF7 to promote bud tip progenitor cell gene expression, we hypothesized that that removing CHIR-99021 and RA from the culture media would promote an environment that is permissive for differentiation of bud tip-like cells.

Induced pluripotent stem cells (iPSC) derived foregut spheroids were used to generate PLOs (iPSC line 20-1 (iPSC20-1); (Spence et al., 2011)). PLOs were cultured for 40 days in 3F medium. At 40 days, patterned lung organoids were passaged through a needle to generate bud tip organoids which were serially passaged and maintained for an additional 35 days. Bud tip organoids were then grown in either 3F medium or FGF7 for 23 days (Figure 5A). At the end of the experiment, control bud tip organoids maintained a clear, thin epithelium with visible a lumen whereas FGF7 treated organoids appeared as large dense cysts, some of which contained a dark and opaque lumen (Figure 5B). Bud tip organoids maintained in 3F medium remained SOX9+/SOX2+ positive, and did not display evidence of differentiation (negative for MUC5AC, FOXJ1, SCGB1A1; negative data not shown).

After 23 days of FGF7 treatment, all cells remained NKX2.1+/ECAD+, signifying that they retained a lung epithelial identity (Figure 5C). Protein staining revealed cells that expressed both alveolar and proximal airway markers in these cultures. Although no *bona fide* alveolar structures were observed, a subset of cells expressed the AECI markers PDPN (8.6% of total cells) and HOPX (5.9% of total cells), with some cells exhibiting elongated nuclei similar to AECI cell morphology in vivo (Figure 5D, H-I); however, no cells expressed the AECI marker, RAGE (Figure 5D, H-I). Approximately ~45% of all counted cells stained positive for AECII markers SFTPB and pro-SFTPC, with overlapping punctate staining clearly seen (Figure 5D, H-I). Transmission electron microscopy also revealed cells with lamellar bodies suggestive of differentiation into AECII-like cells (Figure 5F). Interestingly, only 6.3% of cells stained positive for ABCA3, a marker of mature AECII cells (Figure 5D, H). This may suggest that AECII-like cells did not reach full maturity *in vitro.* Another 43.2% of cells stained positive for nuclear SOX2 (Figure 5G, H-I), a marker of the proximal airway, but did not express nuclear SOX9 (Figure 5H-I). 26.8% of cells stained positive for the goblet cell marker MUC5AC, and secreted MUC5AC was detected within the lumens of almost all differentiated organoids (Figure 5E). Transmission electron microscopy confirmed the presence of mucous filled vacuoles within cells (Figure 5F, 'M' marks mucous). 7% of cells were positive for the club cell marker SCGB1A1 (Figure 4E, H-I). Apical acetylated tubulin staining was present in 2.5% of cells, although these cells did not possess fully formed multiciliated structures, no beating cilia were observed in culture, and FOXJ1 staining was absent (Figure 5E, H-I), suggesting that these were not multiciliated cells. Additionally, 2.0% of cells expressed very clear staining for Chromagranin A (CHGA), a marker for neuroendocrine cells. These cells morphologically looked similar to native neuroendocrine cells in the adult lung and sat on the basal side of epithelial structures (Figure 5E). No positive staining was detected for the basal cell marker P63 (Figure 5E).

Together, this data suggests that SOX2+/SOX9+ bud tip organoids maintained the ability to undergo multilineage differentiation, and could give rise to both alveolar-like and airway-like cell lineages *in vitro* (Summarized in Figure 5J).

Engraftment of hPSC-derived bud tip progenitor cells into the injured mouse airway

We next sought to explore the potential of hPSC-derived bud tip progenitor organoids to contribute to injury repair by determining whether they could engraft into the airways of injured mouse lungs (Figure 6A). We reasoned that damaging the lung epithelium would create additional niches for injected cells to engraft. Sixteen male immunocompromised NSG mice (8 control, 8 treatment group) were given an i.p. injection of 300 mg/kg Naphthaline to induce proximal airway injury (Karagiannis et al., 2012). The lung epithelium was severely damaged 24 hours after naphthaline injury but largely recovered by 7 days after injury (Figure

6B). Bud tip organoids were generated from the iPSC20.1 line, which was transduced with a doxycycline inducible nuclear GFP (tet-O-GFP) lentivirus (Y.-J. Chen et al., 2014). iPSC20.1 bud tip organoids were digested to a single cell suspension and 600,000 cells were intratracheally administed to 8 NSG mice 24 hours following Naphthalene injury (Figure 6A). iPSC20.1 bud tip organoids from the same cohort that were injected were also collected for comparison on the day of injection (Figure 6, Figure Supplement 1). Starting 24 hours after delivery of the cells, mice were given doxycycline in the drinking water for 7 days to determine whether any engrafted human cells could receive a systemic signal from the bloodstream, and animals were sacrificed 8 days after injury. Mice were injected with BrdU 1 hour before sacrifice to assess cell proliferation (Figure 6A). 75% of mice that received iPSC20.1 bud tip progenitor cells survived to 8 days post injury, compared with only 50% of animals that received an injury but no cells, although this survival benefit was not statistically significant (Figure 6C).

The lungs of all surviving animals were analyzed, and 4/6 surviving mice that received human cells had clear patches of engrafted cells as determined by protein staining for HuMITO or NuMA within the proximal airways (Figure 6D). No human cells were found within the alveolar spaces. Human cell engraftment was assessed in each lung by counting the number of patches in a histological section of lung stained with HuMITO or NuMA and with one or more human cells flanked by mouse epithelial cells within the airway. Individual mice possessed cell patches ranging from 3.1 (+/- 0.5) to 9.8 (+/-2.1) cells per patch, depending on the individual mouse, although it is noteworthy that some grafts were as large as 45 cells (Figure 6E). Engrafted human cells retained NKX2.1 expression after integration (Figure 6F). Many human cells found within the airway were positive for BrdU, showing that engrafted lung bud progenitors were actively proliferating after 7 days (Figure 5G). KI67 protein staining further confirmed that 52.8% of engrafted human cells within the mouse airway were proliferating at the time of sacrifice (Figure 6H-I).

Interestingly, 7 days post injection of the cells, 79% of human cells in the mouse airway were still co-labeled by nuclear SOX2 and nuclear SOX9 (Figure 5J). However, the protein stain for SOX9 appeared weaker and exhibited some cytoplasmic staining as compared to *in vitro* grown bud tip organoids (Figure 5-Figure Supplement 1C), suggesting that engrafted cells may be transitioning to a SOX2+, SOX9- state.

Immunofluorescent staining for proximal cell markers revealed that of the SOX2+ cells, 42.8% expressed the club cell marker SCGB1A1, and 25% of cells expressed the goblet cell marker MUC5AC (Figure 5L-O). Markers of multiiliated cells, FOXJ1 (Figure 5N) and Acetylated Tubulin (negative data not shown), were not observed. Staining for the basal cell marker P63 was also absent (negative data not shown). Immunofluorescent staining for differentiated alveolar cell markers (AECI: HOPX, PDPN, RAGE; AECII: Pro-SFTPC, SFTPB, ABCA3) were not observed in any engrafted human cells (data not shown).

Staining for ECAD demonstrated that human cells possessed basal and lateral cellular membranes in continuity with the mouse airway (Figure 5L, P). Furthermore, we observed that 35% of all human cells expressed GFP, indicating that engrafted human cells had access to systemic factors delivered by the host bloodstream, and indicating that these cells can respond to orally administered drugs. Taken together, our data suggests that hPSC-derived lung bud tip progenitor-like cells can engraft into the injured airway. Most engrafted cells retain expression of progenitor markers after 7 days but a subset of cells begin to express differentiation markers, These results additionally suggest that hPSC-derived bud tip progenitor cells may hold a therapeutic benefit to repopulate lung epithelium that may be dysfunctional, such as with cystic fibrosis, or lost to disease or immune attack, such as with complications from lung transplantation.

Discussion:

The ability to study human lung development, homeostasis and disease is limited by our ability to carry out functional experiments in human tissues. This has led to the development of many different *in vitro* model systems using primary human tissue, and using cells and tissues derived from hPSCs (Dye et al., 2016c; Miller and Spence, 2017). Current approaches to differentiate hPSCs have used many techniques, including the stochastic differentiation of lung-specified cultures into many different lung cell lineages (Y.-W. Chen et al., 2017; Huang et al., 2013; Wong et al., 2012), FACS based sorting methods to purify lung progenitors from mixed cultures followed by subsequent differentiation (Gotoh et al., 2014; Konishi et al., 2015; Longmire et al., 2012; McCauley et al., 2017), and by expanding 3-dimensional ventral foregut spheroids into lung organoids (Dye et al., 2016b; 2015). During normal development, early lung progenitors transition through a SOX9+ distal bud tip progenitor cell state on their way to terminal differentiation, and it is assumed that in many hPSC-differentiation studies, NKX2.1-positive cells specified to the lung lineage also transition through a SOX9+ distal epithelial progenitor state prior to differentiating; however, this has not been shown definitively. For example, studies have identified methods to sort and purify lung epithelial progenitor cells from a mixed population (Gotoh et al., 2014; Konishi et al., 2015; McCauley et al., 2017). However, whether or not these populations represents a true bud tip epithelial progenitor or is representative of an earlier stage lung progenitor is unknown.

Capturing the bud tip progenitor state in vitro has remained elusive, in part, because the complex signaling networks required to induce and/or maintain this progenitor cell state are not well understood. A more recent study observed putative SOX9+/SOX2+ human bud tip progenitor cells, but these cells were rare, were not easily expanded in culture and their multipotent ability was not tested (Y.-W. Chen et al., 2017). The current study aimed to elucidate the signaling

interactions that are required to maintain and expand the bud tip progenitor population in mouse and human fetal lungs, and to induce, expand and maintain a nearly homogenous population of these cells from hPSCs. Passing through a distal progenitor cell state is a critical aspect of normal lung epithelial development *en route* to becoming an alveolar or airway cell type (Rawlins et al., 2009), and so achieving this with hPSC-derived models is an important step toward faithfully modeling the full complement of developmental events that take place during lung organogenesis *in vivo*. Moreover, capturing this cell state *in vitro* will facilitate future studies aimed at understanding the precise mechanisms by which progenitor cells make cell fate choices in order to differentiate into mature cell types.

Our study has identified a minimum core group of signaling events that synergize to efficiently support the maintenance of mouse and human bud tip progenitor cells cultured *ex vivo*, and we have used the resulting information to differentiate multipotent lung bud tip-like progenitor cells from hPSCs. The ability to induce, *de novo*, populations of cells from hPSCs suggest that biologically robust experimental findings can be used in a manner that predicts how a naïve cell will behave in the tissue culture dish with a high degree of accuracy, and across multiple cell lines (D'Amour et al., 2005; Green et al., 2011; Spence et al., 2011). Thus, the robustness of our results culturing and expanding isolated mouse and human bud tip progenitors is highlighted by the ability to use this information in a predictive manner in order to accurately induced a bud tip-like population of cells from hESCs and iPSCs. Using isolated embryonic tissue side-by-side with *in vitro* hPSC differentiation highlights the power of using the embryo as guide, but also shows the strength of hPSC-directed differentiation. In this context, hPSCs and embryos can be viewed as complementary models that, when paired together, are a powerful platform of discovery and validation.

Our studies also identified significant species-specific differences between the human and fetal mouse lung. Differences included both gene/protein expression differences, as well as functional differences when comparing how cells responded to diverse signaling environments *in vitro.* For example, in mice, SOX9 is exclusively expressed in the bud tip progenitors and SOX2 is exclusively expressed in the proximal airway. In contrast, the bud tip progenitors in the human fetal lung robustly co-express SOX2 and SOX9 until around 16 weeks of gestation. Others have noted similar differences with regards to expression Hedgehog signaling machinery (M. Zhang et al., 2010). These mouse-human differences highlight the importance of validating observations made in hPSC-derived tissues by making direct comparisons with human tissues, as predictions or conclusions about human cell behavior based on results generated from the developing mouse lung may be misleading.

Significantly, our studies also suggest that hPSC derived lung epithelium may have therapeutic potential, especially for chronic and fatal diseases such as cystic fibrosis or bronchiolitis obliterans, which occurs following lung

transplantation. The present study has shown that lung bud tip progenitors derived from iPSCs are able to successfully engraft into the airway of an injured host mammalian lung, integrate into an existing epithelial layer, proliferate, differentiate into multiple cell types, and can respond to systemic circulating drugs and nutrients (Doxycycline, BrdU). While this result is promising, a significant amount of future work is needed to determine whether engrafted cells survive long-term in the host airway, whether they eventually reduce proliferation and avoid tumor formation, and how they interact with the host lung neuronal and vascular networks. In the future, an deepened mechanistic understanding of how a hPSC-derived lung bud tip progenitor gives rise to any one specific lung lineage may allow cell based therapies that rely less on progenitors, and more on specific cell populations.

Our experimental findings, in combination with previously published work, have also raised new questions that may point to interesting avenues for future mechanistic studies to determine how specific cell types of the lung are born. Previously, we have shown that lung organoids grown in high concentrations of FGF10 predominantly give rise to airway-like tissues, with a small number of alveolar cell types and a lack of alveolar structure (Dye et al., 2016b; 2015). Here, our results suggest that high concentrations of FGF10 alone do not play a major role in supporting robust growth of bud tip progenitor cells. When comparing our previously published work and our current work, we also note that lung organoids grown in high FGF10 possess abundant P63+ basal-like cells (Dye et al., 2015), whereas bud tip organoids grown in 3F media lack this population. Similarly, lung organoids grown in high FGF10 lacked secretory cells (Dye et al., 2015), whereas we find evidence for robust differentiation of club and goblet cells in patterned lung organoids grown in 3F media. This data suggests that FGF10 may have different functional roles in the human fetal lung or that there are still unappreciated roles for FGF7 and FGF10 during lung morphogenesis. These findings may also suggest that we still do not fully appreciate how these signaling pathways interact to control cell fate decisions. Additionally, one unique element of the currently described bud tip organoids is that they lack mesenchymal cells, yet they undergo complex epithelial budding and branching-like events, supporting previous *in vitro* results suggesting the mesenchyme is not essential for branching (Varner et al., 2015). The lack of mesenchyme also presents a powerful opportunity to explore questions related to the role of specific growth factors, cell types, mechanical forces, vascular or neuronal factors that may influence cell fate or lung development specifically in the epithelium. Collectively, these observations lay the groundwork for many future studies.

Taken together, our current work has identified that multiple signals are integrated into a network that is critical *in vitro* tissue growth, expansion and maintenance of mouse and human distal bud tip epithelial progenitors, and we have utilized this information to generate and expand*, de novo*, a population of lung bud tip-like progenitor cells from hPSCs. These conditions generated

patterned lung organoids that underwent complex epithelial budding and branching, in spite of a complete absence of mesenchyme. They contained mature secretory cells, and maintained a bud tip progenitor domain for over 115 days in culture. Regular needle passaging allowed us to expand a nearly homogenous population of proliferative bud tip-like progenitor cells for over 16 weeks in culture, which maintained a multipotent lineage capability *in vitro* and which were able to engraft into injured mouse lungs and respond to systemic factors. We believe the result of the current studies, as well as the predictive approach incorporating primary mouse and human tissue to inform differentiation of hPSCs will be a valuable tool to more carefully understand how specific elements of an environment control the differentiation of hPSCs.

Methods:

EXPERIMENTAL MODEL AND SUBJECT DETAILS

Mouse models:

All animal research was approved by the University of Michigan Committee on Use and Care of Animals. Lungs from Sox9-eGFP (MGI ID:3844824), Sox9CreER;Rosa$^{Tomato/Tomato}$ (MGI ID:5009223 and 3809523)(Kopp et al., 2011), or wild type lungs from CD1 embryos (Charles River) were dissected at embryonic day (E) 13.5, and buds were isolated as described below and as previously described (del Moral and Warburton, 2010). 8-10 week old Immunocompromised NSG *scid* mice (Jackson laboratories 0005557) were used for engraftment studies. Pilot studies identified that females had a more severe reaction and died at a higher rate from naphthalene injection, therefore male mice were used for engraftment experiments.

Human fetal lung tissue:

All research utilizing human fetal tissue was approved by the University of Michigan institutional review board. Normal human fetal lungs were obtained from the University of Washington Laboratory of Developmental Biology, and epithelial bud tips were dissected as described below. All tissues were shipped overnight in Belzer's solution at 4 degrees Celsius and were processed and cultured within 24 hours of obtaining the specimen. Experiments to evaluate the effect on progenitor maintenance in culture by media conditions were repeated using tissues from 3 individual lung specimens; (1) 84 day post fertilization of unknown gender, (2), 87 day post fertilization male, and (3), 87 day post fertilization of unknown gender. RNAseq experiments utilized tissue from 2 additional individual lungs; (4) 59 day male and (5) 87 day of unknown gender. Fetal progenitor organoids grown from sample (5) were injected into injured mouse lungs to assess engraftment.

Cell lines and culture conditions:

Mouse and human primary cultures:

Isolated mouse bud tips were cultured in 4-6 µl droplets of matrigel, covered with media, and kept at 37 degrees Celsius with 5% CO2. Isolated human fetal lung bud tips were cultured in 25-50 µl droplets of matrigel, covered with media, and kept at 37 degrees Celsius with 5% CO2. Cultures were fed every 2-4 days.

Generation and culture of hPSC-derived lung organoids:
The University of Michigan Human Pluripotent Stem Cell Research Oversight (hPSCRO) Committee approved all experiments using human embryonic stem cell (hESC) lines. Patterned lung organoids were generated from 4 independent pluripotent cell lines in this study: hESC line UM63-1 (NIH registry #0277) was obtained from the University of Michigan and hESC lines H9 and H1 (NIH registry #0062 and #0043, respectively) were obtained from the WiCell Research Institute. iPSC20.1 was previously described (Spence et al., 2011). ES cell lines were routinely karyotyped to ensure normal karyotype and ensure the sex of each line (H9 - XX, UM63-1 – XX, H1 - XY). All cell lines are routinely monitored for mycoplasma infection monthly using the MycoAlert Mycoplasma Detection Kit (Lonza). Stem cells were maintained on hESC-qualified Matrigel (Corning Cat# 354277) using mTesR1 medium (Stem Cell Technologies). hESCs were maintained and passaged as previously described (Spence et al., 2011) and ventral foregut spheroids were generated as previously described (Dye et al., 2016b; 2015). Following differentiation, free-floating foregut spheroids were collected from differentiated stem cell cultures and plated in a matrigel droplet on a 24-well tissue culture grade plate.

METHOD DETAILS

Isolation and culture of mouse lung epithelial buds

Mouse buds were dissected from E13.5 embryos. For experiments using Sox9CreER;Rosa$^{Tomato/Tomato}$ mice, 50 ug/g of tamoxifen was dissolved in corn oil and given by oral gavage on E12.5, 24 hours prior to dissection. Briefly, in a sterile environment, whole lungs were placed in 100% dispase (Corning Cat# 354235) on ice for 30 minutes. Lungs were then transferred using a 25uL wiretrol tool (Drummond Scientific Cat# 5-000-2050) to 100% FBS (Corning Cat#35-010-CV) on ice for 15 minutes, and then transferred to a solution of Dulbecco's Modified Eagle Medium: Nutrient Mixture F12 (DMEM/F12, ThermoFisher SKU# 12634-010) with 10% FBS and 1x Pennicillin-Streptomycin (ThermoFisher Cat# 15140122) on ice. To dissect buds, a single lung or lung lobe was transferred by wiretrol within a droplet of media to a 100mm sterile petri dish. Under a dissecting microscope, the mesenchyme was carefully removed and epithelial bud tips were torn away from the bronchial tree using tungsten needles (Point Technologies, Inc.). Care was taken to remove the trachea and any connective tissue from dissected lungs. Isolated bud tips were picked up using a p20 pipette and added to an eppendorf tube with cold Matrigel (Corning Ref# 354248) on ice. The buds were picked up in a p20 pipette with 4-6 uL of Matrigel and plated on a 24-well tissue culture well (ThermoFisher Cat# 142475). The plate was moved to a tissue culture incubator and incubated for 5 minutes at 37 degrees Celsius and

5% CO2 to allow the Matrigel droplet to solidify. 500uL of media was then added to the dish in a laminar flow hood. Media was changed every 2-3 days.

Isolation and culture of human fetal lung epithelial buds

Distal regions of 12 week fetal lungs were cut into ~2mm sections and incubated with dispase, 100% FBS and then 10% FBS as described above, and moved to a sterile petri dish. Mesenchyme was removed by repeated pipetting of distal lung pieces after dispase treatment. Buds were washed with DMEM until mesenchymal cells were no longer visible in the media. Buds were then moved to a 1.5 mL eppendorf tube containing 200uL of Matrigel, mixed using a p200 pipette, and plated in ~20uL droplets in a 24 well tissue culture plate. Plates were placed at 37 degrees Celsius with 5% CO2 for 20 minutes while droplets solidified. 500uL of media was added to each well containing a droplet. Media was changed every 2-4 days.

RNA-sequencing and Bioinformatic Analysis

RNA was isolated using the mirVana RNA isolation kit, following the "Total RNA" isolation protocol (Thermo-Fisher Scientific, Waltham MA). RNA sequencing library preparation and sequencing was carried out by the University of Michigan DNA Sequencing Core and Genomic Analysis Services (https://seqcore.brcf.med.umich.edu/). 50bp single end cDNA libraries were prepared using the Truseq RNA Sample Prep Kit v2 (Illumina), and samples were sequenced on an Illumina HiSeq 2500. Transcriptional quantitation analysis was conducted using 64-bit Debian Linux stable version 7.10 ("Wheezy"). Pseudoalignment of RNA-sequencing reads was computed using kallisto v0.43.0 and a normalized data matrix of pseudoaligned sequences (Transcripts Per Million, TPM) and differential expression was calculated using the R package DEseq2 (Bray et al., 2016; Love et al., 2014). Data analysis was performed using the R statistical programming language (http://www.R-project.org/) and was carried out as previously described (Dye et al., 2015; Finkbeiner et al., 2015; Tsai et al., 2016). The complete sequence alignment, expression analysis and all corresponding scripts can be found at https://github.com/hilldr/Miller_Lung_Organoids_2017 (in process). All raw data files generated by RNA-sequencing have been deposited to the EMBL-EBI ArrayExpress database (In process).

Naphthaline injury

Naphthaline (Sigma #147141) was dissolved in corn oil at a concentration of 40 mg/ml. NSG *scid* males (8-10 weeks of age) were given i.p. injections at a dose of 300 mg/kg weight.

Intratracheal injection of fetal progenitor organoids and hPSC-derived bud tip organoid cells into immunocompromised mouse lungs

Generating single cells from organoid tissues

2-3 matrigel droplets containing organoid tissues were removed from the culture plate and combined in a 1.5mL eppendorf tube with 1mL of room temperature Accutase (Sigma #A6964). The tube was laid on its side to prevent organoids from settling to the bottom. Tissue was pipetted up and down 15-20 times with a 1mL tip every 5 minutes for a total of 20 minutes. Single cell status was determined by hemocytometer. Cells were diluted to a concentration of 500,000-600,000 cells per 0.03 mL in sterile PBS.

Intratracheal injection of cells

Injection of cells into the mouse trachea was performed as previously described (Badri et al., 2011; Cao et al., 2017). Briefly, animals were anesthetized and intubated. Animals were given 500,000-600,000 single cells in 30-35 uL of sterile PBS through the intubation cannula.

Culture media, growth factors and small molecules

Serum-free basal media

All mouse bud, human fetal bud, and hPSC-derived human lung organoids were grown in serum-free basal media (basal media) with added growth factors. Basal media consisted of Dulbecco's Modified Eagle Medium: Nutrient Mixture F12 (DMEM/F12, ThermoFisher SKU# 12634-010) supplemented with 1X N2 supplement (ThermoFisher Catalog# 17502048) and 1X B27 supplement (ThermoFisher Catalog# 17504044), along with 2mM Glutamax (ThermoFisher Catalog# 35050061), 1x Pennicillin-Streptomycin (ThermoFisher Cat# 15140122) and 0.05% Bovine Serum Albumin (BSA; Sigma product# A9647). BSA was weighed and dissolved in DMEM F/12 media before being passed through a SteriFlip 0.22 uM filter (Millipore Item# EW-29969-24) and being added to basal media. Media was stored at 4 degrees Celsius for up to 1 month. On the day of use, basal media was aliquoted and 50ug/mL Ascorbic acid and 0.4 uM Monothioglycerol was added. Once ascorbic acid and monothioglycerol had been added, media was used within one week.

Growth factors and small molecules

Recombinant Human Fibroblast Growth Factor 7 (FGF7) was obtained from R&D systems (R&D #251-KG/CF) and used at a concentration of 10 ng/mL unless otherwise noted. Recombinant Human Fibroblast Growth Factor 10 (FGF10) was obtained either from R&D systems (R&D #345-FG) or generated in house (see below), and used at a concentration of 10 ng/mL (low) or 500 ng/mL (high) unless otherwise noted. Recombinant Human Bone Morphogenic Protein 4 (BMP4) was purchased from R&D systems (R&D Catalog # 314-BP) and used at a concentration of 10 ng/mL. All-trans Retinoic Acid (RA) was obtained from Stemgent (Stemgent Catalog# 04-0021) and used at a concentration of 50 nM. CHIR-99021, a GSK3β inhibitor that stabilizes β-CATENIN, was obtained from STEM CELL technologies (STEM CELL Technologies Catalog# 72054) and used at a concentration of 3 uM. Y27632, a ROCK inhibitor (APExBIO Cat# A3008) was used at a concentration of 10uM.

Generation and Isolation of human recombinant FGF10

Recombinant human FGF10 was produced in-house. The recombinant human FGF10 (rhFGF10) expression plasmid pET21d-FGF10 in *E. coli* strain BL21*trxB*(DE3) was a gift from James A. Bassuk at the University of Washington School of Medicine(Bagai et al., 2002). *E. coli* strain was grown in standard LB media with peptone derived from meat, carbenicillin and glucose. rhFGF10 expression was induced by addition of isopropyl-1-thio-β-D-galactopyranoside (IPTG). rhFGF10 was purified by using a HiTrap-Heparin HP column (GE Healthcare, 17040601) with step gradients of 0.5M to 2M LiCl. From a 200 ml culture, 3 mg of at least 98% pure rFGF-10 (evaluated by SDS-PAGE stained with Coomassie Blue R-250) was purified. rFGF10 was compared to commercially purchased human FGF10 (R&D Systems) to test/validate activity based on the ability to phosphorylate ERK1/2 in an A549 alveolar epithelial cell line (ATCC Cat#CCL-185) as assessed by western blot analysis.

RNA extraction and quantitative RT-PCR analysis

RNA was extracted using the MagMAX-96 Total RNA Isolation System (Life Technologies). RNA quality and concentration was determined on a Nanodrop 2000 spectrophotometer (Thermo Scientific). 100 ng of RNA was used to generate a cDNA library using the SuperScript VILO cDNA master mix kit (Invitrogen) according to manufacturer's instructions. qRT-PCR analysis was conducted using Quantitect SYBR Green Master Mix (Qiagen) on a Step One Plus Real-Time PCR system (Life Technologies). Expression was calculated as a change relative to GAPDH expression using arbitrary units, which were calculated by the following equation: [2^(GAPDH Ct - Gene Ct)] x 10,000. A Ct value of 40 or greater was considered not detectable. A list of primer sequences used can be found in Table 1.

Tissue preparation, Immunohistochemistry and imaging

Paraffin sectioning and staining

Mouse bud, human bud, and HLO tissue was fixed in 4% Paraformaldehyde (Sigma) for 2 hours and rinsed in PBS overnight. Tissue was dehydrated in an alcohol series, with 30 minutes each in 25%, 50%, 75% Methanol:PBS/0.05% Tween-20, followed by 100% Methanol, and then 100% Ethanol. Tissue was processed into paraffin using an automated tissue processor (Leica ASP300). Paraffin blocks were sectioned 5-7 uM thick, and immunohistochemical staining was performed as previously described (Spence et al., 2009). A list of antibodies, antibody information and concentrations used can be found in Table 2. PAS Alcian blue staining was performed using the Newcomer supply Alcian Blue/PAS Stain kit (Newcomer Supply, Inc.) according to manufacturer's instructions.

Whole mount staining

For whole mount staining tissue was placed in a 1.5mL eppendorf tube and fixed in 4% paraformaldehyde (Sigma) for 30 minutes. Tissue was then washed with PBS/0.05% Tween-20 (Sigma) for 5 hours, followed by a 2.5-hour incubation with

blocking serum (PBS-Tween-20 plus 5% normal donkey serum). Primary antibodies were added to blocking serum and tissue was incubated for at least 24 hours at 4 degrees Celcius. Tissue was then washed for 5 hours with several changes of fresh PBS-Tween-20. Secondary antibodies were added to fresh blocking solution and tissue was incubated for 12-24 hours, followed by 5 hours of PBS-Tween-20 washes. Tissue was then dehydrated to 100% methanol and carefully moved to the center of a single-well EISCO concave microscope slide (ThermoFisher Cat# S99368) using a glass transfer pipette. 5-7 drops of Murray's clear (2 parts Benzyl alcohol, 1 part Benzyl benzoate [Sigma]) were added to the center of the slide, and slides were coverslipped and sealed with clear nail polish.

In situ hybridization

In situ hybridization for ID2 was performed using the RNAscope 2.5 HD manual assay with brown chromogenic detection (Advanced Cell Diagnostics, Inc.) according to manufacturers instructions. The human 20 base pair ID2 probe was generated by Advanced Cell Diagnostics targeting 121-1301 of ID2 (gene accession NM_002166.4) and is commercially available.

Imaging and image processing

Images of fluorescently stained slides were taken on a Nikon A-1 confocal microscope. When comparing groups within a single experiment, exposure times and laser power were kept consistent across all images. All Z-stack imaging was done on a Nikon A-1 confocal microscope and Z-stacks were 3-D rendered using Imaris software. Brightness and contrast adjustments were carried out using Adobe Photoshop Creative Suite 6 and adjustments were made uniformly among all images.

Brightfield images of live cultures were taken using an Olympus S2X16 dissecting microscope. Image brightness and contrast was enhanced equally for all images within a single experiment using Adobe Photoshop. Images were cropped where noted in figure legends to remove blank space surrounding buds or cultures. Brightfield images of Alcian Blue stains were taken using an Olympus DP72 inverted microscope.

Quantification and Statistical Analysis

All plots and statistical analysis were done using Prism 6 Software (GraphPad Software, Inc.). For statistical analysis of qRT-PCR results, at least 3 biological replicates for each experimental group were analyzed and plotted with the standard error of the mean. If only two groups were being compared, a two-sided student’s T-test was performed. In assessing the effect of length of culture with FGF7 on gene expression in mouse buds (Figure 1 – Figure Supplement 1G), a one-way, unpaired Analysis of Variance (ANOVA) was performed for each individual gene over time. The mean of each time point was compared to the mean of the expression level for that gene at day 0 of culture. If more than two

groups were being compared within a single experiment, an unpaired one-way analysis of variance was performed followed by Tukey's multiple comparison test to compare the mean of each group to the mean of every other group within the experiment. For all statistical tests, a significance value of 0.05 was used. For every analysis, the strength of p values is reported in the figures according the following: $P > 0.05$ ns, $P \leq 0.05$ *, $P \leq 0.01$ **, $P \leq 0.001$ ***, $P \leq 0.0001$ ****. Details of statistical tests can be found in the figure legends.

Acknowledgements:
JRS is supported by the NIH-NHLBI (R01 HL119215). AJM is supported by the NIH Cellular and Molecular Biology training grant at Michigan (T32 GM007315), and by the Tissue Engineering and Regeneration Training Grant (DE00007057-40). The University of Washington Laboratory of Developmental Biology was supported by NIH Award Number 5R24HD000836 from the Eunice Kennedy Shriver National Institute of Child Health & Human Development.

KEY RESOURCES TABLES

TABLE 1: qRT-PCR primer sequences

Species	Gene Target	Forward Primer Sequence	Reverse Primer Sequence
Mouse	*Aqp5*	TAGAAGATGGCTCGGAGCAG	CTGGGACCTGTGAGTGGTG
Mouse	*Foxj1*	TGTTCAAGGACAGGTTGTGG	GATCACTCTGTCGGCCATCT
Mouse	*Gapdh*	TGTCAGCAATGCATCCTGCA	CCGTTCAGCTCTGGGATGAC
Mouse	*Id2*	AGAAAAGAAAAAGTCCCCAAATG	GTCCTTGCAGGCATCTGAAT
Mouse	*Nmyc*	AGCACCTCCGGAGAGGATA	TCTCTACGGTGACCACATCG
Mouse	*P63*	AGCTTCTTCAGTTCGGTGGA	CCTCCAACACAGATTACCCG
Mouse	*Scgb1a1*	ACTTGAAGAAATCCTGGGCA	CAAAGCCTCCAACCTCTACC
Mouse	*Sftpb*	ACAGCCAGCACACCCTTG	TTCTCTGAGCAACAGCTCCC
Mouse	*Sox2*	AAAGCGTTAATTTGGATGGG	ACAAGAGAATTGGGAGGGGT
Mouse	*Sox9*	TCCACGAAGGGTCTCTTCTC	AGGAAGCTGGCAGACCAGTA
Human	*FOXJ1*	CAACTTCTGCTACTTCCGCC	CGAGGCACTTTGATGAAGC
Human	*GAPDH*	AATGAAGGGGTCATTGATGG	AAGGTGAAGGTCGGAGTCAA
Human	*HOPX*	GCCTTTCCGAGGAGGAGAC	TCTGTGACGGATCTGCACTC
Human	*ID2*	GACAGCAAAGCACTGTGTGG	TCAGCACTTAAAAGATTCCGTG
Human	*MUC5AC**	GCACCAACGACAGGAAGGATGAG	CACGTTCCAGAGCCGGACAT
Human	*NKX2.1*	CTCATGTTCATGCCGCTC	GACACCATGAGGAACAGCG
Human	*NMYC*	CACAGTGACCACGTCGATTT	CACAAGGCCCTCAGTACCTC
Human	*P63*	CCACAGTACACGAACCTGGG	CCGTTCTGAATCTGCTGGTCC
Human	*SCGB1A1*	ATGAAACTCGCTGTCACCCT	GTTTCGATGACACGCTGAAA
Human	*SFTPB*	CAGCACTTTAAAGGACGGTGT	GGGTGTGTGGGACCATGT
Human	*SOX2*	GCTTAGCCTCGTCGATGAAC	AACCCCAAGATGCACAACTC
Human	*SOX9*	GTACCCGCACTTGCACAAC	ATTCCACTTTGCGTTCAAGG
Human	*SFTPC*	AGCAAAGAGGTCCTGATGGA	CGATAAGAAGGCGTTTCAGG

Note: All primer sequences were obtained from http://primerdepot.nci.nih.gov (human) or http://mouseprimerdepot.nci.nih.gov (mouse) unless otherwise noted. All annealing temperatures are near 60°C.

*MUC5AC Huang, SX et al. Efficient generation of lung and airway epithelial cells from human pluripotent stem cells. Nature Biotechnol. 1–11 (2013). doi:10.1038/nbt.2754

Table 2: Antibody information

Primary Antibody	Source	Catalog #	Used for Species	Dilution (Sections)	Dilution (Whole mount)	Clone
Goat anti-CC10 (SCGB1A1)	Santa Cruz Biotechnology	sc-9770	Mouse, Human	1:200		C-20
Goat anti-Chromogranin A (CHGA)	Santa Cruz Biotechnology	sc-1488	Human	1:100		C-20
Goat anti-SOX2	Santa Cruz Biotechnology	Sc-17320	Mouse, Human	1:200	1:100	polyclonal
Mouse anti-ABCA3	Seven Hills Bioreagents	WMAB-17G524	Human	1:500		17-H5-24
Mouse anti-Acetylated Tubulin (ACTTUB)	Sigma-Aldrich	T7451	Mouse, Human	1:1000		6-11B-1
Mouse anti-E-Cadherin (ECAD)	BD Transduction Laboratories	610181	Mouse, Human	1:500		36/E-Cadherin
Mouse anti- human mitochondria	Millipore	MAB1273	Human	1:500		113-1
Mouse anti-human nuclear	Thermofisher	PA5-22285	Human	1:500		polyclonal

matrix protein-22 (NuMA)						
Mouse anti-Surfactant Protein B (SFTPB)	Seven Hills Bioreagents	Wmab-1B9	Mouse, Human	1:250		monoclonal
Rabbit anti-Aquaporin 5 (Aqp5)	Abcam	Ab78486	Mouse	1:500		polyclonal
Rabbit anti-Clara Cell Secretory Protein (CCSP; SCGB1A1)	Seven Hills Bioreagents	Wrab-3950	Mouse, Human	1:250		polyclonal
Rabbit anti-HOPX	Santa Cruz Biotechnology	Sc-30216	Human	1:250		polyclonal
Rabbit anti-NKX2.1	Abcam	ab76013	Human	1:200		EP1584Y
Rabbit anti-PDPN	Santa Cruz Biotechnology	Sc-134482	Human	1:500		polyclonal
Rabbit anti-Pro-Surfactant protein C (Pro-SFTPC)	Seven Hills Bioreagents	Wrab-9337	Human, Mouse	1:500		polyclonal
Rabbit anti-P63	Santa Cruz Biotechnology	sc-8344	Mouse, Human	1:200		H-129
Rabbit anti-SOX9	Millipore	AB5535	Mouse, Human	1:500	1:250	polyclonal
Rat anti-KI67	Biolegend	652402	Mouse	1:100		16A8
*Biotin-Mouse anti MUC5AC	Abcam	ab79082	Human	1:500		Monoclonal
Secondary Antibody	**Source**	**Catalog #**		**Dilution**		
Donkey anti-goat 488	Jackson Immuno	705-545-147		1:500		
Donkey anti-goat 647	Jackson Immuno	705-605-147		1:500		
Donkey anti-goat Cy3	Jackson Immuno	705-165-147		1:500		
Donkey anti-mouse 488	Jackson Immuno	715-545-150		1:500		
Donkey anti-mouse 647	Jackson Immuno	415-605-350		1:500		
Donkey anti-mouse Cy3	Jackson Immuno	715-165-150		1:500		
Donkey anti-rabbit 488	Jackson Immuno	711-545-152		1:500		
Donkey anti-rabbit 647	Jackson Immuno	711-605-152		1:500		
Donkey anti-rabbit Cy3	Jackson Immuno	711-165-102		1:500		
Donkey anti-goat 488	Jackson Immuno	705-545-147		1:500		
Donkey anti-goat 647	Jackson Immuno	705-605-147		1:500		
Donkey anti-goat Cy3	Jackson Immuno	705-165-147		1:500		
Donkey anti-mouse 488	Jackson Immuno	715-545-150		1:500		
Donkey anti-mouse 647	Jackson Immuno	415-605-350		1:500		
Donkey anti-mouse Cy3	Jackson Immuno	715-165-150		1:500		
Donkey anti-rabbit 488	Jackson Immuno	711-545-152		1:500		
Donkey anti-rabbit 647	Jackson Immuno	711-605-152		1:500		
Donkey anti-rabbit Cy3	Jackson Immuno	711-165-102		1:500		
Streptavidin 488	Jackson Immuno	016-540-084		1:500		

References:

Abler, L.L., Mansour, S.L., Sun, X., 2009. Conditional gene inactivation reveals roles for Fgf10 and Fgfr2 in establishing a normal pattern of epithelial branching in the mouse lung. Dev. Dyn. 238, 1999–2013. doi:10.1002/dvdy.22032

Badri, L., Walker, N.M., Ohtsuka, T., Wang, Z., Delmar, M., Flint, A., Peters-Golden, M., Toews, G.B., Pinsky, D.J., Krebsbach, P.H., Lama, V.N., 2011. Epithelial Interactions and Local Engraftment of Lung-Resident Mesenchymal Stem Cells. American Journal of Respiratory Cell and Molecular Biology 45, 809–816. doi:10.1165/rcmb.2010-0446OC

Bagai, S., Rubio, E., Cheng, J.-F., Sweet, R., Thomas, R., Fuchs, E., Grady, R., Mitchell, M., Bassuk, J.A., 2002. Fibroblast growth factor-10 is a mitogen for urothelial cells. J. Biol. Chem. 277, 23828–23837. doi:10.1074/jbc.M201658200

Bellusci, S., Furuta, Y., Rush, M.G., Henderson, R., Winnier, G., Hogan, B.L., 1997a. Involvement of Sonic hedgehog (Shh) in mouse embryonic lung growth and morphogenesis. Development 124, 53–63.

Bellusci, S., Grindley, J., Emoto, H., Itoh, N., Hogan, B.L., 1997b. Fibroblast growth factor 10 (FGF10) and branching morphogenesis in the embryonic mouse lung. Development 124, 4867–4878.

Bellusci, S., Henderson, R., Winnier, G., Oikawa, T., Hogan, B.L., 1996. Evidence from normal expression and targeted misexpression that bone morphogenetic protein (Bmp-4) plays a role in mouse embryonic lung morphogenesis. Development 122, 1693–1702.

Branchfield, K., Li, R., Lungova, V., Verheyden, J.M., McCulley, D., Sun, X., 2015. A three-dimensional study of alveologenesis in mouse lung. Developmental Biology. doi:10.1016/j.ydbio.2015.11.017

Bray, N.L., Pimentel, H., Melsted, P., Pachter, L., 2016. Near-optimal probabilistic RNA-seq quantification. Nat Biotechnol 34, 525–527. doi:10.1038/nbt.3519

Cao, P., Aoki, Y., Badri, L., Walker, N.M., Manning, C.M., Lagstein, A., Fearon, E.R., Lama, V.N., 2017. Autocrine lysophosphatidic acid signaling activates β-catenin and promotes lung allograft fibrosis. Journal of Clinical Investigation 127, 1517–1530. doi:10.1172/JCI88896

Cardoso, W.V., Itoh, A., Nogawa, H., Mason, I., Brody, J.S., 1997. FGF-1 and FGF-7 induce distinct patterns of growth and differentiation in embryonic lung epithelium. Dev. Dyn. 208, 398–405. doi:10.1002/(SICI)1097-0177(199703)208:3<398::AID-AJA10>3.0.CO;2-X

Chang, D.R., Martinez Alanis, D., Miller, R.K., Ji, H., Akiyama, H., McCrea, P.D., Chen, J., 2013. Lung epithelial branching program antagonizes alveolar differentiation. Proceedings of the National Academy of Sciences. doi:10.1073/pnas.1311760110

Chen, Y.-J., Finkbeiner, S.R., Weinblatt, D., Emmett, M.J., Tameire, F., Yousefi, M., Yang, C., Maehr, R., Zhou, Q., Shemer, R., Dor, Y., Li, C., Spence, J.R., Ben Z Stanger, 2014. De Novo Formationof Insulin-Producing "'Neo-b Cell

Islets'" from Intestinal Crypts. Cell Rep 1–13. doi:10.1016/j.celrep.2014.02.013

Chen, Y.-W., Huang, S.X., de Carvalho, A.L.R.T., Ho, S.-H., Islam, M.N., Volpi, S., Notarangelo, L.D., Ciancanelli, M., Casanova, J.-L., Bhattacharya, J., Liang, A.F., Palermo, L.M., Porotto, M., Moscona, A., Snoeck, H.-W., 2017. A three-dimensional model of human lung development and disease from pluripotent stem cells. Nat. Cell Biol. 19, 542–549. doi:10.1038/ncb3510

Cornett, B., Snowball, J., Varisco, B.M., Lang, R., Whitsett, J., Sinner, D., 2013. Wntless is required for peripheral lung differentiation and pulmonary vascular development. Developmental Biology 379, 38–52. doi:10.1016/j.ydbio.2013.03.010

D'Amour, K.A., Agulnick, A.D., Eliazer, S., Kelly, O.G., Kroon, E., Baetge, E.E., 2005. Efficient differentiation of human embryonic stem cells to definitive endoderm. Nat Biotechnol 23, 1534–1541. doi:10.1038/nbt1163

del Moral, P.-M., Warburton, D., 2010. Explant culture of mouse embryonic whole lung, isolated epithelium, or mesenchyme under chemically defined conditions as a system to evaluate the molecular mechanism of branching morphogenesis and cellular differentiation. Methods Mol. Biol. 633, 71–79. doi:10.1007/978-1-59745-019-5_5

Desai, T.J., Chen, F., Lü, J., Qian, J., Niederreither, K., Dollé, P., Chambon, P., Cardoso, W.V., 2006. Distinct roles for retinoic acid receptors alpha and beta in early lung morphogenesis. Developmental Biology 291, 12–24. doi:10.1016/j.ydbio.2005.10.045

Desai, T.J., Malpel, S., Flentke, G.R., Smith, S.M., Cardoso, W.V., 2004. Retinoic acid selectively regulates Fgf10 expression and maintains cell identity in the prospective lung field of the developing foregut. Developmental Biology 273, 402–415. doi:10.1016/j.ydbio.2004.04.039

Domyan, E.T., Ferretti, E., Throckmorton, K., Mishina, Y., Nicolis, S.K., Sun, X., 2011. Signaling through BMP receptors promotes respiratory identity in the foregut via repression of Sox2. Development 138, 971–981. doi:10.1242/dev.053694

Domyan, E.T., Sun, X., 2010. Patterning and plasticity in development of the respiratory lineage. Dev. Dyn. 240, 477–485. doi:10.1002/dvdy.22504

Dye, B.R., Dedhia, P.H., Miller, A.J., Nagy, M.S., White, E.S., Shea, L.D., Spence, J.R., 2016a. A bioengineered niche promotes in vivo engraftment and maturation of pluripotent stem cell derived human lung organoids. Elife 5, e19732. doi:10.7554/eLife.19732

Dye, B.R., Dedhia, P.H., Miller, A.J., Nagy, M.S., White, E.S., Shea, L.D., Spence, J.R., Rossant, J., 2016b. A bioengineered niche promotes in vivo engraftment and maturation of pluripotent stem cell derived human lung organoids. Elife 5, e19732. doi:10.7554/eLife.19732

Dye, B.R., Hill, D.R., Ferguson, M.A., Tsai, Y.-H., Nagy, M.S., Dyal, R., Wells, J.M., Mayhew, C.N., Nattiv, R., Klein, O.D., White, E.S., Deutsch, G.H., Spence, J.R., 2015. In vitro generation of human pluripotent stem cell derived lung organoids. Elife 4. doi:10.7554/eLife.05098

Dye, B.R., Miller, A.J., Spence, J.R., 2016c. How to Grow a Lung: Applying

Principles of Developmental Biology to Generate Lung Lineages from Human Pluripotent Stem Cells. Curr Pathobiol Rep 4, 1–11. doi:10.1007/s40139-016-0102-x

Finkbeiner, S.R., Hill, D.R., Altheim, C.H., Dedhia, P.H., Taylor, M.J., Tsai, Y.-H., Chin, A.M., Mahe, M.M., Watson, C.L., Freeman, J.J., Nattiv, R., Thomson, M., Klein, O.D., Shroyer, N.F., Helmrath, M.A., Teitelbaum, D.H., Dempsey, P.J., Spence, J.R., 2015. Transcriptome-wide Analysis Reveals Hallmarks of Human Intestine Development and Maturation In Vitro and In Vivo. Stem Cell Reports 4, 1140–1155. doi:10.1016/j.stemcr.2015.04.010

Firth, A.L., Dargitz, C.T., Qualls, S.J., Menon, T., Wright, R., Singer, O., Gage, F.H., Khanna, A., Verma, I.M., 2014. Generation of multiciliated cells in functional airway epithelia from human induced pluripotent stem cells. Proceedings of the National Academy of Sciences 111, E1723–30. doi:10.1073/pnas.1403470111

Ghaedi, M., Calle, E.A., Mendez, J.J., Gard, A.L., Balestrini, J., Booth, A., Bove, P.F., Gui, L., White, E.S., Niklason, L.E., 2013. Human iPS cell-derived alveolar epithelium repopulates lung extracellular matrix. J. Clin. Invest. 123, 4950–4962. doi:10.1172/JCI68793

Gilpin, S.E., Ren, X., Okamoto, T., Guyette, J.P., Mou, H., Rajagopal, J., Mathisen, D.J., Vacanti, J.P., Ott, H.C., 2014. Enhanced lung epithelial specification of human induced pluripotent stem cells on decellularized lung matrix. Ann. Thorac. Surg. 98, 1721–9– discussion 1729. doi:10.1016/j.athoracsur.2014.05.080

Goss, A.M., Tian, Y., Tsukiyama, T., Cohen, E.D., Zhou, D., Lu, M.M., Yamaguchi, T.P., Morrisey, E.E., 2009. Wnt2/2b and β-Catenin Signaling Are Necessary and Sufficient to Specify Lung Progenitors in the Foregut. Developmental Cell 17, 290–298. doi:10.1016/j.devcel.2009.06.005

Gotoh, S., Ito, I., Nagasaki, T., Yamamoto, Y., Konishi, S., Korogi, Y., Matsumoto, H., Muro, S., Hirai, T., Funato, M., Mae, S.-I., Toyoda, T., Sato-Otsubo, A., Ogawa, S., Osafune, K., Mishima, M., 2014. Generation of alveolar epithelial spheroids via isolated progenitor cells from human pluripotent stem cells. Stem Cell Reports 3, 394–403. doi:10.1016/j.stemcr.2014.07.005

Green, M.D., Chen, A., Nostro, M.-C., d'Souza, S.L., Schaniel, C., Lemischka, I.R., Gouon-Evans, V., Keller, G., Snoeck, H.-W., 2011. Generation of anterior foregut endoderm from human embryonic and induced pluripotent stem cells. Nat Biotechnol 1–7. doi:10.1038/nbt.1788

Harris-Johnson, K.S., Domyan, E.T., Vezina, C.M., Sun, X., 2009. beta-Catenin promotes respiratory progenitor identity in mouse foregut. Proceedings of the National Academy of Sciences 106, 16287–16292. doi:10.1073/pnas.0902274106

Hashimoto, S., Chen, H., Que, J., Brockway, B.L., Drake, J.A., Snyder, J.C., Randell, S.H., Stripp, B.R., 2012. β-Catenin-SOX2 signaling regulates the fate of developing airway epithelium. Journal of Cell Science 125, 932–942. doi:10.1242/jcs.092734

Herriges, J.C., Verheyden, J.M., Zhang, Z., Sui, P., Zhang, Y., Anderson, M.J.,

Swing, D.A., Zhang, Y., Lewandoski, M., Sun, X., 2015. FGF-Regulated ETV Transcription Factors Control FGF-SHH Feedback Loop in Lung Branching. Developmental Cell 35, 322–332. doi:10.1016/j.devcel.2015.10.006

Hines, E.A., Sun, X., 2014. Tissue crosstalk in lung development. J Cell Biochem 115, 1469–1477. doi:10.1002/jcb.24811

Huang, S.X.L., Islam, M.N., O'Neill, J., Hu, Z., Yang, Y.-G., Chen, Y.-W., Mumau, M., Green, M.D., Vunjak-Novakovic, G., Bhattacharya, J., Snoeck, H.-W., 2013. efficient generation of lung and airway epithelial cells from human pluripotent stem cells. Nat Biotechnol 1–11. doi:10.1038/nbt.2754

Karagiannis, T.C., Li, X., Tang, M.M., Orlowski, C., El-Osta, A., Tang, M.L., Royce, S.G., 2012. Molecular model of naphthalene-induced DNA damage in the murine lung. Human & Experimental Toxicology 31, 42–50. doi:10.1177/0960327111407228

Kim, H.Y., Nelson, C.M., 2012. Extracellular matrix and cytoskeletal dynamics during branching morphogenesis. Organogenesis 8, 56–64. doi:10.4161/org.19813

Konishi, S., Gotoh, S., Tateishi, K., Yamamoto, Y., Korogi, Y., Nagasaki, T., Matsumoto, H., Muro, S., Hirai, T., Ito, I., Tsukita, S., Mishima, M., 2015. Directed Induction of Functional Multi-ciliated Cells in Proximal Airway Epithelial Spheroids from Human Pluripotent Stem Cells. Stem Cell Reports 0. doi:10.1016/j.stemcr.2015.11.010

Kopp, J.L., Dubois, C.L., Schaffer, A.E., Hao, E., Shih, H.P., Seymour, P.A., Ma, J., Sander, M., 2011. Sox9+ ductal cells are multipotent progenitors throughout development but do not produce new endocrine cells in the normal or injured adult pancreas. Development 138, 653–665. doi:10.1242/dev.056499

Lange, A.W., Sridharan, A., Xu, Y., Stripp, B.R., Perl, A.-K., Whitsett, J.A., 2015. Hippo/Yap signaling controls epithelial progenitor cell proliferation and differentiation in the embryonic and adult lung. Journal of Molecular Cell Biology 7, 35–47. doi:10.1093/jmcb/mju046

Longmire, T.A., Ikonomou, L., Hawkins, F., Christodoulou, C., Cao, Y., Jean, J.C., Kwok, L.W., Mou, H., Rajagopal, J., Shen, S.S., Dowton, A.A., Serra, M., Weiss, D.J., Green, M.D., Snoeck, H.-W., Ramirez, M.I., Kotton, D.N., 2012. Efficient derivation of purified lung and thyroid progenitors from embryonic stem cells. Cell Stem Cell 10, 398–411. doi:10.1016/j.stem.2012.01.019

Love, M.I., Huber, W., Anders, S., 2014. Moderated estimation of fold change and dispersion for RNA-seq data with DESeq2. Genome Biol. 15, 31–21. doi:10.1186/s13059-014-0550-8

Lu, B.C., Cebrian, C., Chi, X., Kuure, S., Kuo, R., Bates, C.M., Arber, S., Hassell, J., MacNeil, L., Hoshi, M., Jain, S., Asai, N., Takahashi, M., Schmidt-Ott, K.M., Barasch, J., D'Agati, V., Costantini, F., 2009. Etv4 and Etv5 are required downstream of GDNF and Ret for kidney branching morphogenesis. Nat Genet 41, 1295–1302. doi:10.1038/ng.476

Mahoney, J.E., Mori, M., Szymaniak, A.D., Varelas, X., Cardoso, W.V., 2014. The Hippo Pathway Effector Yap Controls Patterning and Differentiation of

Airway Epithelial Progenitors. Dev. Cell 1–14. doi:10.1016/j.devcel.2014.06.003

McCauley, K.B., Hawkins, F., Serra, M., Thomas, D.C., Jacob, A., Kotton, D.N., 2017. Efficient Derivation of Functional Human Airway Epithelium from Pluripotent Stem Cells via Temporal Regulation of Wnt Signaling. Cell Stem Cell. doi:10.1016/j.stem.2017.03.001

Metzger, R.J., Klein, O.D., Martin, G.R., Krasnow, M.A., 2008. The branching programme of mouse lung development. Nature 453, 745–750. doi:10.1038/nature07005

Miller, A.J., Spence, J.R., 2017. In Vitro Models to Study Human Lung Development, Disease and Homeostasis. Physiology (Bethesda) 32, 246–260. doi:10.1152/physiol.00041.2016

Min, H., Danilenko, D.M., Scully, S.A., Bolon, B., Ring, B.D., Tarpley, J.E., DeRose, M., Simonet, W.S., 1998. Fgf-10 is required for both limb and lung development and exhibits striking functional similarity to Drosophila branchless. Genes & Development 12, 3156–3161.

Moens, C.B., Auerbach, A.B., Conlon, R.A., Joyner, A.L., Rossant, J., 1992. A targeted mutation reveals a role for N-myc in branching morphogenesis in the embryonic mouse lung. Genes Dev. 6, 691–704. doi:10.1101/gad.6.5.691

Morrisey, E.E., Cardoso, W.V., Lane, R.H., Rabinovitch, M., Abman, S.H., Ai, X., Albertine, K.H., Bland, R.D., Chapman, H.A., Checkley, W., Epstein, J.A., Kintner, C.R., Kumar, M., Minoo, P., Mariani, T.J., McDonald, D.M., Mukouyama, Y.-S., Prince, L.S., Reese, J., Rossant, J., Shi, W., Sun, X., Werb, Z., Whitsett, J.A., Gail, D., Blaisdell, C.J., Lin, Q.S., 2013. Molecular determinants of lung development. Ann Am Thorac Soc 10, S12–6. doi:10.1513/AnnalsATS.201207-036OT

Morrisey, E.E., Hogan, B.L.M., 2010. Preparing for the First Breath: Genetic and Cellular Mechanisms in Lung Development. Developmental Cell 18, 8–23. doi:10.1016/j.devcel.2009.12.010

Motoyama, J., Liu, J., Mo, R., Ding, Q., Post, M., Hui, C.C., 1998. Essential function of Gli2 and Gli3 in the formation of lung, trachea and oesophagus. Nat Genet 20, 54–57. doi:10.1038/1711

Nikolić, M.Z., Caritg, O., Jeng, Q., Johnson, J.-A., Sun, D., Howell, K.J., Brady, J.L., Laresgoiti, U., Allen, G., Butler, R., Zilbauer, M., Giangreco, A., Rawlins, E.L., 2017. Human embryonic lung epithelial tips are multipotent progenitors that can be expanded in vitro as long-term self-renewing organoids. Elife 6, e26575. doi:10.7554/eLife.26575

Nyeng, P., Norgaard, G.A., Kobberup, S., Jensen, J., 2008. FGF10 maintains distal lung bud epithelium and excessive signaling leads to progenitor state arrest, distalization, and goblet cell metaplasia. BMC Dev Biol 8, 2. doi:10.1186/1471-213X-8-2

Okubo, T., Knoepfler, P.S., Eisenman, R.N., Hogan, B.L.M., 2005. Nmyc plays an essential role during lung development as a dosage-sensitive regulator of progenitor cell proliferation and differentiation. Development 132, 1363–1374. doi:10.1242/dev.01678

Ornitz, D.M., Yin, Y., 2012. Signaling Networks Regulating Development of the

Lower Respiratory Tract. Cold Spring Harb Perspect Biol 4, a008318–a008318. doi:10.1101/cshperspect.a008318

Perl, A.-K.T., Kist, R., Shan, Z., Scherer, G., Whitsett, J.A., 2005. Normal lung development and function after Sox9 inactivation in the respiratory epithelium. genesis 41, 23–32. doi:10.1002/gene.20093

Que, J., Okubo, T., Goldenring, J.R., Nam, K.T., Kurotani, R., Morrisey, E.E., Taranova, O., Pevny, L.H., Hogan, B.L.M., 2007. Multiple dose-dependent roles for Sox2 in the patterning and differentiation of anterior foregut endoderm. Development 134, 2521–2531. doi:10.1242/dev.003855

Rawlins, E.L., 2010. The building blocks of mammalian lung development. Dev. Dyn. 240, 463–476. doi:10.1002/dvdy.22482

Rawlins, E.L., Clark, C.P., Xue, Y., Hogan, B.L.M., 2009. The Id2+ distal tip lung epithelium contains individual multipotent embryonic progenitor cells. Development 136, 3741–3745. doi:10.1242/dev.037317

Rock, J.R., Hogan, B.L.M., 2011. Epithelial Progenitor Cells in Lung Development, Maintenance, Repair, and Disease. Annu. Rev. Cell Dev. Biol. 27, 493–512. doi:10.1146/annurev-cellbio-100109-104040

Rockich, B.E., Hrycaj, S.M., Shih, H.-P., Nagy, M.S., Ferguson, M.A.H., Kopp, J.L., Sander, M., Wellik, D.M., Spence, J.R., 2013. Sox9 plays multiple roles in the lung epithelium during branching morphogenesis. Proceedings of the National Academy of Sciences. doi:10.1073/pnas.1311847110

Sekine, K., Ohuchi, H., Fujiwara, M., Yamasaki, M., Yoshizawa, T., Sato, T., Yagishita, N., Matsui, D., Koga, Y., Itoh, N., Kato, S., 1999. Fgf10 is essential for limb and lung formation. Nat Genet 21, 138–141. doi:10.1038/5096

Shu, W., Guttentag, S., Wang, Z., Andl, T., Ballard, P., Lu, M.M., Piccolo, S., Birchmeier, W., Whitsett, J.A., Millar, S.E., Morrisey, E.E., 2005. Wnt/beta-catenin signaling acts upstream of N-myc, BMP4, and FGF signaling to regulate proximal-distal patterning in the lung. Dev Biol 283, 226–239.

Spence, J.R., Lange, A.W., Lin, S.-C.J., Kaestner, K.H., Lowy, A.M., Kim, I., Whitsett, J.A., Wells, J.M., 2009. Sox17 Regulates Organ Lineage Segregation of Ventral Foregut Progenitor Cells. Developmental Cell 17, 62–74. doi:10.1016/j.devcel.2009.05.012

Spence, J.R., Mayhew, C.N., Rankin, S.A., Kuhar, M.F., Vallance, J.E., Tolle, K., Hoskins, E.E., Kalinichenko, V.V., Wells, S.I., Zorn, A.M., Shroyer, N.F., Wells, J.M., 2011. Directed differentiation of human pluripotent stem cells into intestinal tissue in vitro. Nature 470, 105–109. doi:10.1038/nature09691

Treutlein, B., Brownfield, D.G., Wu, A.R., Neff, N.F., Mantalas, G.L., Espinoza, F.H., Desai, T.J., Krasnow, M.A., Quake, S.R., 2014. Reconstructing lineage hierarchies of the distal lung epithelium using single-cell RNA-seq. Nature 509, 371–375. doi:10.1038/nature13173

Tsai, Y.-H., Hill, D.R., Kumar, N., Huang, S., Chin, A.M., Dye, B.R., Nagy, M.S., Verzi, M.P., Spence, J.R., 2016. LGR4 and LGR5 Function Redundantly During Human Endoderm Differentiation. Cell Mol Gastroenterol Hepatol 2, 648–662.e8. doi:10.1016/j.jcmgh.2016.06.002

Varner, V.D., Gleghorn, J.P., Miller, E., Radisky, D.C., Nelson, C.M., 2015. Mechanically patterning the embryonic airway epithelium. Proceedings of the

National Academy of Sciences 201504102. doi:10.1073/pnas.1504102112

Varner, V.D., Nelson, C.M., 2014. Cellular and physical mechanisms of branching morphogenesis. Development 141, 2750–2759. doi:10.1242/dev.104794

Volckaert, T., Campbell, A., Dill, E., Li, C., Minoo, P., De Langhe, S., 2013. Localized Fgf10 expression is not required for lung branching morphogenesis but prevents differentiation of epithelial progenitors. Development 140, 3731–3742. doi:10.1242/dev.096560

Weaver, M., Dunn, N.R., Hogan, B.L., 2000. Bmp4 and Fgf10 play opposing roles during lung bud morphogenesis. Development 127, 2695–2704.

White, A.C., Xu, J., Yin, Y., Smith, C., Schmid, G., Ornitz, D.M., 2006. FGF9 and SHH signaling coordinate lung growth and development through regulation of distinct mesenchymal domains. Development 133, 1507–1517. doi:10.1242/dev.02313

Wong, A.P., Bear, C.E., Chin, S., Pasceri, P., Thompson, T.O., Huan, L.-J., Ratjen, F., Ellis, J., Rossant, J., 2012. Directed differentiation of human pluripotent stem cells into mature airway epithelia expressing functional CFTR protein. Nat Biotechnol. doi:10.1038/nbt.2328

Yin, Y., Wang, F., Ornitz, D.M., 2011. Mesothelial- and epithelial-derived FGF9 have distinct functions in the regulation of lung development. Development 138, 3169–3177. doi:10.1242/dev.065110

Yin, Y., White, A.C., Huh, S.-H., Hilton, M.J., Kanazawa, H., Long, F., Ornitz, D.M., 2008. An FGF–WNT gene regulatory network controls lung mesenchyme development. Developmental Biology 319, 426–436. doi:10.1016/j.ydbio.2008.04.009

Zhang, M., Wang, H., Teng, H., Shi, J., Zhang, Y., 2010. Expression of SHH signaling pathway components in the developing human lung. Histochem. Cell Biol. 134, 327–335. doi:10.1007/s00418-010-0738-2

Zhang, Y., Yokoyama, S., Herriges, J.C., Zhang, Z., Young, R.E., Verheyden, J.M., Sun, X., 2016. E3 ubiquitin ligase RFWD2 controls lung branching through protein-level regulation of ETV transcription factors. Proceedings of the National Academy of Sciences 201603310. doi:10.1073/pnas.1603310113

Zhao, R., Fallon, T.R., Saladi, S.V., Pardo-Saganta, A., Villoria, J., Mou, H., Vinarsky, V., Gonzalez-Celeiro, M., Nunna, N., Hariri, L.P., Camargo, F., Ellisen, L.W., Rajagopal, J., 2014. Yap tunes airway epithelial size and architecture by regulating the identity, maintenance, and self-renewal of stem cells. Developmental Cell 30, 151–165. doi:10.1016/j.devcel.2014.06.004

Figure legends:

Figure 1. Characterization of bud tip progenitors during the pseudoglandular stage of human fetal lung branching morphogenesis.
(A) Human fetal bud tip cells co-express SOX2 and SOX9 until ~16 weeks gestation. Scale bar represents 50 μm.
(B) ID2, a marker of bud tip cells in mice, is expressed in the bud tip region of developing human lungs at 15 weeks gestation as identified by *in situ* hybridization. Scale bar represents 50 μm.
(C) By 15 weeks gestation, bud tip cells show positive staining for Pro-SFTPC. PDPN and HOPX are absent from bud tip cells, but are present in the transition zone and in the airways adjacent to the bud tips. ABCA3 and SFTPB are not present in the bud tip cells in the fetal lung at 15 weeks. Scale bars represent 50μm (low magnification images) and 25 μm (high magnification images).
(D) Volcano plot of genes identified as differentially expressed by comparing different RNA-sequencing data sets; Isolated, uncultured bud tips (n=2; 59 days and 89 days gestation; isolation procedure Figure 2A-B) were compared to publically available datasets of whole adult human lung (E-MTAB-1733). A total of 7,166 genes that were differentially expressed (adjusted P-value < 0.01).
(E) A subset of genes known to be markers of lung epithelial cells in mouse and human were interrogated to evaluate expression levels between adult human and isolated fetal lung bud tips.
(F) 37 human bud-tip enriched transcription factors (Nikolić et al., 2017) were examined in the differential expression analysis comparing isolated fetal bud tips versus human adult lung (as shown in D). In total, 20 of the 37 transcription factors were statistically significantly enriched in the current analysis (denoted by the asterisk "*").
(G) Summary of markers expressed by bud tip cells at 14-15 weeks gestation as identified by protein staining and confirmed by RNA-sequencing.

Figure 2: FGF7, CHIR-99021 and RA are sufficient to maintain human fetal bud tip progenitor cells cultured *ex vivo.*
(A-B) Distal epithelial lung bud tips were collected from 3 human fetal lungs ((1) 84 day post fertilization of unknown gender, (2), 87 day post fertilization male, and (3), 87 day post fertilization of unknown gender) and cultured in Matrigel droplets. Scalebar in (B) represents 500μm.
(C) Wholemount immunofluorescent staining for SOX9, SOX2, ECAD in freshly isolated bud tips from an 87 day post-fertilization fetal lung. A maximum intensity projection of the confocal Z-series was rendered (3D rendering), and the resulting images demonstrated overlapping SOX2 and SOX9 expression at bud tips. Scalebar represents 100μm.
(D) Isolated human fetal bud tips were cultured for over 6 weeks in serum-free media supplemented with FGF7, CHIR-99021 and RA ('3-factor', or '3F' medium). Organoids grown from isolated human fetal lung bud tips are called 'fetal progenitor organoids'. Scale bar represents 500μm.

(E) Protein staining of tissue sections shows that almost all cells in fetal progenitor organoids grown in 3F medium were double positive for both SOX2 and SOX9. Scale bar represents 100μm.
(F) Whole mount staining, confocal Z-stack imaging and 3D rendering demonstrating co-expression of SOX2 and SOX9 in 3F grown fetal progenitor organoids. Scale bar represents 100μm.
(G) Fetal progenitor organoids express Pro-SFTPC at 4 weeks in culture. Scale bars represent 100μm at lower magnification and 25μm at higher magnification.
(H) Fetal progenitor organoids express low levels of the distal progenitor marker ID2 after 4 weeks in culture as determined by *in situ* hybridization. Scale bar represents 50 μm.
(I) Heatmap of key genes expressed during lung development in the epithelium and mesenchyme based on RNA-sequencing from peripheral (distal) portion of whole fetal lung tissue (n=4, 59-125 days post fertilization), freshly isolated uncultured fetal lung buds (n=2, 59 and 89 days post fertilization) and fetal progenitor organoids cultured for 2 weeks (n=2, 59 and 89 days post fertilization).
(J) RNAseq analysis from whole human adult lung was compared to uncultured isolated lung buds (n=2, 59 and 89 days post fertilization) and to cultured fetal progenitor organoids (n=2, 59 and 89 days post fertilization, cultured for 2 weeks). The top 1000 most highly upregulated genes from each comparison were identified (log2FoldChange < 0; adjusted p-value < 0.05) and plotted in a Venn diagram to assess gene overlap. 27.5% of genes were common to both groups. A hypergeometric means test found that the shared genes between isolated human bud tips and cultured fetal progenitor organoids were highly significant (overlapping p-value=1.4e-278).

Figure 3: FGF7, CHIR-99021 and RA generate patterned epithelial lung organoids from hPSCs

(A) Schematic of deriving patterned lung organoids from human pluripotent stem cells.
(B) Brightfield images of hPSC-derived foregut spheroids cultured in 3F media (FGF7, CHIR-99021 and RA) and grown *in vitro.* Images taken at 2, 3, 5, 6 or 10 weeks. Scale bars represent 200μm.
(C) Immunostaining for NKX2.1 and SOX2 in PLOs at 2, 6 and 16 weeks, respectively. Scale bars represent 50 μm.
(D) Quantitative analysis of cells co-expressing NKX2.1 and SOX2 in PLOs at 2, 6 and 16 weeks, as shown in (B). Each data point represents an independent biological replicate, and the mean +/- the standard error of the mean is shown for each group.
(E) Brightfield image of a patterned lung organoid after 6 weeks (45 days) in culture, showing clear distal budded regions and interior airway-like regions, and a schematic representing a patterned lung organoid, highlighting bud tip region and interior regions.

(F) Patterned lung organoids were co-stained for SOX9 and SOX2 protein expression by immunofluorescence. Inset shows high magnification of boxed region. Scale bar represents 100 μm.
(G) Low and high magnification immunofluorescent images of Pro-SFTPC and SOX9 co-expression in bud tip region of patterned lung organoids. Scale bars represent 50 μm.
(H) Bud tips of patterned lung organoids express ID2 mRNA, visualized by *In situ* hybridization (brown dots). Scale bar represents 100 μm.
(I) Interior regions of patterned lung organoids (top) and adult human airway (bottom) co-stained for SCGB1A1, Acetylated Tubulin (AC-TUB) and P63. Note that in the patterned lung organoids P63 staining is absent and AC-TUB staining is apically localized but does not show mature cilia. Scale bars represent 100 μm (left panels, low magnification) or 50 μm (right panels, high magnification).
(J) Interior regions of patterned lung organoids (top) and adult human airway (bottom) co-stained for MUC5AC and the epithelial marker β–catenin (bCAT). Scale bars represent 100 μm (left panels, low magnification) or 50 μm (right panels, high magnification).
(K-L) Percent of cells expressing MUC5AC or SCGB1A1, plotted as aggregate data ((I); # cells positive in all organoids/total cells counted in all organoids) and for each individual patterned lung organoid counted ((J); # cells positive in individual organoid/all cells counted in individual organoid).

Figure 4: A highly enriched population of proliferative SOX9+/SOX2+ progenitors can be expanded from patterned lung organoids
(A) hPSC-derived epithelial patterned lung organoids were passaged through a 27-gague needle 2-3 times to break them apart.
(B) Epithelial fragments were replated in a fresh Matrigel droplet. Fragments subsequently formed cystic structures, called 'bud tip organoids'. Scale bar represents 1mm.
(C) Quantitative assessment of organoid passaging and expansion. One single patterned lung organoid was needle passaged into 6 wells (passage 1), generating 75 new bud tip organoids in total (average 12.5 per well). A single well of the resulting bud tip organoids were then passaged into 6 new wells after 2 weeks in culture (1:6 split ratio), generating 200 new organoids in total (average 33 per well). This 1:6 passaging was carried out two additional times, every 1-2 weeks for up to 4 passages before growth slowed. 3 biological replicates were performed for expansion experiments; graph plots the mean +/- the SEM.
(D) Immunostaining for SOX9 and SOX2 in bud tip organoids. Scale bar represents 50um.
(E) Quantitation of the percent of SOX9+ cells in patterned lung organoids versus bud tip organoids (# SOX9+ cells/total cells). Each data point represents an independent biological replicate and graphs indicate the mean +/- the standard error of the mean for each experimental group. An unpaired, one-way analysis of variance was performed for each gene followed by Tukey's multiple comparison

to compare the mean of each group to the mean of every other group within the experiment. A significance level of 0.05 was used. Significance is shown on the graph according to the following: P > 0.05 ns, P ≤ 0.05 *, P ≤ 0.01 **, P ≤ 0.001 ***, P ≤ 0.0001 ****.

(F-G) Immunostaining for KI67 and SOX9 in patterned lung organoids (F) and bud tip organoids (G). Scale bar represents 100um.

(H) Quantitation of the percent of all cells that were KI67+ in patterned and bud tip organoids (# KI67+ cells /total cells).

(I) Quantitation of the percent of proliferating SOX9+ cells in patterned and bud tip organoids (# KI67+/SOX9+ cells/total cells). For (H) and (I), each data point represents an independent biological replicate and graphs indicate the mean +/- the standard error of the mean for each experimental group. Significance was determined by an unpaired Student's T test. A significance value of 0.05 was used. P > 0.05 ns, P ≤ 0.05 *, P ≤ 0.01 **, P ≤ 0.001 ***, P ≤ 0.0001 ****.

(J) RNA-sequencing was conducted to compare the global transcriptome of hPSCs, foregut spheroids, hPSC-derived patterned lung organoids, hPSC-derived bud tip organoids, whole peripheral (distal) fetal lung, freshly isolated (uncultured) fetal lung buds and fetal progenitor organoids. Principal component analysis (PCA) is shown for the first 3 principal components (PC1-3).

(K) Heatmap of key genes expressed during lung development in the epithelium based on RNA-sequencing from freshly isolated (uncultured) fetal lung buds (n=2, 59 and 89 days post fertilization) and fetal progenitor organoids cultured for 2 weeks (n=2, 59 and 89 days post fertilization).

(L-N) RNAsequencing analysis identified differentially expressed genes when comparing whole human adult lung versus uncultured isolated lung buds (n=2, 59 and 89 days post fertilization), cultured fetal progenitor organoids (n=2, 59 and 89 days post fertilization, cultured for 2 weeks), and hPSC-derived bud tip organoids (n=2, H9-derived bud tip organoids 97 days, iPSC20-1-derived bud tip organoids 60 days). The top 1000 upregulated genes relative to adult for each group were identified (log2FoldChange < 0; adjusted p-value < 0.05), and plotted in a Venn diagram to identify overlapping genes (L-N). **(L)** A hypergeometric means test found that the shared enriched genes identified in isolated human bud tips and hPSC-derived bud tip organoids was highly significant (overlapping p-value=9.3e-901), **(M)** as were the shared enriched genes identified in cultured fetal progenitor organoids and hPSC-derived bud tip organoids (overlapping p-value=1.2e-1021). **(N)** A comparison of the 1000 most highly upregulated genes relative to adult human lung for isolated human fetal buds, fetal progenitor organoids and hPSC-derived bud tip organoids showed 285 overlapping genes between groups. These genes represented 14.3% of all genes included in the comparison, and included several genes previously associated with human or mouse fetal bud tips. A small subset of genes previously associated with human or mouse bud-tip progenitor cells are highlighted as “Selected overlapping genes” (L-N).

Figure 5: Bud tip organoids retain multilineage potential *in vitro*

(A) Schematic of experimental setup. iPSC20-1 bud tip organoids were initially cultured in 3F medium and subsequently grown in 3F medium or media containing FGF7 alone ('differentiation media') for 24 days.
(B) Brightfield images of bud tip organoids growing in 3F media (left) and FGF7 alone (right). Scale bar represents 500 μm.
(C) NKX2.1 immunofluorescence of bud tip organoids grown in FGF7 for 24 days. Scale bar represents 50 μm.
(D) Immunostaining for AECI (PDPN, HOPX, RAGE) and AECII cells (ABCA3, Pro-SFTPC, SPB) in alveolar regions of the native human adult lung (left panels) and in hPSC-derived bud tip organoids exposed to differentiation media (right panels). Positive ABCA3 staining and PDPN staining were both observed in differentiated organoids, but staining did not overlap. Two separate regions of the same slide are shown to illustrate PDPN+ or ABCA3+ cells. Bud tip organoids contain cells that co-stain for SFTPB and ProSFTPC, suggesting these are AECII-like cells. Interestingly, some cells expressed AECI-marker HOPX, but no positive staining for RAGE was observed (bottom row). This suggests AECI-like cells were present but were perhaps immature, as RAGE does not appear in the human fetal lung until 16 weeks (Figure 1 – Figure Supplement 1). Scale bars represents 50 μm.
(E) Immunostaining for airway cell types (MUC5AC, FOXJ1, SCGB1A1, P63, SOX2, Ac-TUB, CHGA) in bronchiolar regions of the native human adult lung (left panels) and in hPSC-derived bud tip organoids exposed to differentiation media (right panels). Clear MUC5AC staining was observed in differentiated organoids, and positive mucous staining was observed within the lumens of most organoids. Although positive staining for SCGB1A1 was observed in organoids, ciliated cells were absent, as indicated by a lack of FOXJ1 staining and acetylated tubulin staining that, while apical, is within the cell and does not mark mature ciliated structures. Clear CHGA+ cells were observed (bottom row), suggesting the presence of neuroendocrine cells. Scale bar represents 50 μm.
(F) Transmission Electron Microscopy (TEM) was performed on hPSC-derived bud tip organoids exposed to differentiation media. Mucous containing vessicles were observed (marked "M") and lamellar bodies were seen in many cells (marked "LB").
(G) Immunostaining for SOX9 and SOX2 in bud tip organoids grown in differentiation media. Scale bar represents 50 um.
(H-I) Quantitation of cell type markers in bud tip organoids grow in differentiation media plotted as aggregate data ((H) numbers at top of bars represent positive cells/total cells counted across 5 individual organoids), and as individual data per organoid ((I) number of positive cells per organoid). Each data point in (I) represents an independent biological replicate and graphs indicate the mean +/- the standard error of the mean.
(J) Summary of mature lung epithelial cell types generated *in vitro*.

Figure 6: Engraftment of hPSC-derived bud tip progenitor organoid cells into the injured mouse airway

(A) Schematic of experimental design. 16 immunocompromised NSG male mice were injected with 300mg/kg of Naphthalene. 24 hours post-injury, mice were randomly assigned (8 per group) to receive an intratracheal injection of 600,000 single cells isolated from bud tip organoids maintained, or no injection of cells. Doxycycline (1mg/ml) was added to the drinking water for all mice starting on day 2 post-injury. 8 days post-injury, animals were injected with BrdU to assess cell proliferation and sacrificed one hour later.
(B) H&E staining showing the kinetics of Naphthalene injury in NSG mice, before injury and 24 hours and 7 days post-injury. Scale bar represents 50um.
(C) Mouse survival data. 75% (6/8) of animals that received Naphthalene and an injection of cells survived until the day of harvest, compared with 50% (4/8) of animals that did not receive cells (not statistically significant, log-rank test $p>0.05$).
(D-E) Characterization of surviving cell-injected mice. Engraftment was assessed based on human specific antibodies (NuMA, huMITO) in 3 independent histological sections from each surviving mouse. (D) Engraftment was observed in 4/6 animals. (E) Quantitation of the number of human cells in each engrafted cell 'patch'. Each data point represents the number of cells in a single patch of cells.
(F) Immunostaining for the human specific mitochondrial marker, HuMITO and NKX2.1 in transplanted lungs. Scale bar represents 50um.
(G) Immunostaining for human nuclear specific antibody (NuMA) and BrdU in transplanted lungs . Low magnification (top) and high magnification (bottom) images are shown. Scale bars represent 50um.
(H-I) Immunostaining for HuMito and KI67 demonstrates proliferating human cells in transplanted lungs (H). Low magnification (top) and high magnification (bottom) images are shown. Scale bars represent 50um. (I) Quantitation of human cells that co-express the proliferation marker KI67 comparing proliferation *in vitro* bud tip organoids (day 0) and following *in vivo* engraftmet (day 7). Aggregate data is plotted showing total number of cells positive for KI67, and the total number of cells counted from 3 non-serial sections from 3 different mice is plotted for day 7.
(J-K) Immunostaining for HuMITO, SOX9 and SOX2 in transplanted lungs(J). Low magnification (top) and high magnification (bottom) images are shown. Scale bars represent 50um. (K) shows quantification of immunostaining, comparing *in vitro* bud tip organoids (day 0) and following *in vivo* engraftmet (day 7). Aggregate data from 3 non-serial sections from 3 mice is plotted for day 7.
(L-M) Immunostaining for NuMA and MUC5AC in transplanted lungs (L). Low magnification (top) and high magnification (bottom) images are shown. Scale bars represent 50um. (M) shows quantification of immunostaining, comparing *in vitro* bud tip organoids (day 0) and following *in vivo* engraftmet (day 7). Aggregate data from 3 non-serial sections from 3 mice is plotted for day 7.
(N-O) Immunostaining for NuMA, SCGB1A1 and FOXJ1 in transplanted lungs (N). Low magnification (top) and high magnification (bottom) images are shown. Note that he FOXJ1+ cell shown is assumed to be of murine origin, since it does not express NuMA. Scale bars represent 50um. (O) shows quantification of

immunostaining, comparing *in vitro* bud tip organoids (day 0) and following *in vivo* engraftmet (day 7). Aggregate data from 3 non-serial sections from 3 mice is plotted for day 7.

(P-Q) Immunostaining for NuMA, ECAD and GFP in transplanted lungs (P). Low magnification (top) and high magnification (bottom) images are shown. Scale bars represent 50um. (Q) shows quantification of GFP+ cells following *in vivo* engraftmet and dox induction for (day 7). Aggregate data from 3 non-serial sections from 3 mice is plotted for day 7.

Figure 1

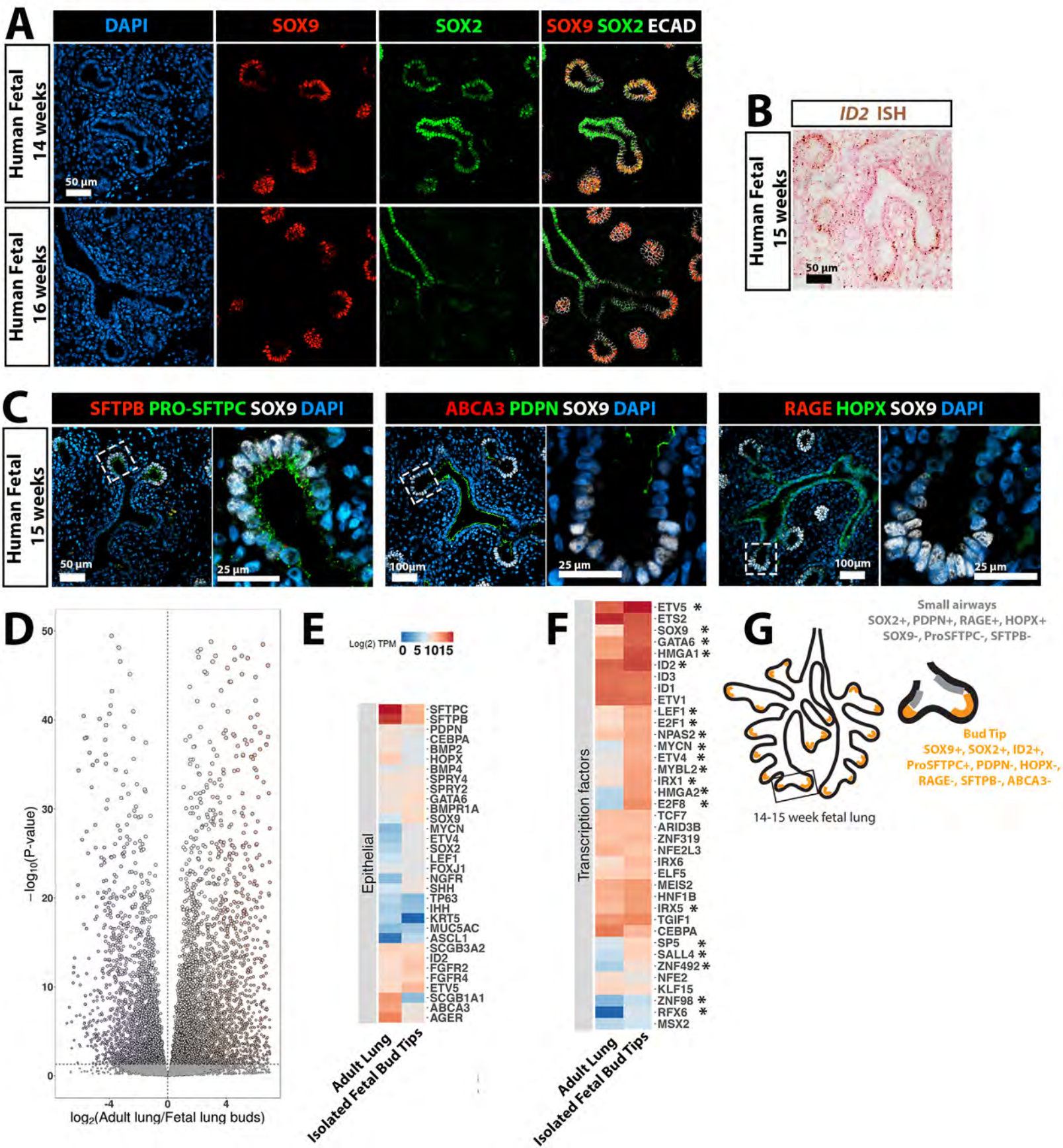
A
DAPI
SOX9
SOX2
SOX9 SOX2 ECAD
Human Fetal 14 weeks
Human Fetal 16 weeks
50 µm
B
ID2 ISH
Human Fetal 15 weeks
50 µm
C
SFTPB PRO-SFTPC SOX9 DAPI
ABCA3 PDPN SOX9 DAPI
RAGE HOPX SOX9 DAPI
Human Fetal 15 weeks
50 µm
25 µm
100µm
25 µm
100µm
25 µm
D
−log10(P-value)
log2(Adult lung/Fetal lung buds)
E
Log(2) TPM 0 5 1015
Epithelial
SFTPC
SFTPB
PDPN
CEBPA
BMP2
HOPX
BMP4
SPRY4
SPRY2
GATA6
BMPR1A
SOX9
MYCN
ETV4
SOX2
LEF1
FOXJ1
NGFR
SHH
TP63
IHH
KRT5
MUC5AC
ASCL1
SCGB3A2
ID2
FGFR2
FGFR4
ETV5
SCGB1A1
ABCA3
AGER
Adult Lung
Isolated Fetal Bud Tips
F
Transcription factors
ETV5 *
ETS2
SOX9 *
GATA6 *
HMGA1 *
ID2 *
ID3
ID1
ETV1
LEF1 *
E2F1 *
NPAS2 *
MYCN *
ETV4 *
MYBL2 *
IRX1 *
HMGA2 *
E2F8 *
TCF7
ARID3B
ZNF319
NFE2L3
IRX6
ELF5
MEIS2
HNF1B
IRX5 *
TGIF1
CEBPA
SP5 *
SALL4 *
ZNF492 *
NFE2
KLF15
ZNF98 *
RFX6 *
MSX2
Adult Lung
Isolated Fetal Bud Tips
G
Small airways
SOX2+, PDPN+, RAGE+, HOPX+
SOX9-, ProSFTPC-, SFTPB-
Bud Tip
SOX9+, SOX2+, ID2+,
ProSFTPC+, PDPN-, HOPX-,
RAGE-, SFTPB-, ABCA3-
14-15 week fetal lung

Figure 2

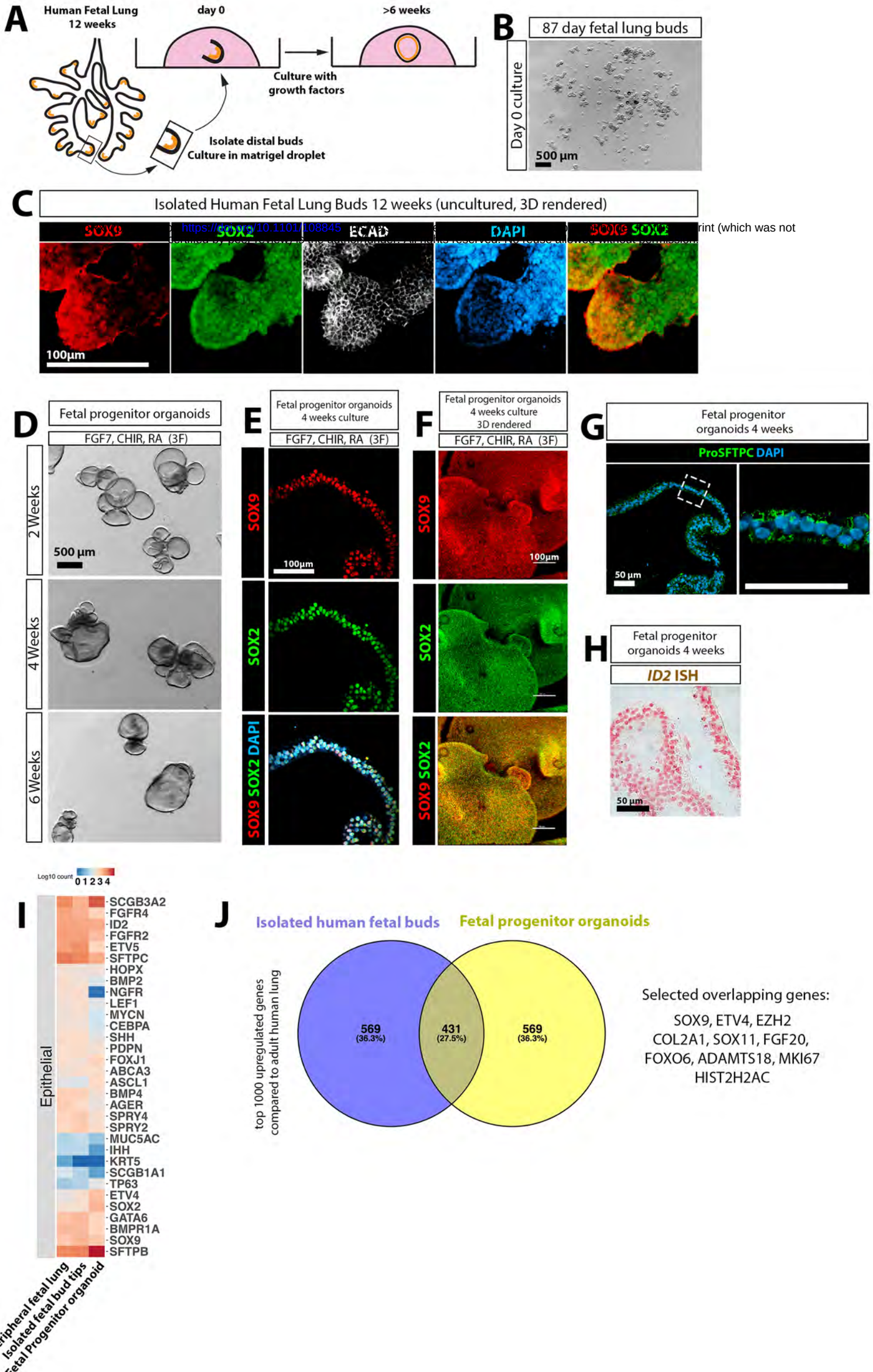

Figure 3

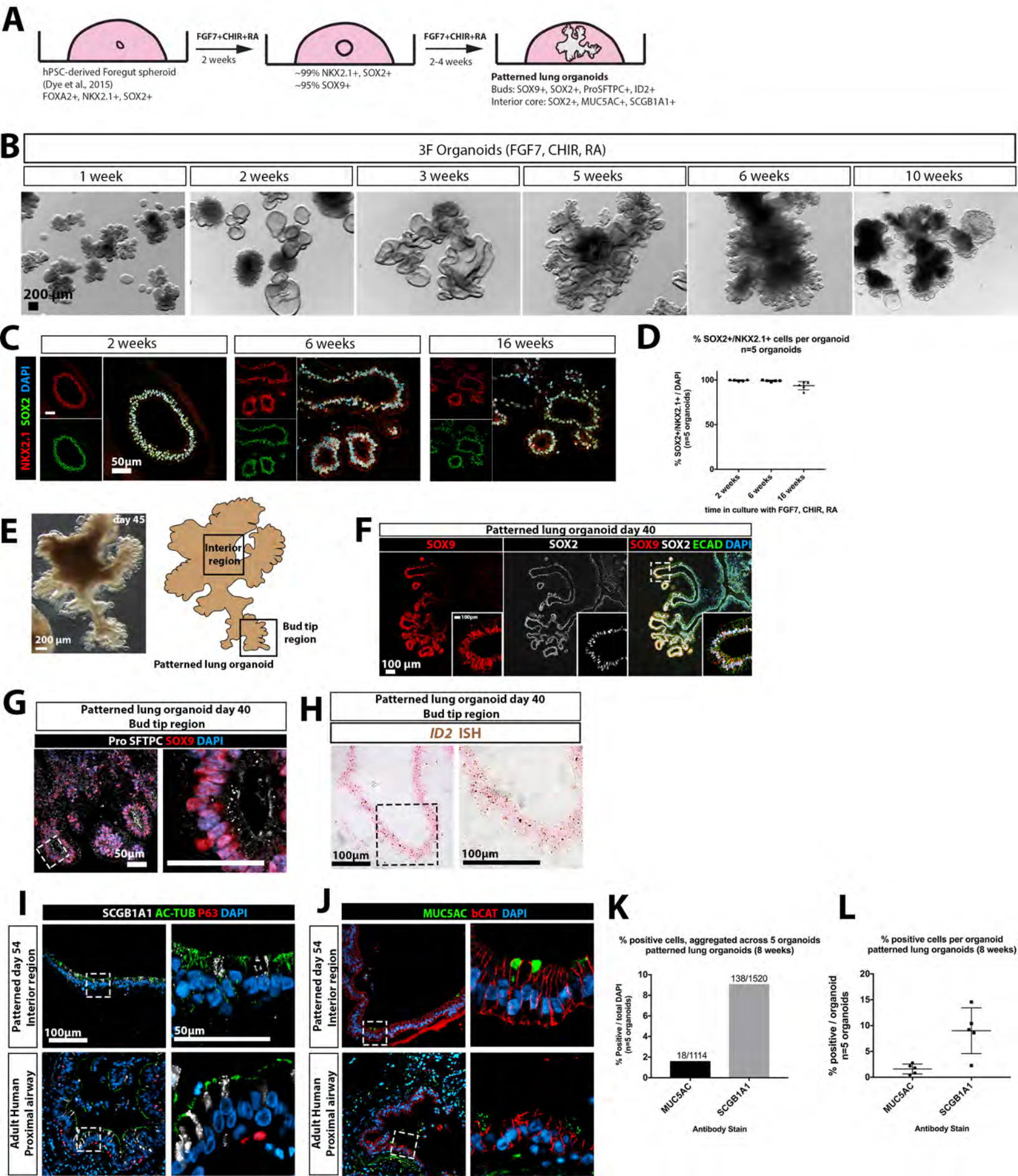
A
FGF7+CHIR+RA
2 weeks
FGF7+CHIR+RA
2-4 weeks
hPSC-derived Foregut spheroid
(Dye et al., 2015)
FOXA2+, NKX2.1+, SOX2+
~99% NKX2.1+, SOX2+
~95% SOX9+
Patterned lung organoids
Buds: SOX9+, SOX2+, ProSFTPC+, ID2+
Interior core: SOX2+, MUC5AC+, SCGB1A1+
B
3F Organoids (FGF7, CHIR, RA)
1 week
2 weeks
3 weeks
5 weeks
6 weeks
10 weeks
200 µm
C
2 weeks
6 weeks
16 weeks
NKX2.1 SOX2 DAPI
50µm
D
% SOX2+/NKX2.1+ cells per organoid
n=5 organoids
% SOX2+/NKX2.1+ / DAPI
(n=5 organoids)
100
50
0
2 weeks
6 weeks
16 weeks
time in culture with FGF7, CHIR, RA
E
day 45
200 µm
Interior region
Bud tip region
Patterned lung organoid
F
Patterned lung organoid day 40
SOX9
SOX2
SOX9 SOX2 ECAD DAPI
100µm
100 µm
G
Patterned lung organoid day 40
Bud tip region
Pro SFTPC SOX9 DAPI
50µm
H
Patterned lung organoid day 40
Bud tip region
ID2 ISH
100µm
100µm
I
SCGB1A1 AC-TUB P63 DAPI
Patterned day 54
Interior region
Adult Human
Proximal airway
100µm
50µm
J
MUC5AC bCAT DAPI
Patterned day 54
Interior region
Adult Human
Proximal airway
K
% positive cells, aggregated across 5 organoids
patterned lung organoids (8 weeks)
% Positive / total DAPI
(n=5 organoids)
10
8
6
4
2
0
18/1114
138/1520
MUC5AC
SCGB1A1
Antibody Stain
L
% positive cells per organoid
patterned lung organoids (8 weeks)
% positive / organoid
n=5 organoids
20
15
10
5
0
MUC5AC
SCGB1A1
Antibody Stain

Figure 4

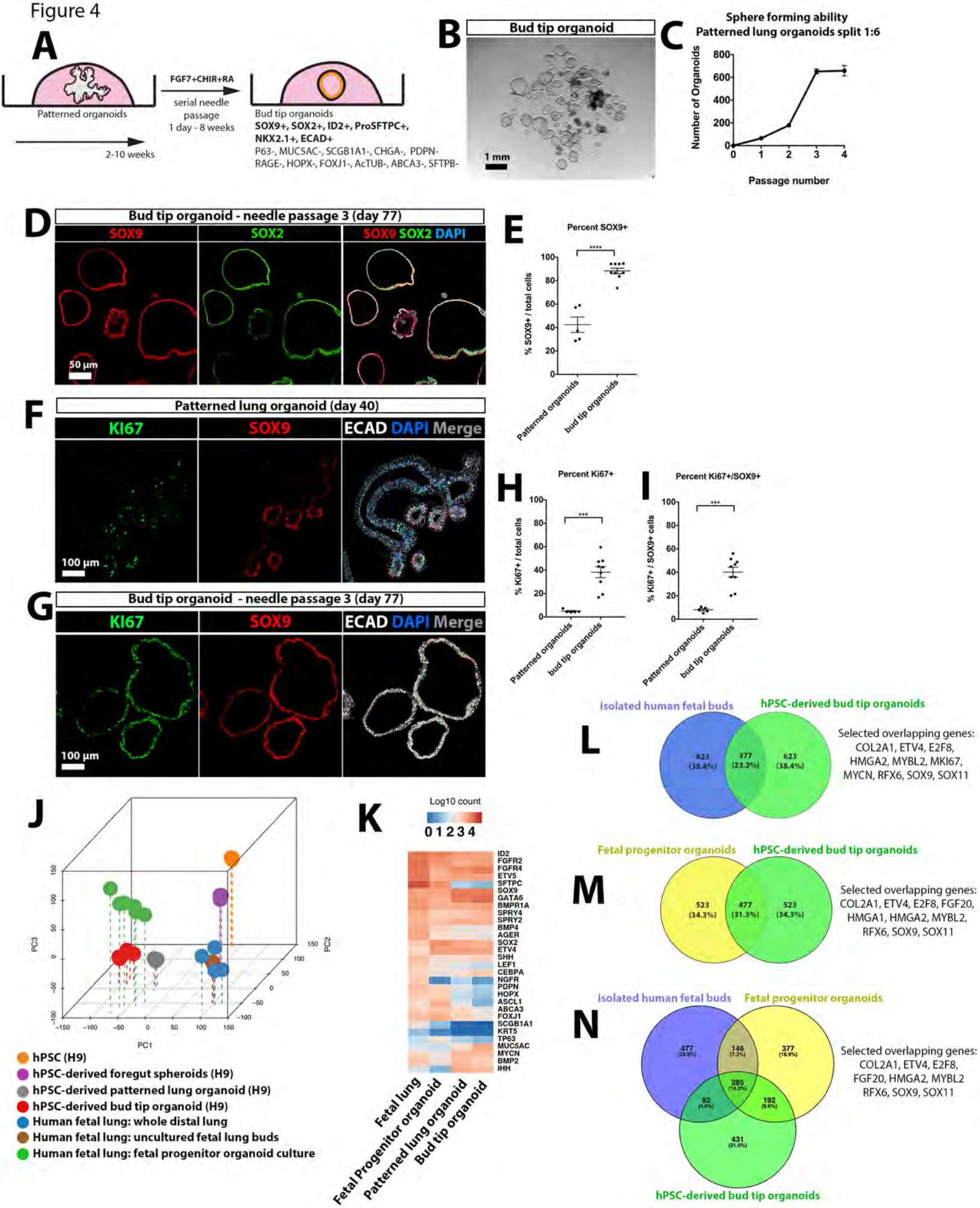
A
Patterned organoids
FGF7+CHIR+RA
serial needle passage
1 day - 8 weeks
2-10 weeks
Bud tip organoids
SOX9+, SOX2+, ID2+, ProSFTPC+, NKX2.1+, ECAD+
P63-, MUC5AC-, SCGB1A1-, CHGA-, PDPN-
RAGE-, HOPX-, FOXJ1-, AcTUB-, ABCA3-, SFTPB-
B
Bud tip organoid
1 mm
C
Sphere forming ability
Patterned lung organoids split 1:6
Number of Organoids
Passage number
D
Bud tip organoid - needle passage 3 (day 77)
SOX9
SOX2
SOX9 SOX2 DAPI
50 µm
E
Percent SOX9+
% SOX9+ / total cells
Patterned organoids
bud tip organoids
F
Patterned lung organoid (day 40)
KI67
SOX9
ECAD DAPI Merge
100 µm
G
Bud tip organoid - needle passage 3 (day 77)
KI67
SOX9
ECAD DAPI Merge
100 µm
H
Percent Ki67+
% Ki67+ / total cells
Patterned organoids
bud tip organoids
I
Percent Ki67+/SOX9+
% Ki67+ / SOX9+ cells
Patterned organoids
bud tip organoids
J
PC1
PC2
PC3
hPSC (H9)
hPSC-derived foregut spheroids (H9)
hPSC-derived patterned lung organoid (H9)
hPSC-derived bud tip organoid (H9)
Human fetal lung: whole distal lung
Human fetal lung: uncultured fetal lung buds
Human fetal lung: fetal progenitor organoid culture
K
Log10 count
0 1 2 3 4
ID2
FGFR2
FGFR4
ETV5
SFTPC
SOX9
GATA6
BMPR1A
SPRY4
SPRY2
BMP4
AGER
SOX2
ETV4
SHH
LEF1
CEBPA
NGFR
PDPN
HOPX
ASCL1
ABCA3
FOXJ1
SCGB1A1
KRT5
TP63
MUC5AC
MYCN
BMP2
IHH
Fetal lung
Fetal Progenitor organoid
Patterned lung organoid
Bud tip organoid
L
Isolated human fetal buds
hPSC-derived bud tip organoids
623 (38.4%)
377 (23.2%)
623 (38.4%)
Selected overlapping genes:
COL2A1, ETV4, E2F8, HMGA2, MYBL2, MKI67, MYCN, RFX6, SOX9, SOX11
M
Fetal progenitor organoids
hPSC-derived bud tip organoids
523 (34.3%)
477 (31.3%)
523 (34.3%)
Selected overlapping genes:
COL2A1, ETV4, E2F8, FGF20, HMGA1, HMGA2, MYBL2, RFX6, SOX9, SOX11
N
Isolated human fetal buds
Fetal progenitor organoids
477 (23.9%)
146 (7.3%)
377 (18.9%)
285 (14.3%)
92 (4.6%)
192 (9.6%)
431 (21.6%)
hPSC-derived bud tip organoids
Selected overlapping genes:
COL2A1, ETV4, E2F8, FGF20, HMGA2, MYBL2 RFX6, SOX9, SOX11

Figure 5

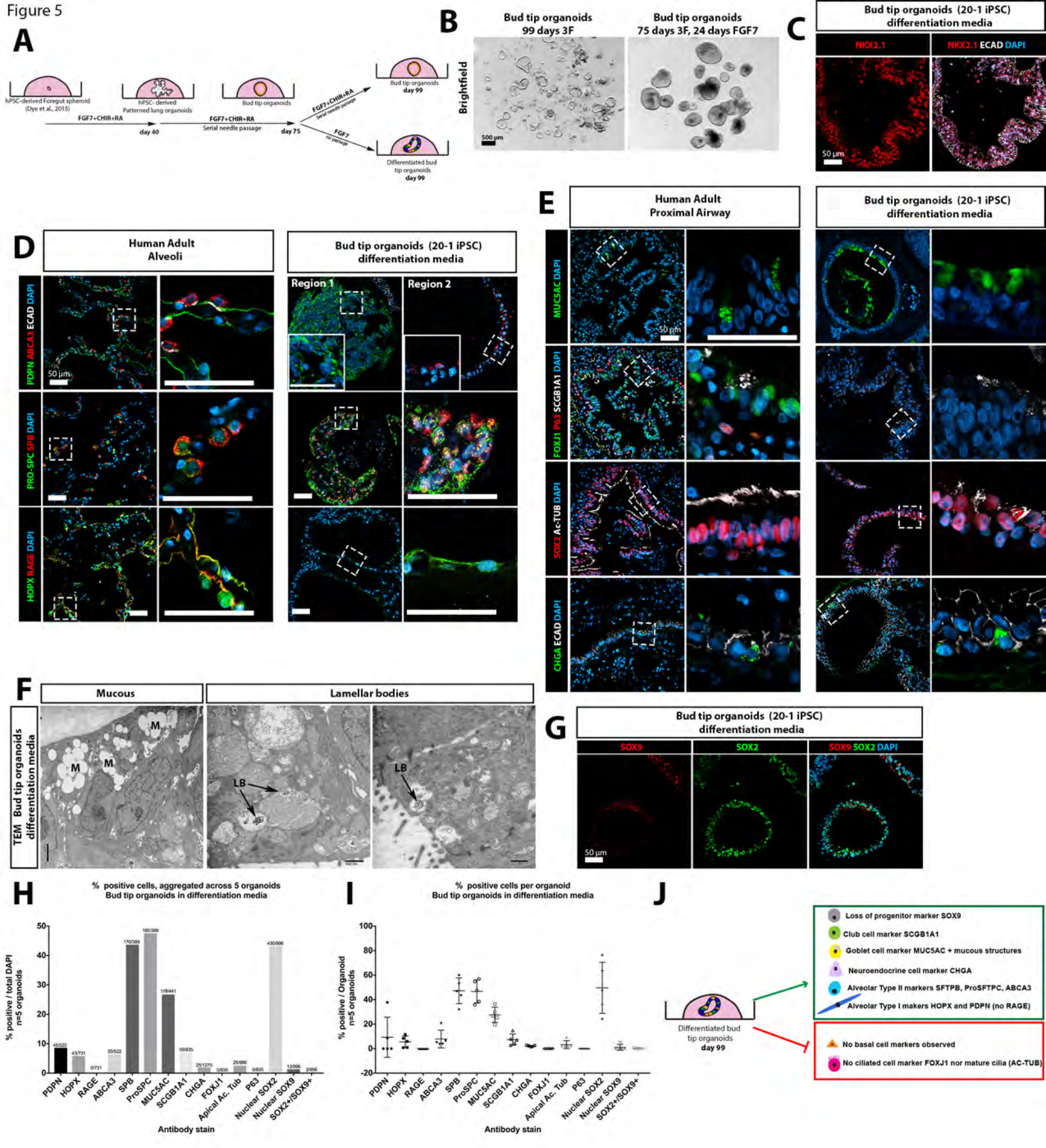
A
hPSC-derived Foregut spheroid (Dye et al., 2015)
FGF7+CHIR+RA
day 40
hPSC- derived Patterned lung organoids
FGF7+CHIR+RA
Serial needle passage
day 75
Bud tip organoids
FGF7+CHIR+RA
Serial needle passage
Bud tip organoids day 99
FGF7
no passage
Differentiated bud tip organoids day 99
B
Bud tip organoids 99 days 3F
Bud tip organoids 75 days 3F, 24 days FGF7
Brightfield
500 µm
C
Bud tip organoids (20-1 iPSC) differentiation media
NKX2.1
NKX2.1 ECAD DAPI
50 µm
D
Human Adult Alveoli
Bud tip organoids (20-1 iPSC) differentiation media
Region 1
Region 2
PDPN ABCA3 ECAD DAPI
PRO-SPC SPB DAPI
HOPX RAGE DAPI
50 µm
E
Human Adult Proximal Airway
Bud tip organoids (20-1 iPSC) differentiation media
MUC5AC DAPI
FOXJ1 P63 SCGB1A1 DAPI
SOX2 Ac-TUB DAPI
CHGA ECAD DAPI
50 µm
F
Mucous
Lamellar bodies
TEM Bud tip organoids differentiation media
M
LB
G
Bud tip organoids (20-1 iPSC) differentiation media
SOX9
SOX2
SOX9 SOX2 DAPI
50 µm
H
% positive cells, aggregated across 5 organoids
Bud tip organoids in differentiation media
% positive / total DAPI n=5 organoids
45/522
43/731
0/731
33/622
170/389
185/389
118/441
59/835
25/1275
0/835
25/896
0/835
430/996
13/996
2/996
PDPN
HOPX
RAGE
ABCA3
SPB
ProSPC
MUC5AC
SCGB1A1
CHGA
FOXJ1
Apical Ac. Tub
P63
Nuclear SOX2
Nuclear SOX9
SOX2+/SOX9+
Antibody stain
I
% positive cells per organoid
Bud tip organoids in differentiation media
% positive / Organoid n=5 organoids
Antibody stain
J
Differentiated bud tip organoids day 99
Loss of progenitor marker SOX9
Club cell marker SCGB1A1
Goblet cell marker MUC5AC + mucous structures
Neuroendocrine cell marker CHGA
Alveolar Type II markers SFTPB, ProSFTPC, ABCA3
Alveolar Type I makers HOPX and PDPN (no RAGE)
No basal cell markers observed
No ciliated cell marker FOXJ1 nor mature cilia (AC-TUB)

Figure 6

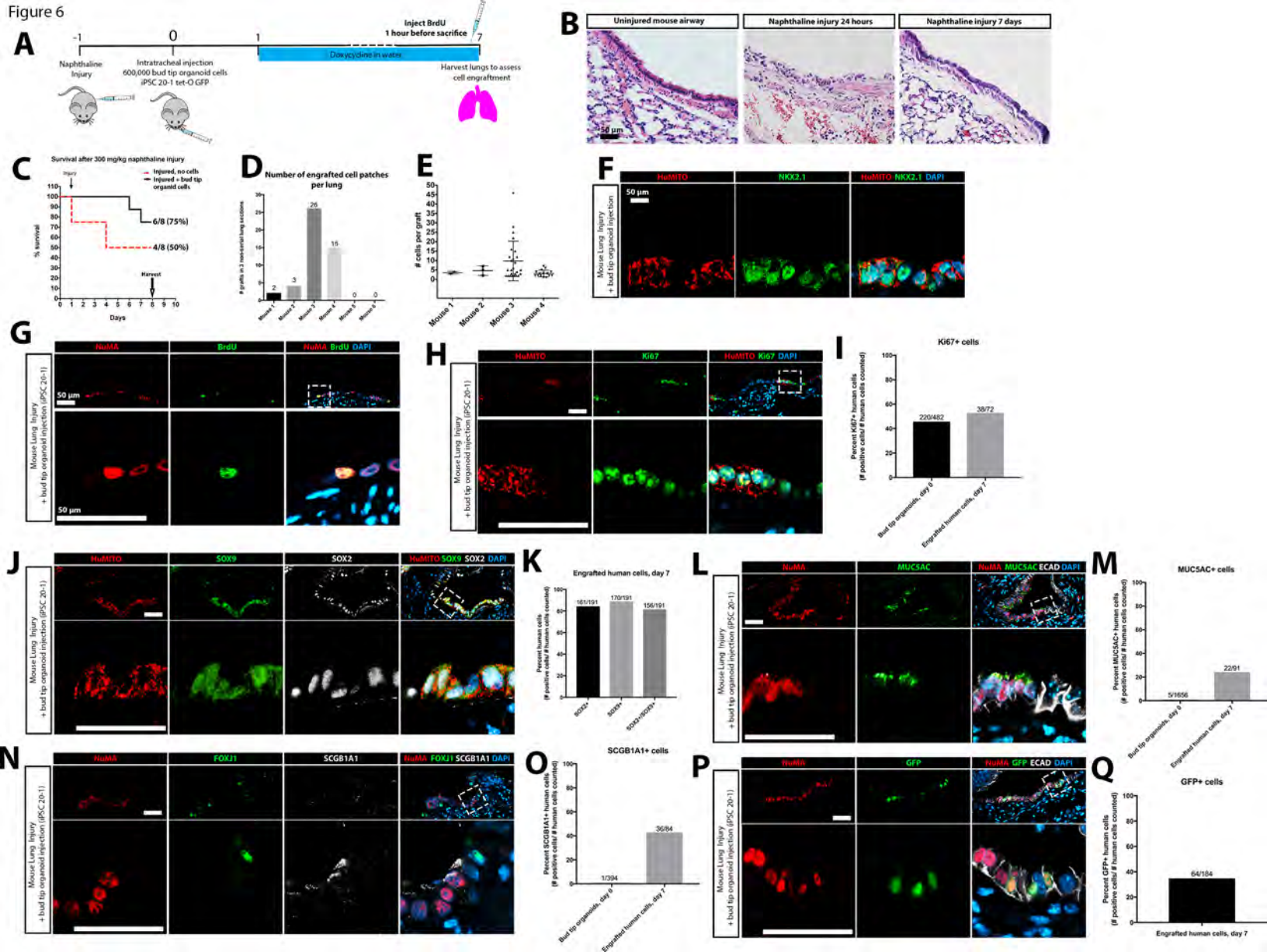
A
-1
0
1
7
Inject BrdU
1 hour before sacrifice
Naphthaline Injury
Intratracheal injection
600,000 bud tip organoid cells
iPSC 20-1 tet-O GFP
Doxycycline in water
Harvest lungs to assess cell engraftment
B
Uninjured mouse airway
Naphthaline injury 24 hours
Naphthaline injury 7 days
50 µm
C
Survival after 300 mg/kg naphthaline injury
Injury
Injured, no cells
Injured + bud tip organoid cells
% survival
6/8 (75%)
4/8 (50%)
Harvest
Days
D
Number of engrafted cell patches per lung
grafts in 3 non-serial lung sections
2
3
26
15
0
0
Mouse 1
Mouse 2
Mouse 3
Mouse 4
Mouse 5
Mouse 6
E
cells per graft
Mouse 1
Mouse 2
Mouse 3
Mouse 4
F
HuMITO
NKX2.1
HuMITO NKX2.1 DAPI
50 µm
Mouse Lung Injury
+ bud tip organoid injection
G
NuMA
BrdU
NuMA BrdU DAPI
50 µm
50 µm
Mouse Lung Injury
+ bud tip organoid injection (iPSC 20-1)
H
HuMITO
Ki67
HuMITO Ki67 DAPI
Mouse Lung Injury
+ bud tip organoid injection (iPSC 20-1)
I
Ki67+ cells
Percent Ki67+ human cells
(# positive cells/ # human cells counted)
220/482
38/72
Bud tip organoids, day 0
Engrafted human cells, day 7
J
HuMITO
SOX9
SOX2
HuMITO SOX9 SOX2 DAPI
Mouse Lung Injury
+ bud tip organoid injection (iPSC 20-1)
K
Engrafted human cells, day 7
Percent human cells
(# positive cells/ # human cells counted)
161/191
170/191
156/191
SOX2+
SOX9+
SOX2+SOX9+
L
NuMA
MUC5AC
NuMA MUC5AC ECAD DAPI
Mouse Lung Injury
+ bud tip organoid injection (iPSC 20-1)
M
MUC5AC+ cells
Percent MUC5AC+ human cells
(# positive cells/ # human cells counted)
5/1656
22/91
Bud tip organoids, day 0
Engrafted human cells, day 7
N
NuMA
FOXJ1
SCGB1A1
NuMA FOXJ1 SCGB1A1 DAPI
Mouse Lung Injury
+ bud tip organoid injection (iPSC 20-1)
O
SCGB1A1+ cells
Percent SCGB1A1+ human cells
(# positive cells/ # human cells counted)
1/394
36/84
Bud tip organoids, day 0
Engrafted human cells, day 7
P
NuMA
GFP
NuMA GFP ECAD DAPI
Mouse Lung Injury
+ bud tip organoid injection (iPSC 20-1)
Q
GFP+ cells
Percent GFP+ human cells
(# positive cells/ # human cells counted)
64/184
Engrafted human cells, day 7

Inventory of Supplemental Information

Figures: 10 supplemental figures
Tables: 1 supplemental table

Figure 1 - Figure Supplement 1: Characterization of human fetal bud tip cells throughout multiple time points during branching morphogenesis

Figure 1 - Figure supplement 2: FGF7 is sufficient to promote growth of mouse SOX9+ bud tip progenitors *ex vivo*

Figure 1 - Figure supplement 3: Removal of BMP4 leads to increased *Sox9* expression.

Figure 1 - Figure supplement 4: Synergistic activity of FGF7, CHIR-99021 and RA maintains SOX9 in mouse bud tip cells *in vitro.*

Figure 2 - Figure supplement 1: FGF7, CHIR-99021 and RA maintain the highest levels of progenitor markers in cultured human fetal bud tips.

Figure 2 - Figure supplement 2: Cultured fetal progenitor organoids successfully engraft into injured mouse airway epithelium

Figure 3 - Figure supplement 1: Patterned lung organoids grown from hPSCs exhibit robust and stereotyped growth

Figure 3 - Figure supplement 2: Patterned lung organoids have molecular similarities to 14 week fetal lung and cultured fetal progenitor organoids

Figure 4 - Figure supplement 1: Characterization of hPSC-derived bud tip organoids

Figure 6 - figure supplement 1: Characterization of bud tip organoids generated from iPSC20-1 on the day of transplantation into the injured mouse airway

Supplemental Table 1: Differentially expressed genes identified by comparing RNAsequencing data between whole adult human lungs vs. freshly isolated human fetal lung bud tips. Note: Positive values (Log2 – fold change (Log2FC)) represent genes enriched in adult tissue while negative values represent genes enriched in bud tips.

Figure 1 - Figure Supplement 1: Characterization of human fetal bud tip cells throughout multiple time points during branching morphogenesis

(A) SOX9 and SOX2 co expression was assessed in paraffin sections from human fetal lung specimens from 10-20 weeks gestation. Bud tip cells co-express SOX9 and SOX2 until 16 weeks gestation when these regions separate. The transition zone, where cells are neither positive for SOX9 nor SOX2 continues to lengthen as branching morphogenesis progresses. Scale bar represents 50 μm.

(B) PDPN and RAGE, along with the bud tip progenitor marker SOX9 were assessed in paraffin sections from human fetal lung specimens from 10-20 weeks gestation. PDPN is present in the more proximal small airways adjacent to SOX9+ bud tips as early as 10 weeks, but SOX9+ cells at the bud tips do not express PDPN from 10-20 weeks. High magnification images show cells within the transition zone. RAGE does not appear until 16 weeks gestation, and is present in PDPN+ cells adjacent to the bud tip region. However, SOX9+ cells at the bud tips do not express RAGE during the time points evaluated. Scale bars represent 50 μm.

(C) ABCA3 and PDPN were co-stained in paraffin sections from human fetal lung specimens from 10-20 weeks gestation. Arrowheads point to bud tips, which are negative for PDPN. No positive staining for ABCA3 was detected from 10-20 weeks gestation. Scale bars represents 50 μm.

(D) Pro-SFTPC and SFTPB were co-stained with SOX9 in paraffin sections from human fetal lung specimens from 10-20 weeks gestation. Weak Pro-SFTPC is detected in the SOX9+ bud tip cells as early as 12 weeks, and staining within the bud tip cells increases over time. SFTPB was not detected at any time point analyzed. Scale bar represents 50 μm.

(E) RAGE and HOPX were evaluated in paraffin sections from human fetal lung specimens from 10-20 weeks gestation. As seen in **(B)**, RAGE does not appear in the transition zone until 16 weeks gestation. Like PDPN, HOPX is excluded from the SOX9+ bud tip cells at all time points evaluated, but is expressed in the nuclei of airway cells as early as 10 weeks,. Scale bar represents 50 μm.

(F) *In situ* hybridization (brown dots indicate positive staining) for *ID2* shows that bud tip cells in the developing human fetal lung express ID2 from 10-20 weeks gestation. Intensity of signal increases with time, and the strongest positive signal in the bud tips occurs at 20 weeks. Scale bar represents 50 μm.

Figure 1 - Figure supplement 2: FGF7 is sufficient to promote growth of mouse SOX9+ bud tip progenitors *ex vivo*

(A) Schematic of *Sox9*-eGFP distal lung buds dissected at E13.5 and cultured in a Matrigel droplet.

(B) Low magnification images of isolated lung buds under brightfield (left) or showing *Sox9*-eGFP expression (right). Scale bar represents 200μm.

(C) Isolated E13.5 embryonic mouse lung buds from wild type versus *Sox9*-eGFP mice did not have significantly different levels of Sox9 transcript as shown by qPCR. Each data point represents an independent biological replicate. Error bars plot the standard error of the mean. The mean of each group was compared

using a two-sided student's T-test with a significance level of 0.05. P > 0.05 ns, P ≤ 0.05 *, P ≤ 0.01 **, P ≤ 0.001 ***, P ≤ 0.0001 ****.

(D) Isolated buds were cultured in basal media or individually with different factors (10ng/mL FGF7, 10ng/mL FGF10, 10ng/mL BMP4, 50nM RA, 3uM CHIR-99021) and imaged at Day 0, Day 5 and Day 14 in culture to assess the ability of each factor to support growth and survival in culture. Scale bar represents 200μm.

(E) Mouse lung buds were growth with FGF7 or with a 50-fold increase in the concentration of FGF10 to test whether FGF10 could provide the same growth support as 10ng/mL of FGF7. After 5 days in culture, buds grown with 500ng/mL of FGF10 were not as large and did not exhibit branched structures. Scale bar represents 200μm.

(F) *Sox9*-Cre^{ER};Rosa26^{Tomato} lungs were induced with Tamoxifen 24 hours prior to isolation of the buds, which were isolated and cultured at E13.5. Lineage labeled buds demonstrated that labeled cells expanded in culture over the course of two weeks. Asterisks (*) mark air bubbles within Matrigel droplets that were auto-fluorescent, and arrowheads point to day 0 isolated lung buds. Scale bar represents 200μm.

(G) QRT-PCR analysis of buds after 0, 3, 5, or 14 days in culture with 10ng/mL FGF7 shows that expression of the progenitor marker *Sox9* decreases over time in culture, whereas expression of the proximal marker *Sox2* remained low. Each data point represents the mean (+/- SEM) of 3 independent biological replicates (n=3). Statistical significance was determined by a one-way, unpaired Analysis of Variance (ANOVA) for each individual gene over time. The mean of each time point was compared to the mean of the expression level for that gene at day 0 of culture. P > 0.05 ns, P ≤ 0.05 *, P ≤ 0.01 **, P ≤ 0.001 ***, P ≤ 0.0001 ****.

Figure 1 - Figure supplement 3: Removal of BMP4 leads to increased *Sox9* expression.

(A) E13.5 isolated mouse lung bud tips cultured with a combination of 5 growth factors in serum free media (10ng/mL FGF7, 10ng/mL FGF10, 10ng/mL BMP4, 50nM RA, 3uM CHIR-99021) with single growth factors removed. Scale bar represents 200 μm.

(B) Removing BMP4 from the 5F media (5F-BMP4) led to a significant increase in *Sox9* expression by QRT-PCR analysis after 5 days when compared to the full 5F media.

(C) *Sox2* expression measured by QRT-PCR is shown for all groups.

(B-C) One-way Analysis of Variance was performed followed by Tukey's multiple comparison to compare the mean of each group to the mean of every other group within the experiment. Each data point represents an independent biological replicate and graphs indicate the mean +/- the standard error of the mean for each experimental group. P > 0.05 ns, P ≤ 0.05 *, P ≤ 0.01 **, P ≤ 0.001 ***, P ≤ 0.0001 ****.

Figure 1 - Figure supplement 4: Synergistic activity of FGF7, CHIR-99021 and RA maintains SOX9 in mouse bud tip cells *in vitro.*

(A) E13.5 mouse bud tips grown with different combinations of growth factors, including '4F' medium (FGF7/FGF10/CHIR-99021/RA) or '3F' medium (FGF7/CHIR-99021/RA), in addition to FGF7/CHIR-99021 and FGF7/RA. Scale bar represents 500μm.

(B) E13.5 bud tips isolated from *Sox9*-Cre^{ER};Rosa26^{Tomato} lungs that were induced with Tamoxifen 24 hours prior to isolation shows that all tested conditions were able to promote the expansion of the original Sox9+ population. Scale bar represents 200μm.

(C-D) Section and whole mount immunohistochemical staining for SOX9 and SOX2 on various growth conditions. Asterisks mark areas within cultures that contained debris with non-specific staining for DAPI. Scale bar represents 50 μm in D.

(E) *Sox9* and *Sox2* mRNA expression levels from E13.5 isolated bud tips and from various growth conditions as assessed by QRT-PCR. Each data point in (E) represents an independent biological replicate. One-way Analysis of Variance was performed followed by Tukey's multiple comparison to compare the mean of each group to the mean of every other group within the experiment. Each data point represents an independent biological replicate and graphs indicate the mean +/- the standard error of the mean for each experimental group. $P > 0.05$ ns, $P \leq 0.05$ *, $P \leq 0.01$ **, $P \leq 0.001$ ***, $P \leq 0.0001$ ****.

Figure 2 - Figure supplement 1: FGF7, CHIR-99021 and RA maintain the highest levels of progenitor markers in cultured human fetal bud tips.

(A) Bright field image of human fetal bud tips cultured in a droplet of matrigel, overlayed with different media combinations, and examined at 2, 4 and 6 weeks. Scale bar represents 500um.

(B) Immunofluorescent co-expression of SOX9 and SOX2 was examined in different media combinations tested. Scalebar represents 50 um.

(C) QRT-PCR analysis of human fetal bud tips after 4 weeks *in vitro* examining expression of *SOX9*, *SOX2, NMYC* and *ID2*. Each data point represents an independent biological replicate and graphs indicate the mean +/- the standard error of the mean for each experimental group. An unpaired, one-way analysis of variance was performed for each experiment followed by Tukey's multiple comparison to compare the mean of each group to the mean of every other group within the experiment. A significance level of 0.05 was used. Significance is shown on the graph according to the following: $P > 0.05$ ns, $P \leq 0.05$ *, $P \leq 0.01$ **, $P \leq 0.001$ ***, $P \leq 0.0001$ ****.

(D-E) QRT-PCR analysis of human fetal bud tips after 4 weeks *in vitro* examining expression of airway cell markers *P63, FOXJ1, SCGB1A1* (D) and alveolar markers *SFTPB* and *HOPX (*E). Each data point represents an independent biological replicate and graphs indicate the mean +/- the standard error of the mean for each experimental group. An unpaired, one-way analysis of variance was performed for each experiment followed by Tukey's multiple comparison to compare the mean of each group to the mean of every other group within the

experiment. A significance level of 0.05 was used. Significance is shown on the graph according to the following: P > 0.05 ns, P ≤ 0.05 *, P ≤ 0.01 **, P ≤ 0.001 ***, P ≤ 0.0001 ****.

Figure 2 - Figure supplement 2: Cultured fetal progenitor organoids successfully engraft into injured mouse airway epithelium

(A) Experimental schematic. 5 male NSG mice were injected with 300 mg/kg of Naphthaline to induce injury to the airway epithelium. 24 hours after injury, mice were given intratracheal injections of 500,000 single cells of fetal progenitor organoids that had been grown in 3F media. Lungs were harvested after 7 days to assess engraftment.

(B) Naphthaline injured lungs exhibit epithelial cell shedding and severe injury in the proximal airway. Scale bar represents 50um.

(C) Brightfield, SOX9 and SOX2 co-expression in fetal progenitor organoids harvested on the day of injection. Fetal progenitor organoids had been grown for 4 weeks in 3F media in culture and were derived from the same sample that was used for cell injection studies. Brightfield scale bare represents 500um; immunofluorescent scale bars represent 100um.

(D) Cell-injected lungs were examined for Human mitochondira (HuMITO), SOX2, SOX9, NKX2.1 and the epithelial marker β–catenin (bCAT). Low magnification cale bars represent 50um; high magnification scale bars represent 25um.

Figure 3 - Figure supplement 1: Patterned lung organoids grown from hPSCs exhibit robust and stereotyped growth

(A) Representative low magnification image of many foregut spheroids on day 1 plated in a Matrigel droplet, and cultured in 3F media for 7 days. Dashed line outlines the Matrigel droplet. Scale bar represents 1mm.

(B) Each experiment yielded many wells of spheroids plated in a 24 well plate on day 1, which were subsequently split into multiple 24 well plates to allow sufficient space for growth by day 35, and each well contained many organoids.

(C) During early stages of growth (day 23-30 shown), epithelial organoids undergo epithelial 'folding', which typically occurs from weeks 3-5. Scale bar represents 200um.

(D) The same organoid was imaged from day 39 through day 46. Asterisks identify buds undergoing bifurcation. Scale bars represent 200 μm.

(E) Patterned lung organoids were frozen and stored in liquid nitrogen, then thawed and grown in 3F media. After thawing, organoids were split as whole intact structures, they were passaged through a 27-gauge needle to generate cystic bud tip organoids.

(F) SOX9 and SOX2 co-expression in bud-tip region of patterned lung organoids after more than 16 weeks (115 days) in vitro. Scale bar represents 100μm.

Figure 3 - Figure supplement 2: Patterned lung organoids have molecular similarities to 14 week fetal lung and cultured fetal progenitor organoids

(A) QRT-PCR comparison of patterned lung organoids to 14 week fetal lung (3 biological replicates of whole lung at 14 weeks gestation) show expression of the progenitor markers *SOX9*, *SOX2*, *NMYC* and *ID2.* Each data point represents an independent biological replicate and graphs indicate the mean +/- the standard error of the mean for each experimental group. An unpaired, Student's T test was performed for each gene. A significance level of 0.05 was used. Significance is shown on the graph according to the following: P > 0.05 ns, P ≤ 0.05 *, P ≤ 0.01 **, P ≤ 0.001 ***, P ≤ 0.0001 ****.
(B) QRT-PCR comparison between undifferentiated hPSCs (H9 hESC line), Foregut (FG) Spheroids, human fetal progenitor organoids and patterned organoids was performed to examine mRNA levels of *SOX9, SOX2, NMYC* and *ID2*. Each data point represents an independent biological replicate and graphs indicate the mean +/- the standard error of the mean for each experimental group. An unpaired, one-way analysis of variance was performed for each gene followed by Tukey's multiple comparison to compare the mean of each group to the mean of every other group within the experiment. A significance level of 0.05 was used. Significance is shown on the graph according to the following: P > 0.05 ns, P ≤ 0.05 *, P ≤ 0.01 **, P ≤ 0.001 ***, P ≤ 0.0001 ****.
(C-D) After 42 days *in vitro* pattered lung organoids were compared to whole fetal lung tissue (3 biological replicates of whole lung at 14 weeks gestation) by QRT-PCR to examine expression of alveolar markers *HOPX*, *SFTPB* and *SFTPC* (**C**) and mature airway markers, *P63 FOXJ1* and *SCGB1A1* (**D**). Each data point represents an independent biological replicate, and the mean +/- the standard error of the mean is shown for each group. An unpaired two-sided student's T test was performed to compare the means of each group for each target. A significance value of 0.05 was used. P > 0.05 ns, P ≤ 0.05 *, P ≤ 0.01 **, P ≤ 0.001 ***, P ≤ 0.0001 ****.

Figure 4 - Figure supplement 1: Characterization of hPSC-derived bud tip organoids

(A) ECAD and NKX2.1 immunofluorescence in bud tip organoids shows that bud tip organoids express NKX2.1. Scale bar represents 50 μm.
(B) Immunofluorescence analysis of HOPX and RAGE in bud tip organoids show that neither marker is expressed, similar to what is seen in 15 week human fetal bud tip cells (Figure 1). Scale bar represents 50 μm.
(C) *In situ* hybridization for ID2 in bud tip organoids (brown dots indicate positive staining) confirms ID2 expression in organoids. Scale bar represents 50 μm.
(D) Immunofluorescence analysis for ProSFTPC, SFTPB and SOX9 in bud tip organoids shows positive ProSFTPC staining but negative SFTPB, similar to what is seen in 15 week human fetal bud tip cells (Figure 1). Scale bar represents 50 μm.
(D) Immunofluorescence analysis of PDPN and ABCA3 in bud tip organoids shows that neither PDPN nor ABCA3 are expressed in organoids – similar to what is seen in 15 week human fetal bud tip cells (Figure 1). Scale bar represents 50um.

Figure 6 - figure supplement 1: Characterization of bud tip organoids generated from iPSC20-1 on the day of transplantation into the injured mouse airway

(A) Bud tip organoids immunostained for NKX2.1 and HuMITO. Scale bar represents 50 um.

(B) Bud tip organoids immunostained for KI67 and HuMITO. Scale bar represents 50 um.

(C) Bud tip organoids immunostained or HuMITO, SOX9 and SOX2 at low magnification (top) and high magnification (bottom). Scale bar for all images represents 50 um.

(D) Bud tip organoids immunostained or NuMA, MUC5AC and ECAD at low magnification (top) and high magnification (bottom). Positive staining for MUC5AC is not observed. Images taken at the same scale as shown in (C).

(E) Bud tip organoids immunostained or FOXJ1 and SCGB1A1. Positive staining was not observed. Scale bar represents 50 um.

(F) Bud tip organoids from untreated cultures (no Doxycycline added to media) immunostained or GFP. Positive staining was not observed. Scale bar represents 50 um.

Figure 1 - Figure Supplement 1

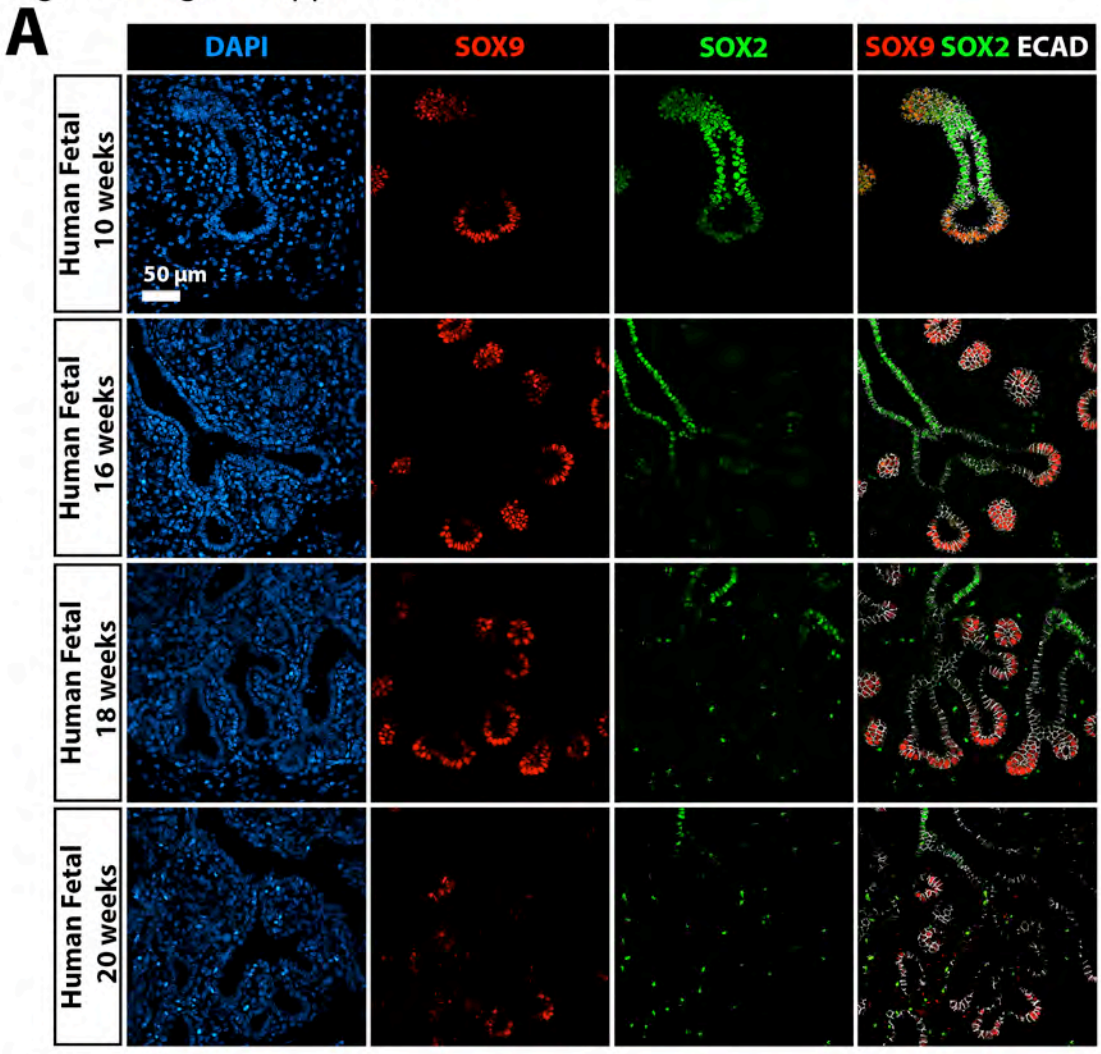

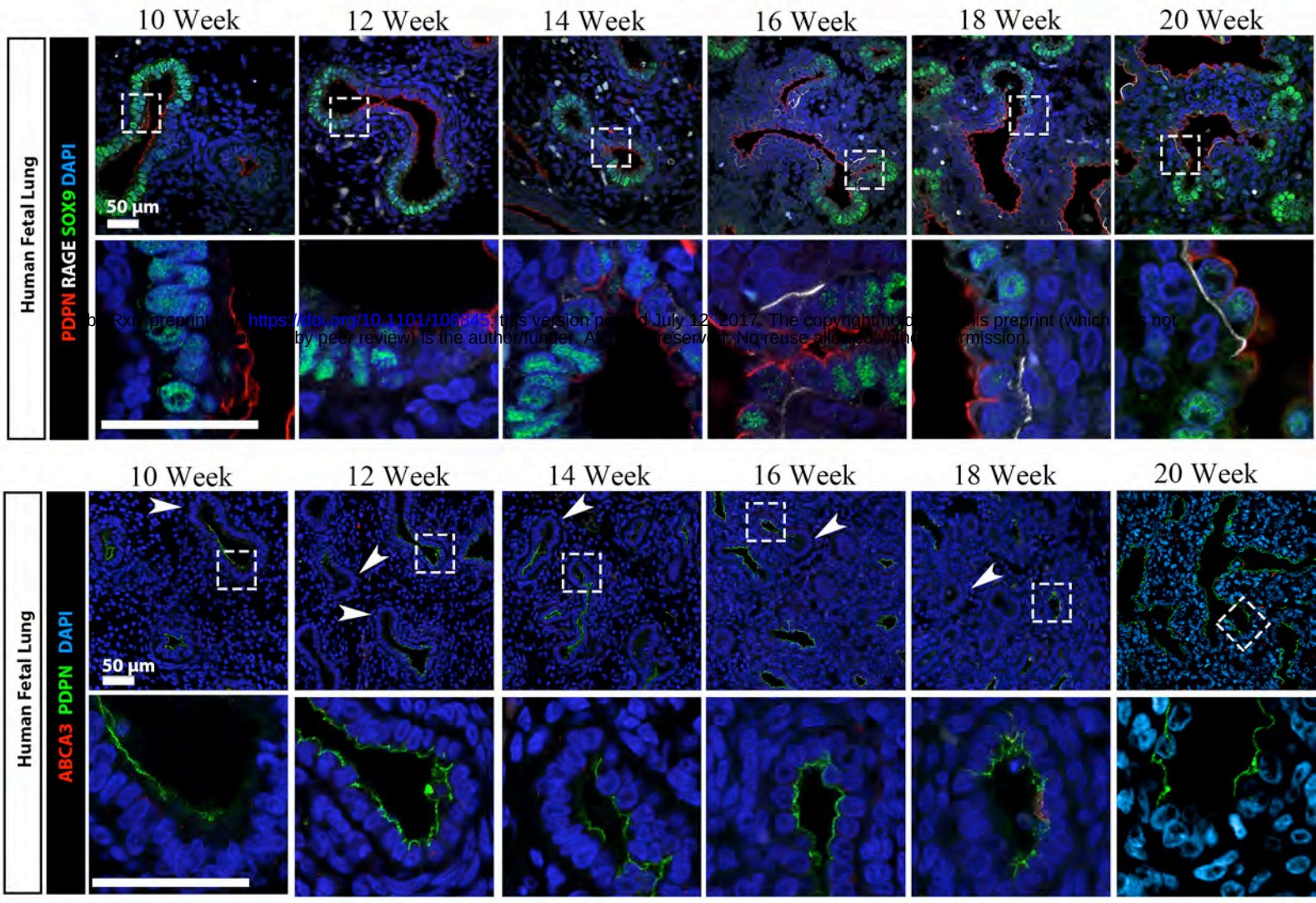

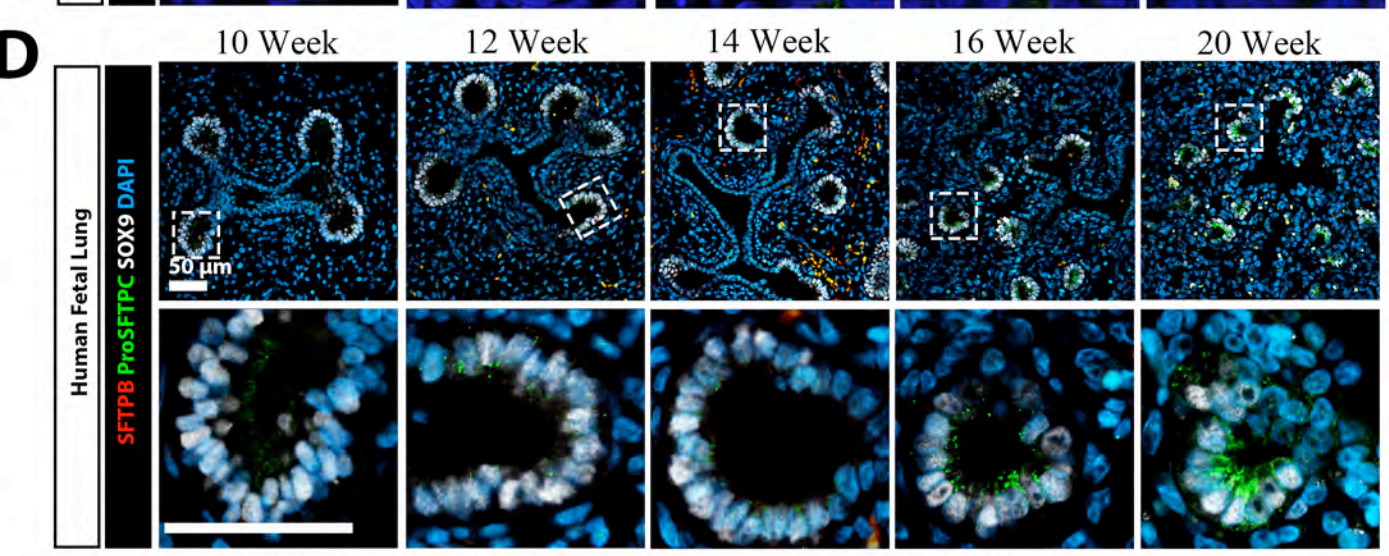

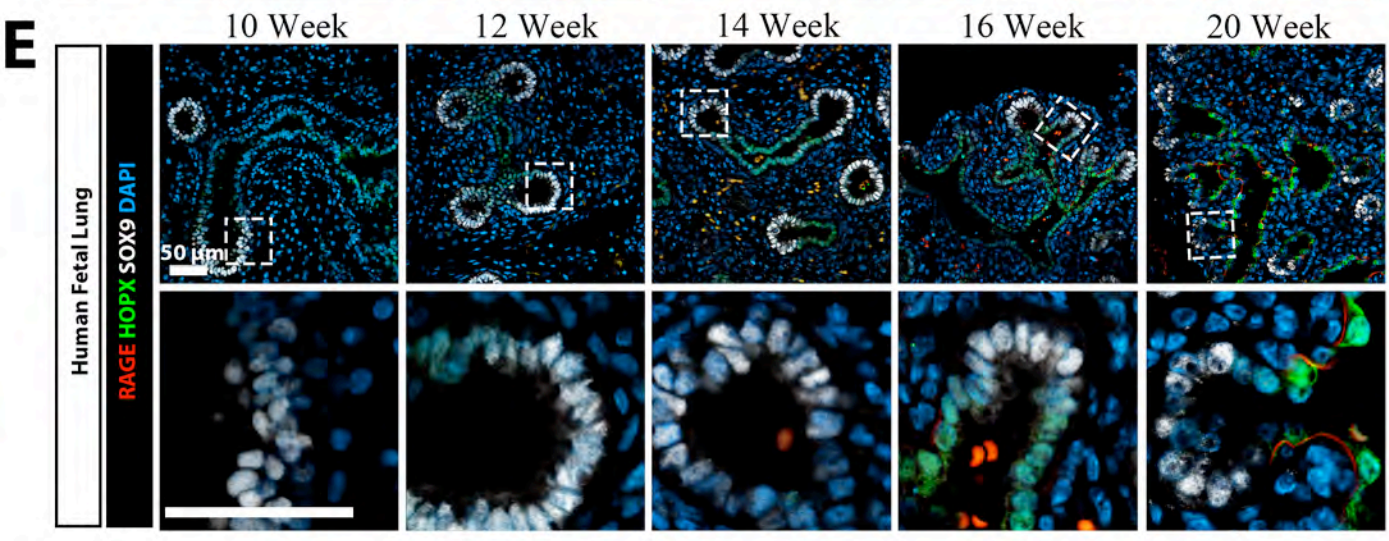

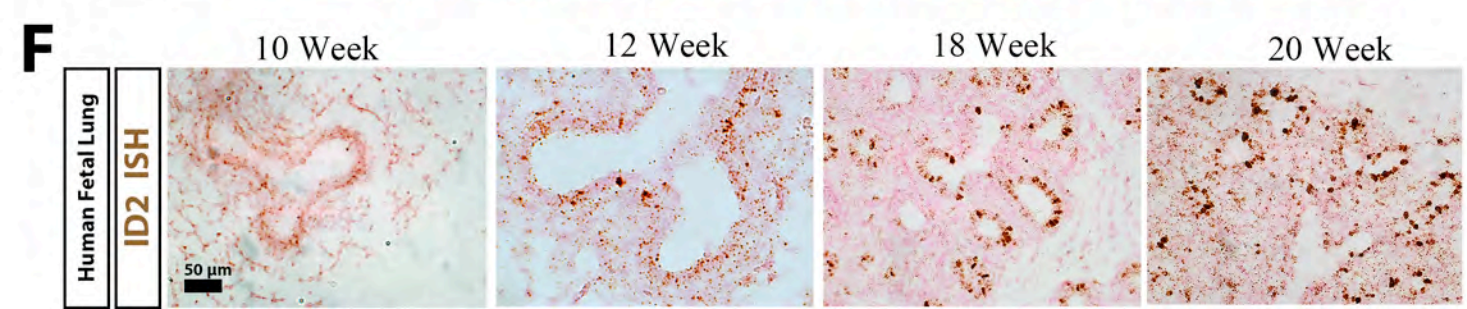

Figure 1 - Figure Supplement 2

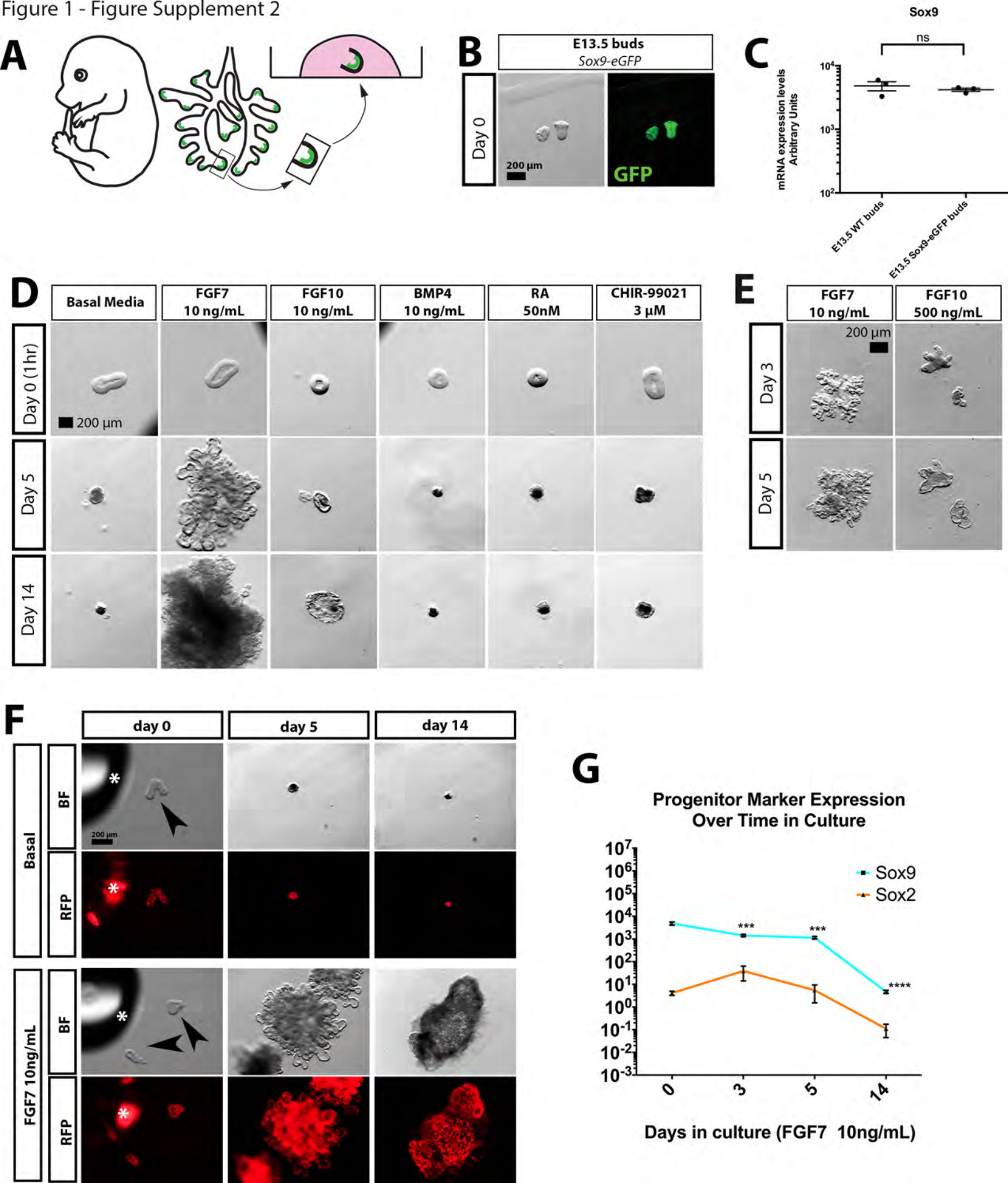

Figure 1 - Figure Supplement 3

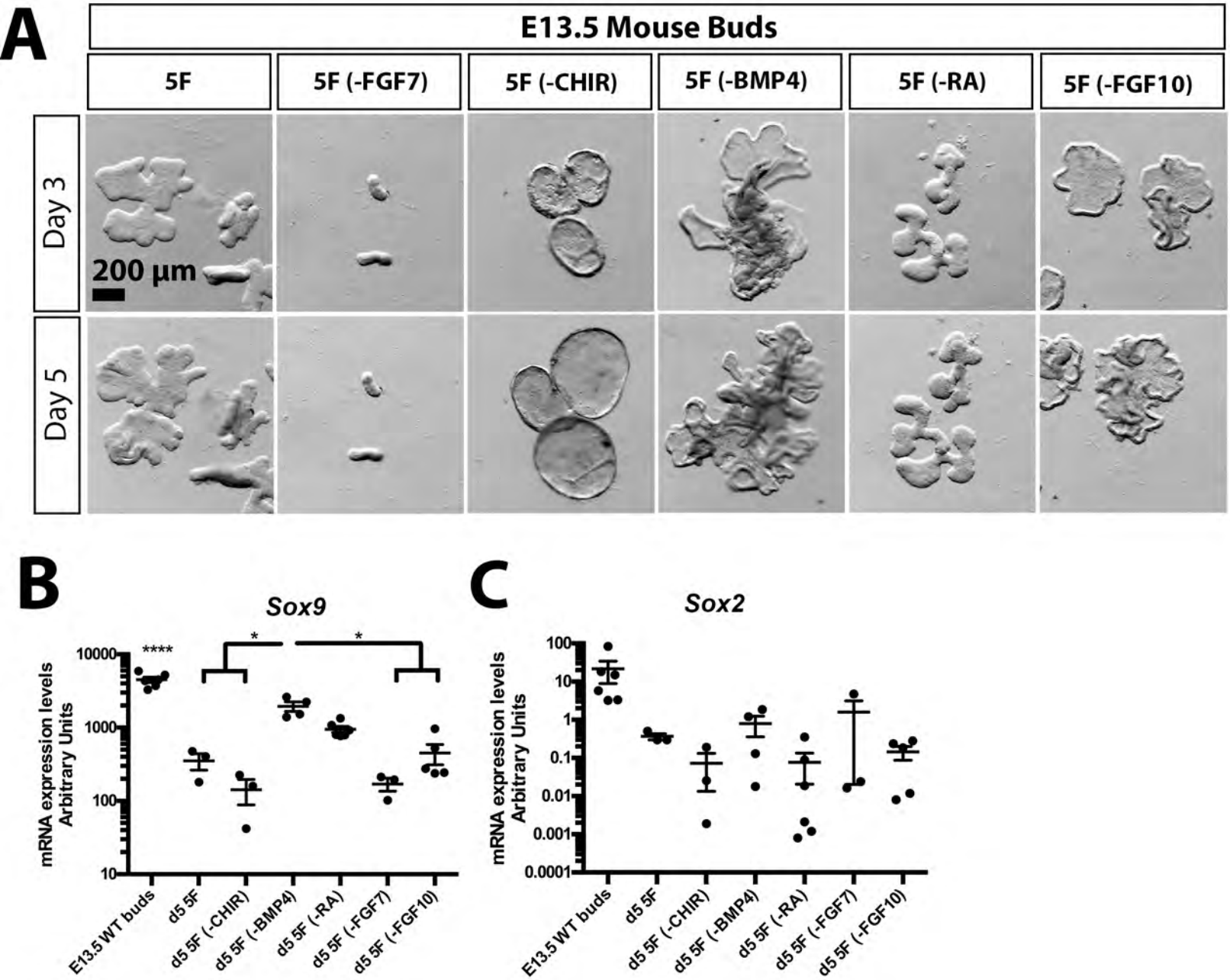

Figure 1 - Figure Supplement 4

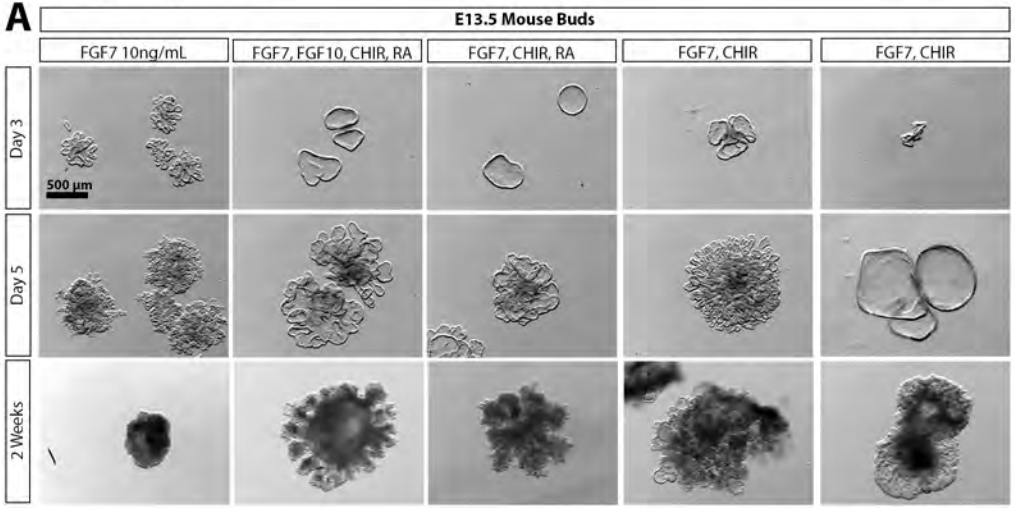

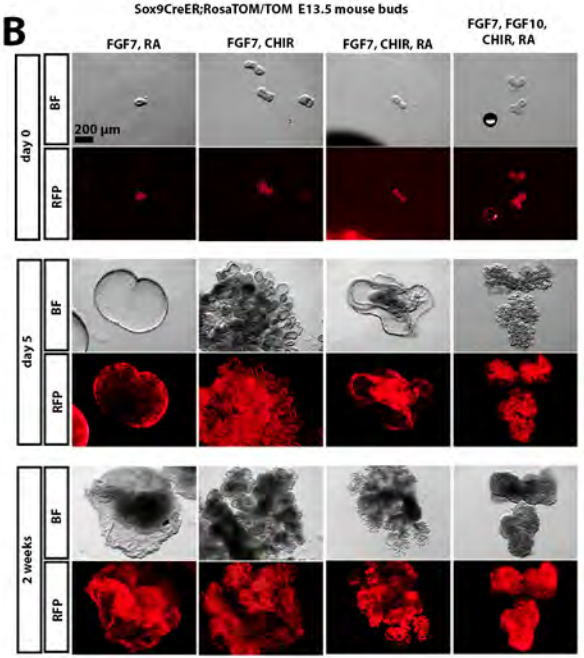

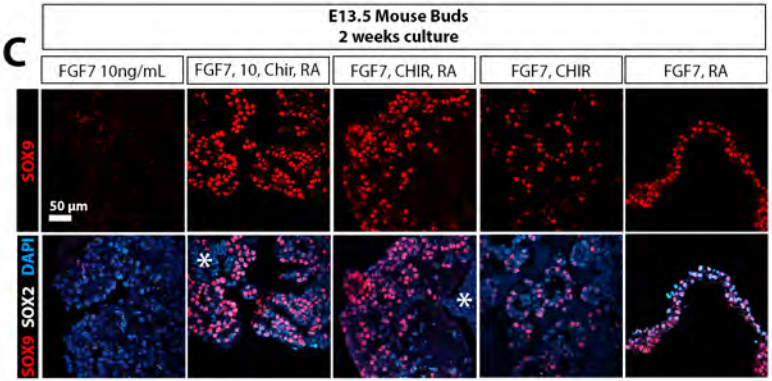

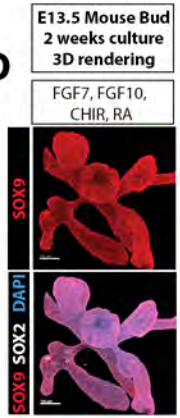

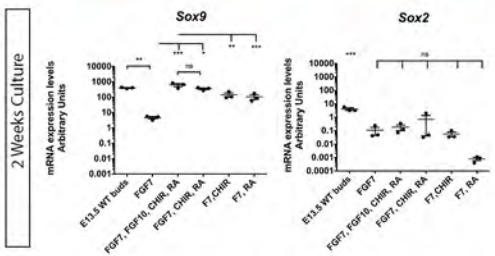

Figure 2 - Figure Supplement 1

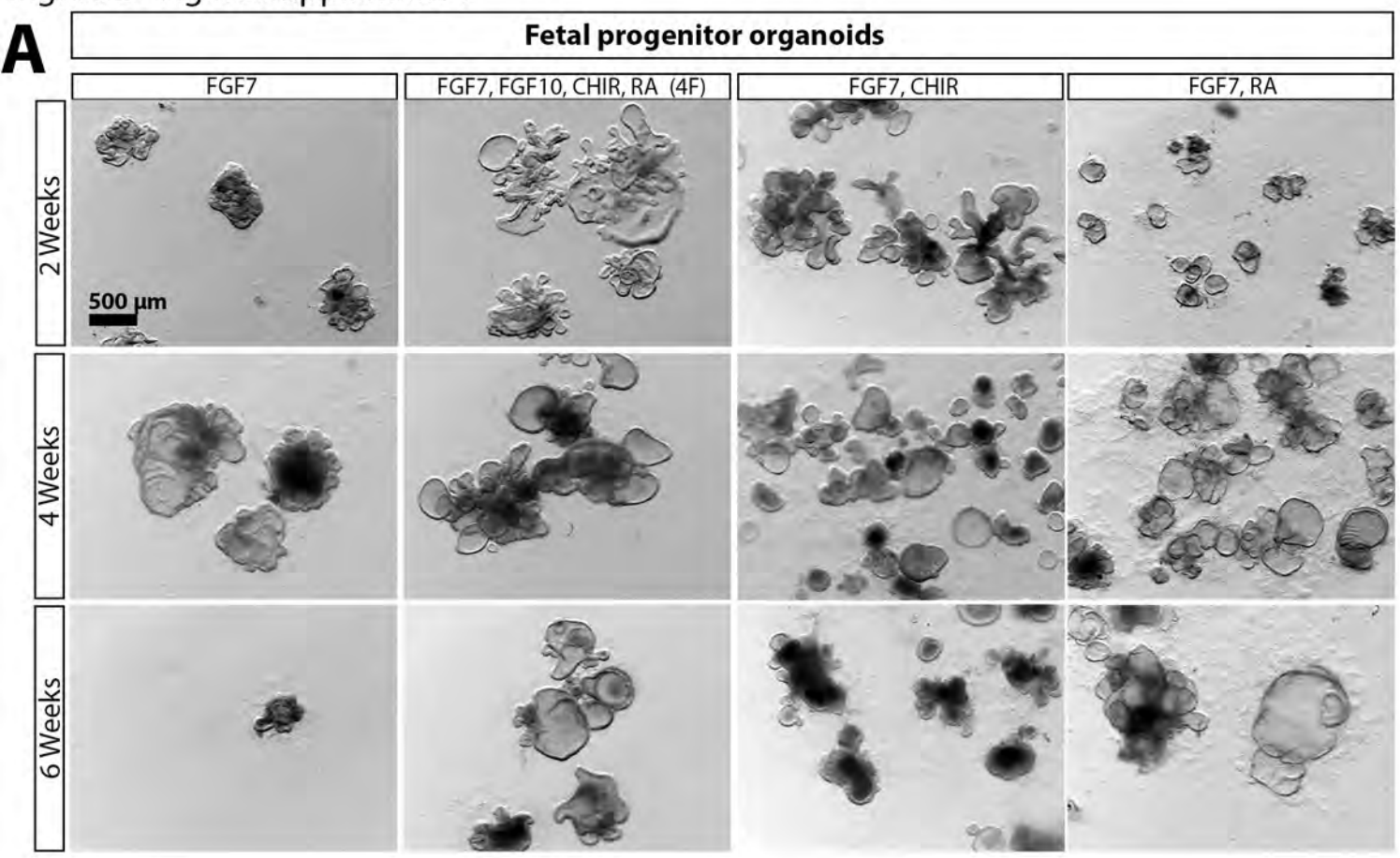

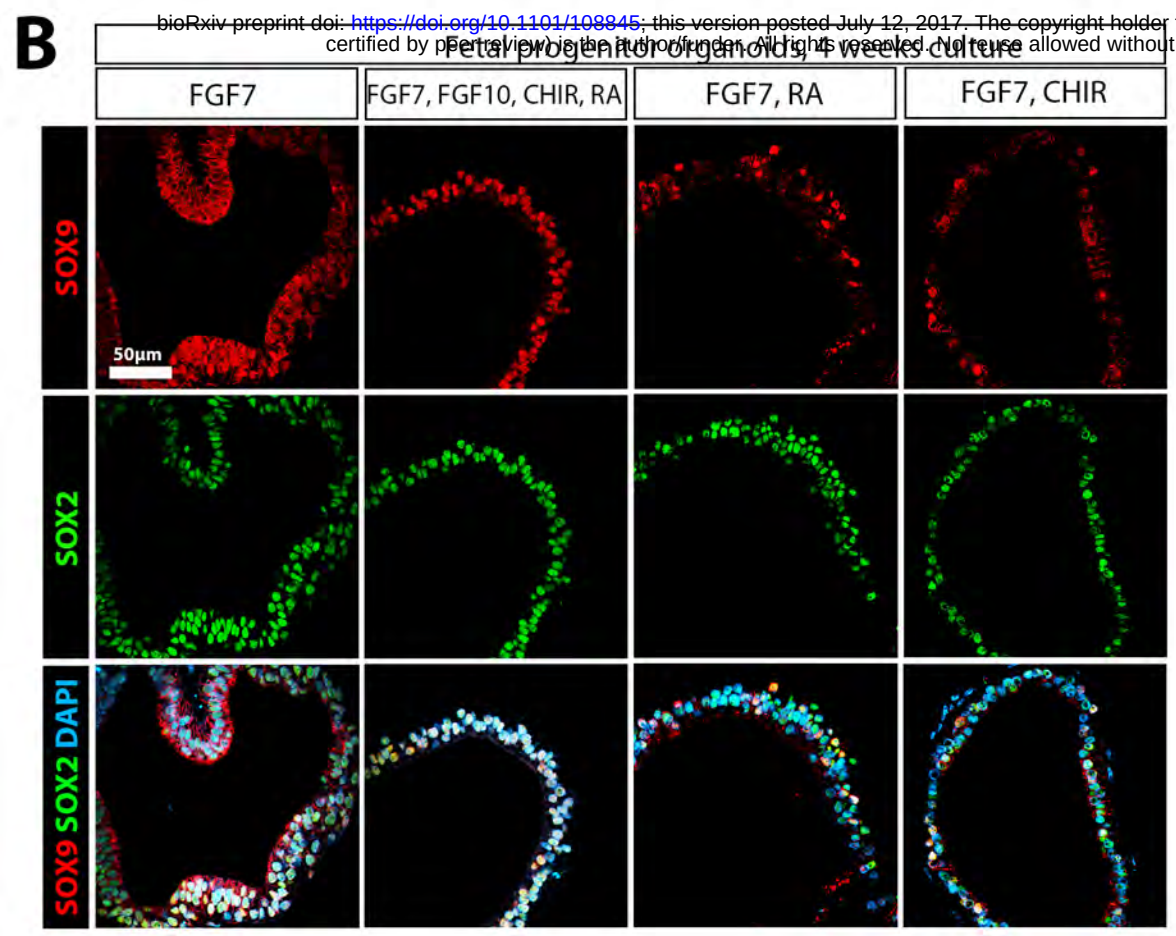

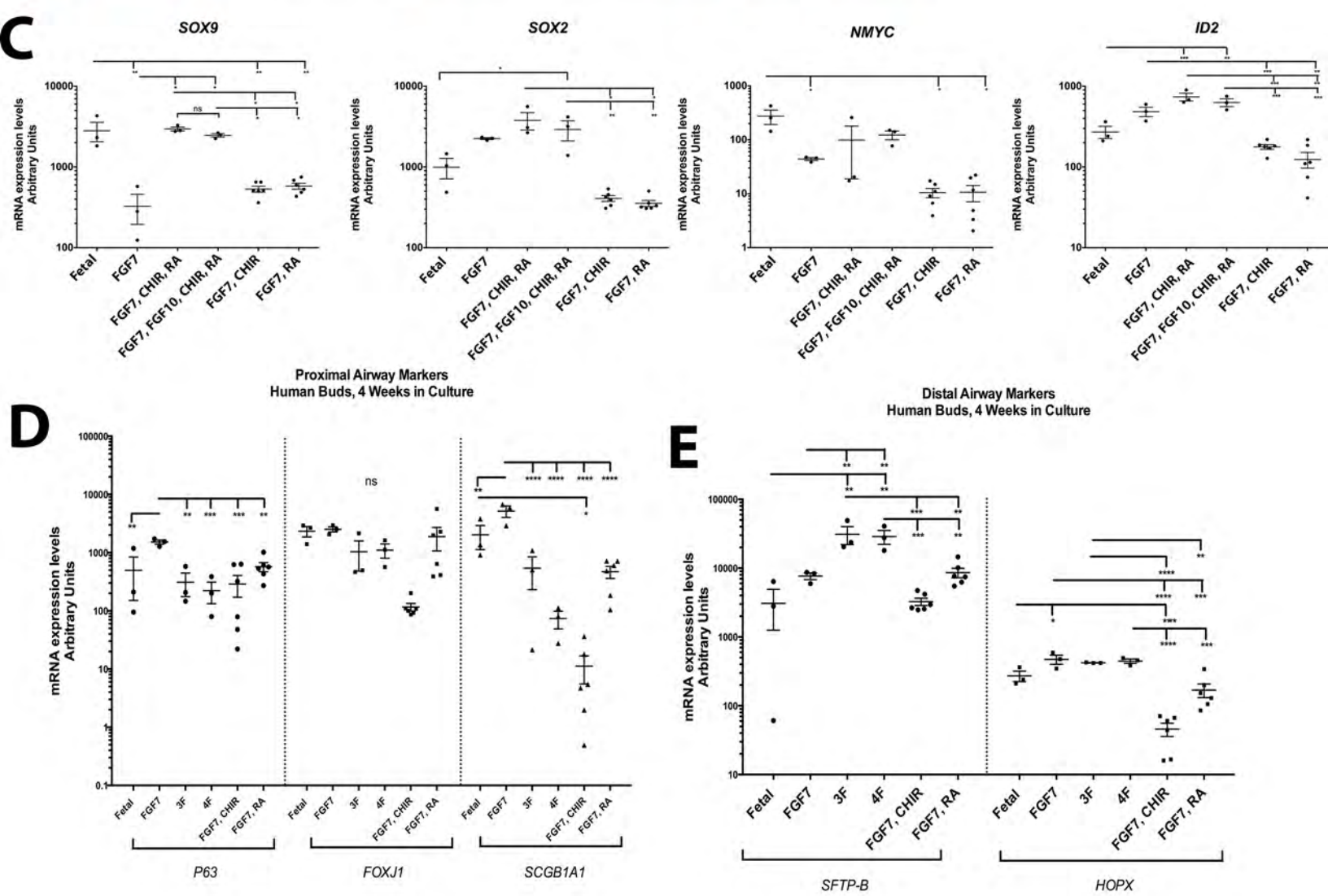

Figure 2 - Figure Supplement 2

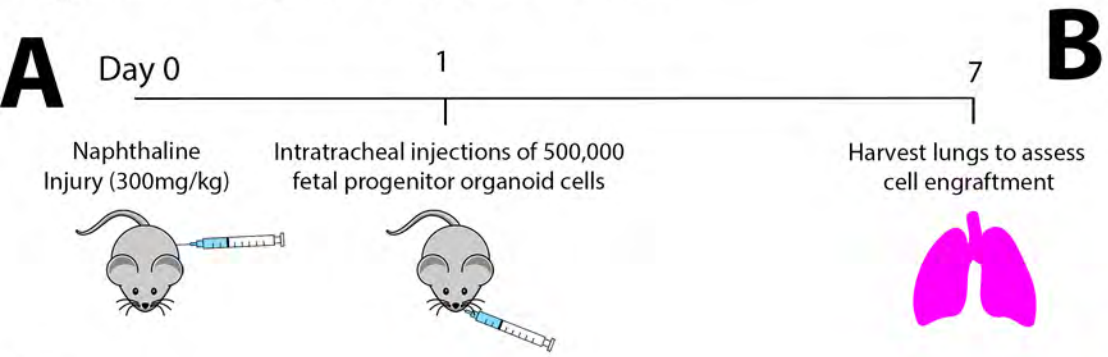

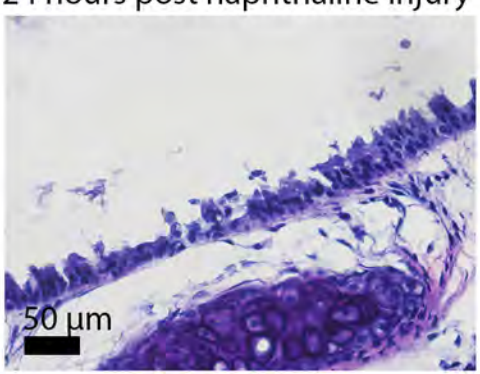

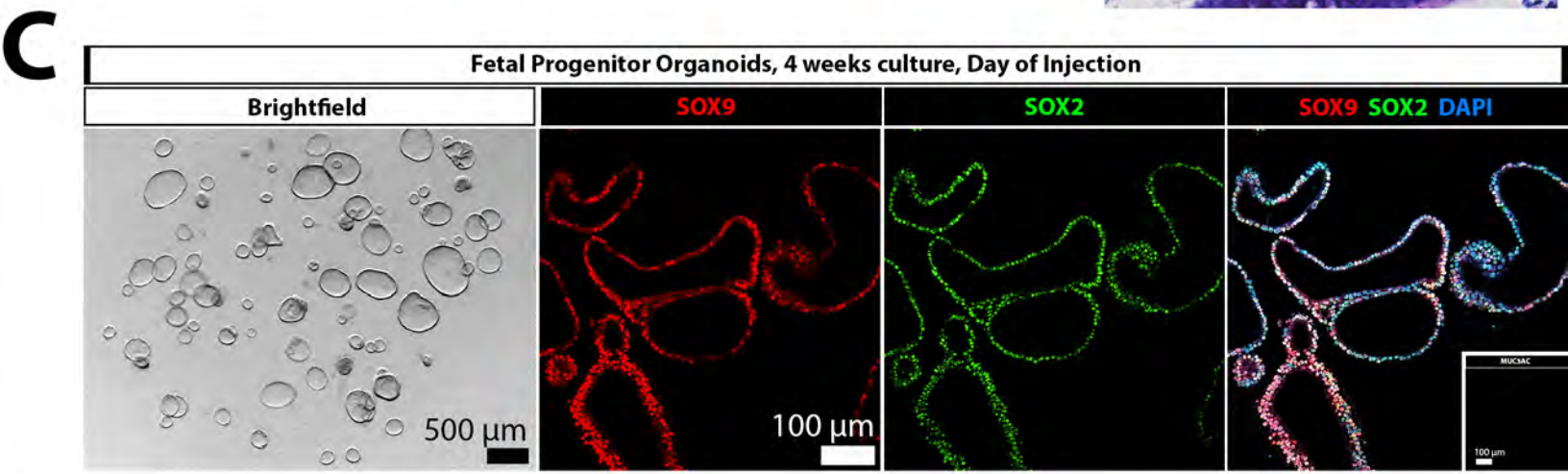

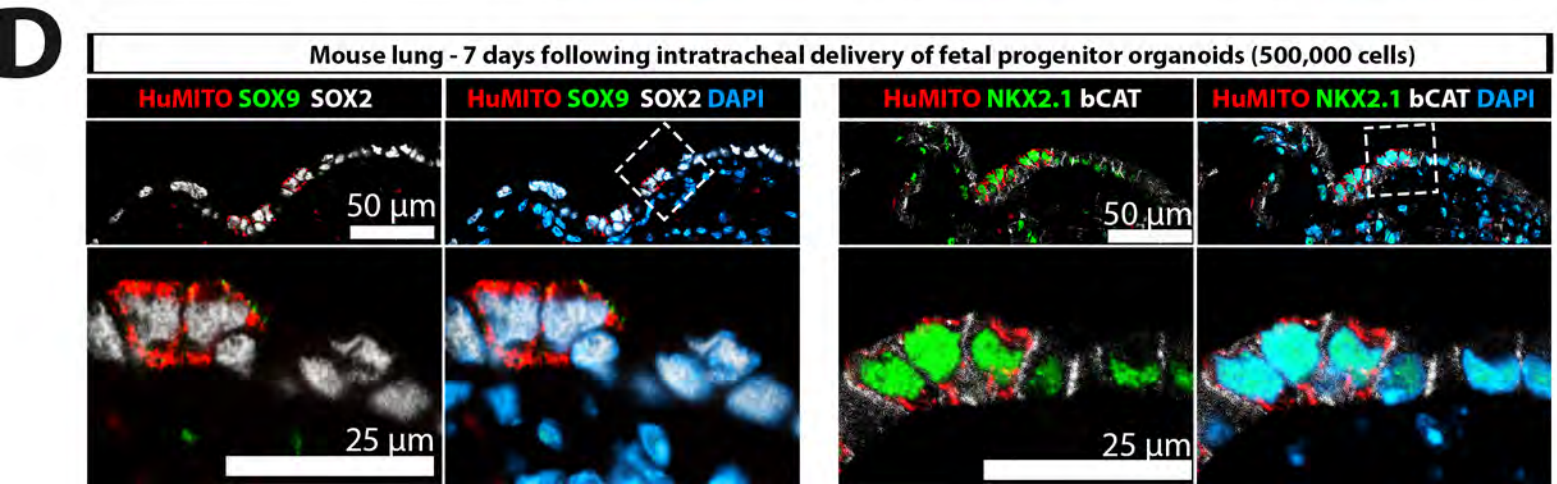

Figure 3 - Figure Supplement 1

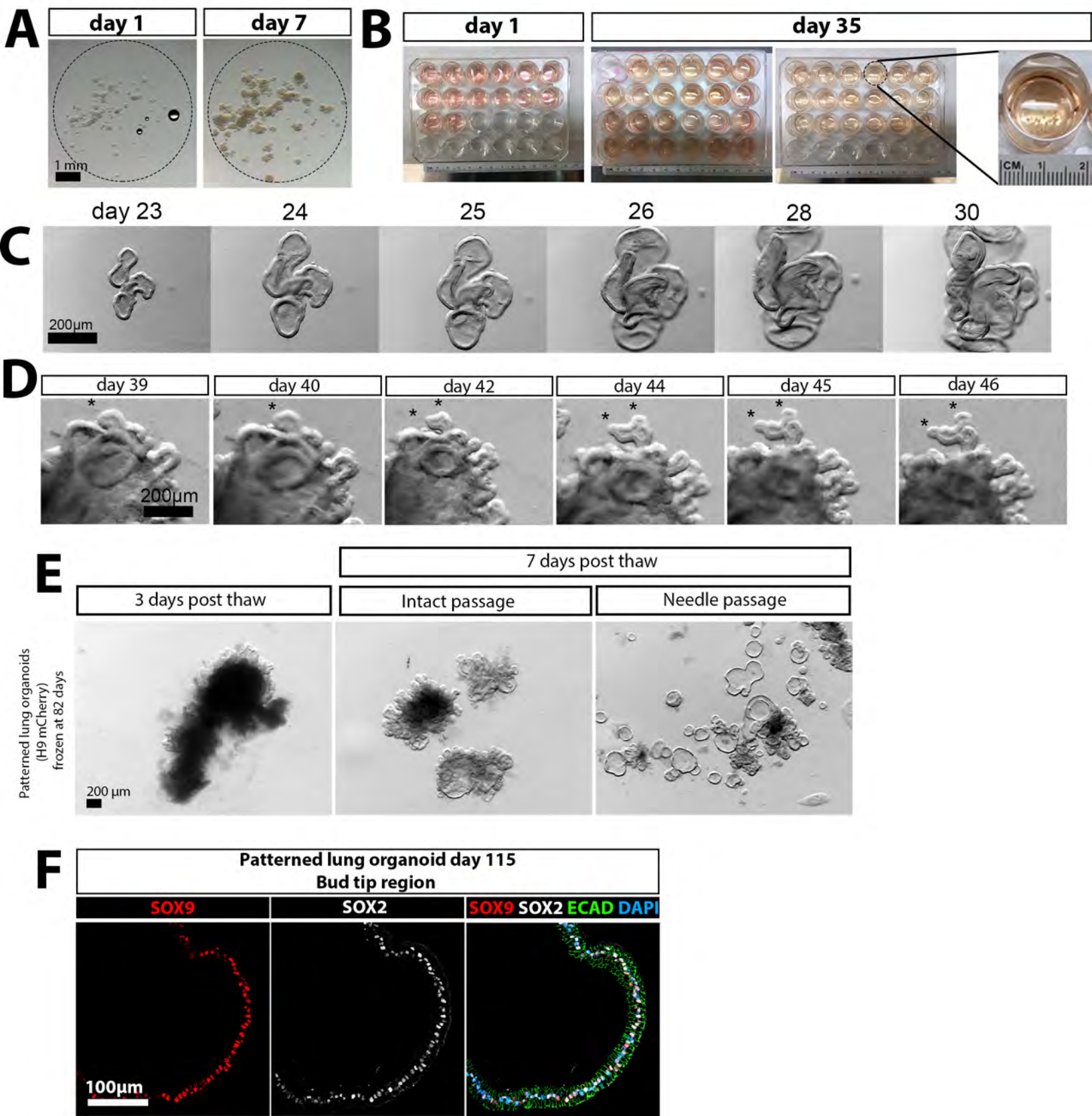

Figure 3 - Figure Supplement 2

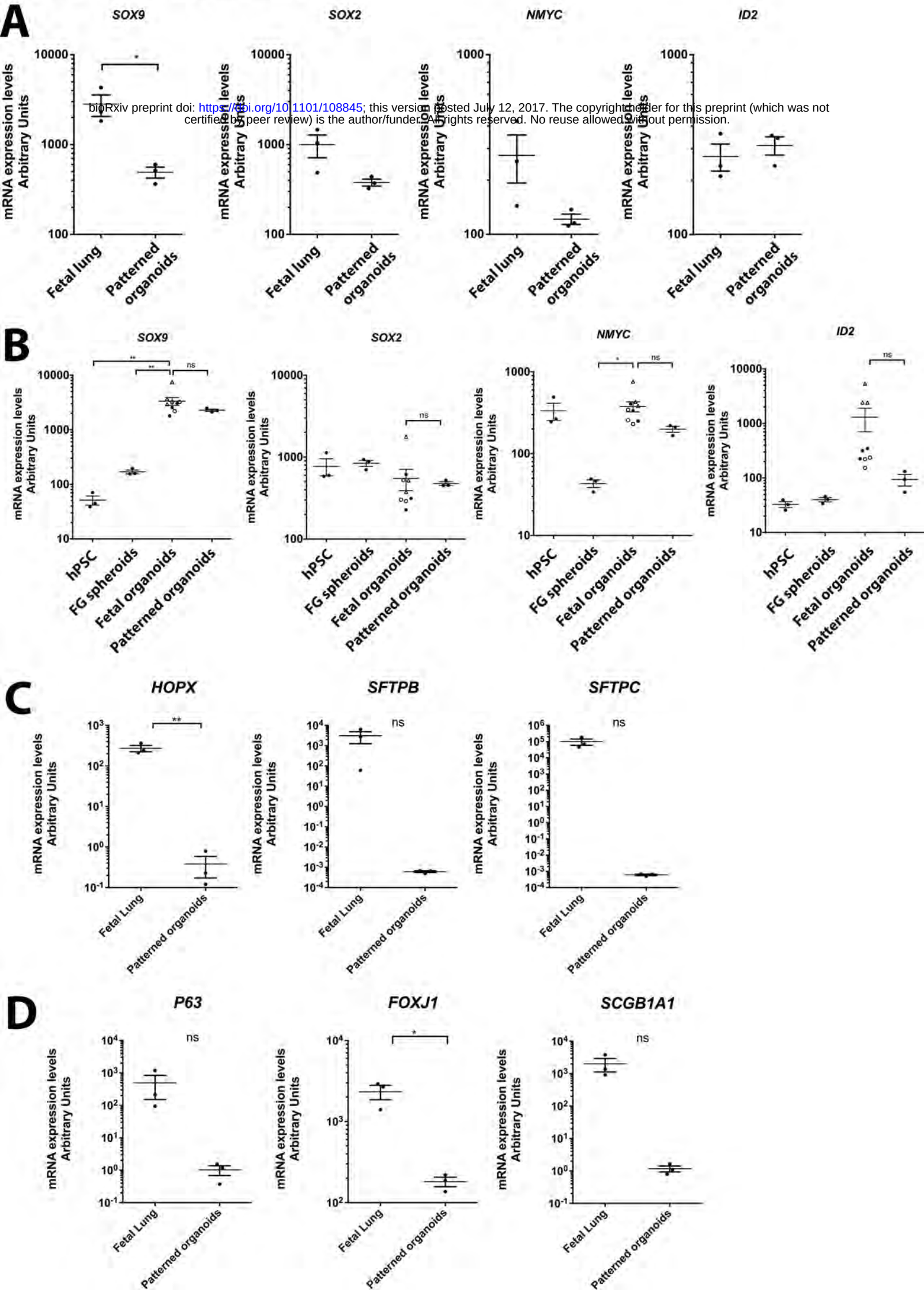

Figure 4 - Figure Supplement 1

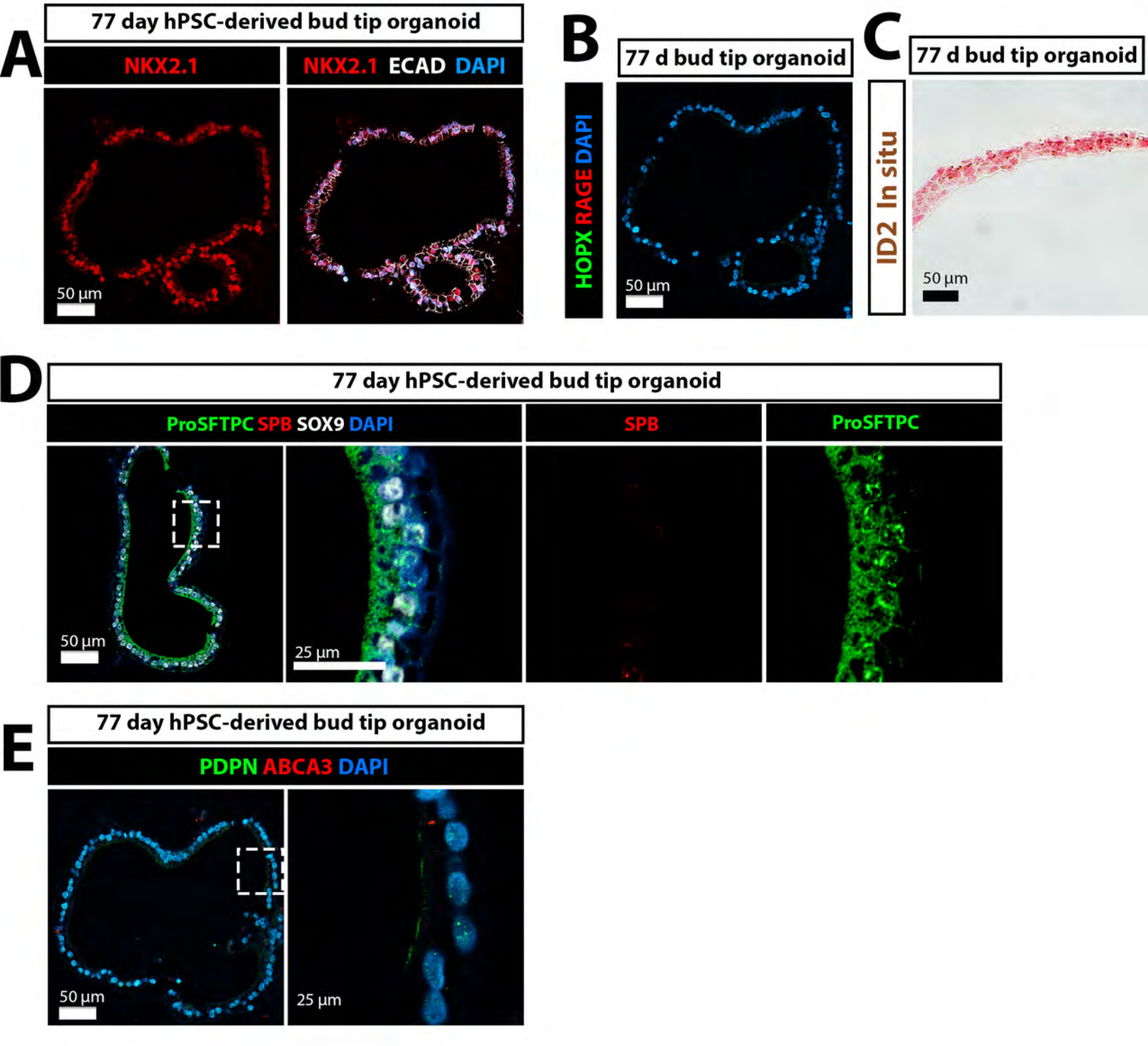

Figure 6 - Figure Supplement 1